Photosynthetic pigments in sediments: development of applications in archaeology and compound-specific radiocarbon analysis

Angela Carol Ballantyne

A thesis submitted in partial fulfilment of the requirements for the degree of Doctor of Philosophy at the University of York

University of York
Department of Chemistry

October 2012

Abstract

Photosynthetic pigments derived from oxygenic aquatic photoautotrophs are biosynthesised from dissolved carbon dioxide that reflects atmospheric concentrations of radiocarbon (^{14}C). Sedimentary pigment signatures are not influenced by a terrestrial signal as terrestrial photosynthetic pigments are overwhelmingly destroyed by photo-oxidation. These properties have been exploited by this study to reveal the presence of archaeological water features and to radiocarbon date the timing of a geochemically significant event.

A new approach for identifying archaeological structures suggested to represent former aquatic features has been developed. HPLC and LC-MS^n analysis of sediment extracts from several suspected water features revealed the presence of photosynthetic pigment derivatives, thus providing evidence of the occurrence of photoautotrophic and heterotrophic aquatic organisms at the time the sediment was deposited. Chlorophyll derivatives diagnostic of heterotrophic communities and bacteriochlorophyll derivatives which provide information on photic zone anoxia and eutrophication have been detected in some sites. Thus, the detection of photosynthetic pigments in archaeological sediments provides a geochemical method for investigating the existence and evolution of water features in past landscapes.

Photosynthetic pigments are ideal candidates for compound specific radiocarbon analysis (CSRA) as they have known primary sources of carbon. Sediments from Kirisjes Pond Antarctica, which have been previously radiocarbon dated using bulk organic material, were extracted and individual pigments isolated and purified by a preparative HPLC system that had been validated with test samples. The younger CSRA results obtained from each layer were more credible than bulk measurements due to the age sequence determined within the section examined, which led to differences in age of up to ca. 1500 years between measurements. CSRA of isolates was used to constrain the timing of a marine incursion to between 7736 and 4688 years before present. Comparison of ^{14}C dates from algal and bacterial pigments suggest a reservoir effect of between ca. 5500 to 6000 years. Radiocarbon measurements of standards showed that no isotopic fractionation had occurred during preparative HPLC.

Contents

List of tables

List of figures

Abbreviation List

$\Delta^{14}C$	Radiocarbon content ‰
^{14}C	Radiocarbon
^{14}C yr $_{BP}$	Radiocarbon years before present
AMS	Accelerator mass spectrometry
APCI	Atmospheric pressure chemical ionisation
ASE	Accelerated solvent extraction
BCC	British Chlorophyll Company
Bchl	Bacteriochlorophyll
BPME	Bacteriophaeophorbide methyl ester
CID	Collision induced dissociation
Chl	Chlorophyll
CSRA	Compound specific radiocarbon analysis
Da	Daltons
EA	Elemental analysis
ESI	Electrospray ionisation
FA	Fatty acid
FAME	Fatty acid methyl ester
FID	Flame ionisation detection
GC	Gas chromatography
GDGT	Glycerol dibiphytanyl glycerol tetraether
HPLC	High performance liquid chromatography
i.d.	Internal diameter
LC	Liquid chromatography
$[M+H]^+$	Protonated molecule
MS	Mass spectrometry
MS/MS	Tandem mass spectrometry
MS^n	Multistage tandem mass spectrometry
m/z	Mass to charge ratio
NP	Normal phase
OM	Organic matter
PDA	Photodiode array
R	Reservoir effect
rf	Radio frequency

RP	Reversed phase
SCE	Steryl chlorin ester
TOC	Total organic carbon
t_R	Retention time
UV/vis	Ultraviolet/visible
V_T	Terminal voltage

Acknowledgements

I would like to thank Prof. Brendan Keely for his help and advice during the supervision of this project. NERC is acknowledged for the provision of a studentship. Dr Jen Harland is thanked for allowing the collection of samples for pigment analysis (Chapter 2) from three archaeological sites. The EAOG are thanked for the provision of a travel grant and Prof. Tim Eglinton and his group for the AMS analysis of my samples discussed in Chapter 4. Dominic Hodgson and BAS are acknowledged for the provision of sediment cores.

I wish to express thanks to thank Drs Chris Knappy and Matt Pickering for introducing me to the Waters HPLC, for providing training and help with MS (and numerous other pieces of instrumentation) and for providing proof reading services. Matt is further thanked for schooling me in the ways of chlorophyll pigments.

The many present and past and members of the BJK group (Matt, Chris, Haslina, Suleman, Neung, Andy, Denize, Kim, Ryan, and Adam) have made the research environment in the lab and office fun and productive. Xmas parties and gigs will not be the same without you guys.

I would like to express my deepest gratitude to my family for their support during my Ph.D. And also for the many hours spent they have spent talking on the phone with me. I would like to thank Graeme who has valiantly put up with me during my writing up period and for his support whether we are in the same city or not!

Author's Declaration

I hereby declare that the work described in this thesis is my own, except where otherwise acknowledged, and has not been submitted previously for a degree at this or any other university.

……...

Angela Ballantyne

Chapter 1. Introduction

1.1. Radiocarbon

1.1.1. Formation and half life of radiocarbon

Cosmic rays comprise protons or nuclei (for example alpha particles) and either originate from outside our solar system or are emitted from the sun (Povinec *et al.*, 2008). These rays interact with air molecules in Earth's upper stratosphere and lower troposphere to produce neutrons that subsequently react with nitrogen to form radiocarbon (^{14}C, Equation 1):

$$^{14}_{7}N + {}^{1}_{0}n \rightarrow {}^{14}_{6}C + {}^{1}_{1}p \qquad (1)$$

The radiocarbon formed quickly oxidises to form $^{14}CO_2$, which mixes with the exchangeable atmospheric reservoir of carbon. As part of this reservoir $^{14}CO_2$ can enter the carbon cycle either by fixation as organic carbon, for example via photosynthesis, or by dissolution in the world's oceans (Currie, 2004; McNichol and Aluwihare, 2007).

The half life ($t_{1/2}$) of ^{14}C was determined to be 5730 years by researchers at the fifth Radiocarbon Dating Conference in Cambridge (Godwin, 1962). Radiocarbon (^{14}C) is the most abundant radioisotope of carbon with a concentration of one atom per one trillion (or 1 x 10^{12}) ^{12}C atoms. Radiocarbon dating has been used to date historical artefacts (for example the shroud of Turin (Damon *et al.*, 1989)) and to determine chronologies of sediments (Macdonald *et al.*, 1991). The theoretical extent to which radiocarbon can be used to date artefacts is nine to ten half lives, ca. 50,000 years before present. Subsequent half lives render substances radiocarbon dead, as nearly all ^{14}C has undergone β decay back to ^{14}N (Hellborg and Skog, 2008).

1.2. Accelerator mass spectrometry

Accelerator mass spectrometric (AMS) instrumentation was developed ca. 35 years ago by Bennett *et al.* (1977) and Nelson *et al.* (1977), who simultaneously reported the use of accelerator tubes. AMS detects the number of each carbon isotopes in a sample, whereas traditionally used decay counting by liquid

scintillation records the number of individual decay events from ^{14}C atoms. AMS has several advantages over decay counting, for example shorter analysis times and smaller sample size requirements.

1.2.1. Sample preparation

Samples for AMS analysis must be converted to CO_2 and analysed as a gas or undergo reduction to form a graphite target. Two principle aims dictate the development of sample preparation methods (Verkouteren and Klouda, 1992):

- Avoid mass fractionation of carbon isotopes
- Reduce preparation time, thus increasing throughput

An example of graphite preparation is the combustion of samples with cupric oxide to form CO_2 followed by hydride reduction over an iron or cobalt catalyst at ca. 500^0C. Samples containing 20 μg of carbon have been converted with a 95% yield into graphite (Ognibene *et al.*, 2003).

Samples can be prepared for gas measurement by using the same preliminary steps as graphitisation (Shah and Pearson, 2007). Elemental analysers can also be used to convert samples to CO_2 and several researchers have been developing methods of coupling elemental analysers to gas ion sources for online sample preparation and measurement (Ramsey and Humm, 2000; Uhl *et al.*, 2004).

1.2.2. AMS instrumentation

The components of a high energy AMS instrument which utilises tandem accelerator tubes are shown schematically in Figure 1. Low energy systems (ca. 200 kV) do not have the large pressure tanks needed to maintain the terminal voltage (ca. 10,000 kV) in high energy systems, as they use vacuum insulation and commercial energy supplies.

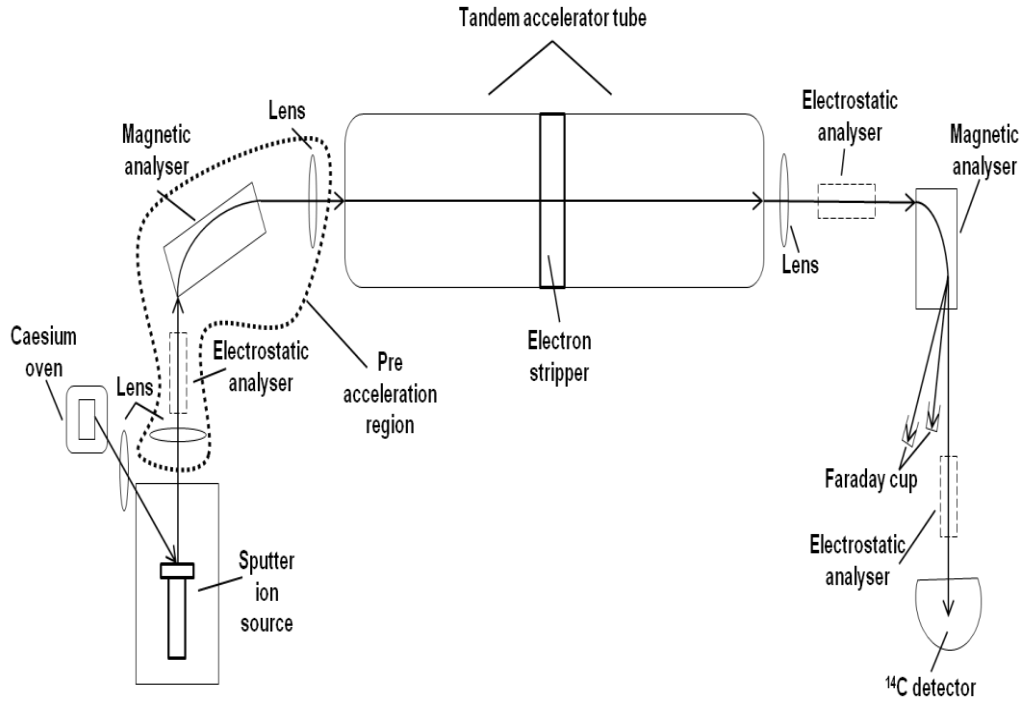

Figure 1. Schematic diagram of a high voltage AMS (modified from Fifield, 1999).

1.2.3. Ion sources

The source, maintained at a negative potential, contains a supply of caesium that is heated in an internal oven until gaseous. Positively charged Cs^+ ions are formed by the gaseous Cs atoms striking a hot tantalum ioniser (Hellborg and Skog, 2008). In sources which ionise graphite samples Cs^+ ions are focused onto the target resulting in the sputtering of free positively and negatively charged ions. Neutral atoms that are sputtered can accept an electron from gaseous atomic Cs in the source that has not been ionised (Hellborg and Skog, 2008). C^- ions are accelerated away from the source as it is held at a negative potential (ca. - 50 kV), thus forming a negative ion beam (Povinec *et al.*, 2008). The current produced by ^{12}C ions from sputtered samples is dependent on sample size and can vary between 30 and 100 µA (Hellborg and Skog, 2008).

Sources have been developed that ionise gaseous CO_2, thus eliminating the need to prepare graphite. For example Bronk and Hedges (1987; 1989) developed a gas ion source for routine use that included automatic sample loading. In spite of their availability, gas ion sources have not been universally

adopted, and are mainly reserved as means to couple gas chromatographs to AMS and for the analysis of small samples (< 50 µg of carbon) (Suter, 2004). The use of gas ion sources is limited as they produce ion currents which can be a factor of 10 lower than solid graphite sources leading to longer analysis times (Ruff *et al.*, 2007). Gas ion sources operate by pumping a mixture of sample CO_2 (ca. 4%) and helium (ca. 96%) from a sample cracker through a capillary to the source at a steady flow rate, for example between 0.4 to 0.5 µg of carbon per minute (Uhl *et al.*, 2004; Ruff *et al.*, 2007). The source contains a titanium pellet in an aluminium holder which has a small aperture for the sample gas to enter (Ruff *et al.*, 2007). At 1000°C it is thought that the carbon dioxide gas forms solid graphite on the titanium pellet and it is sputtered by Cs^+ gas using the same mechanism as that for conventional graphite targets. It is likely that carbon is sputtered from the titanium pellet as neutral atoms and forms C^- ions by accepting an electron from the electron plasma in the source.

Both graphite and gas source types have limitations, for example graphitisation reactions can introduce contamination to the sample and gas sources provide low ion currents (Santos *et al.*, 2007; Hellborg and Skog, 2008).

1.2.4. Pre acceleration region

The C^- ion beam from the source is focused by a lens stack into the pre acceleration region where it enters an electrostatic analyser. The electrostatic analyser separates ions on the basis of kinetic energy (E) and charge (z): only ions with the correct E/q ratio can be transmitted by the analyser (Povinec *et al.*, 2008). Preceding the injection of ions into the accelerator tubes (high energy systems) or unit (low energy systems) a magnetic analyser separates ions in the beam based on mass, kinetic energy and charge to allow sequential injection of ions of masses 12, 13 and 14 amu (Povinec *et al.*, 2008). The magnetic analyser is pulsed in order to inject a beam of ions of specific momentum into the accelerator tube/unit. This is achieved by altering the current in the magnet (Barker and Garner, 1999). Sequential injection is achieved by applying a voltage to the magnet, altering the kinetic energy of each of the three target isotopes in the ion beam to enable separate acceleration of ^{14}C and each of the stable isotopes of carbon (Fifield, 1999). The injection time depends on the abundance of the isotope and the amount of sample graphite or CO_2. Times of

0.4 ms for $^{12}C^-$, 1 ms for $^{13}C^-$ and 100 ms for $^{14}C^-$ have been reported (Matsuzaki *et al.*, 2007). Abundant isotopes can generate high currents (up to 100 μA which can lead to saturation) for this reason millisecond injection times are used to avoid short circuiting the accelerator (Fifield, 1999). High transmission efficiency of ions is ensured because the magnet narrowly focuses the beam, resulting in a good optical fit into the tube (Hellborg and Skog, 2008).

1.2.5. Tandem accelerator tube

In high energy systems the accelerator tube comprises an outer pressure tank filled with sulfur hexafluoride (SF_6) gas at a pressure of 8 Bar. The gas acts to insulate the inner tube from sparks created by dust and moisture (Gottdang *et al.*, 2002). The inner accelerator tube is held under ultra high vacuum with ground potential at both ends (Barker and Garner, 1999). The first tandem accelerator tubes used in AMS were van de Graff tubes that had maximum terminal voltages (V_T) of 7 and 8 MV (Bennett *et al.*, 1977; Nelson *et al.*, 1977). Modern purpose built accelerator tubes have V_T of 1 to 5 MV, which is adequate for radiocarbon analysis, and additionally benefit from lower operational costs than high V_T accelerators. Low energy AMS instruments (V_T = 200 kV) do not have pressure tanks with SF_6 insulating gas, but have a vacuum insulated high voltage terminal which is supplied by a commercial source (Synal *et al.*, 2004).

The injected C^- ions are accelerated to the high voltage terminal in the middle of the tube/unit. The high energy acceleration of the ion beam maintains the beam focus, avoiding ion losses from collisions with the walls of the tube and enabling ions to be of sufficient energy for electrons to be removed in the electron stripper. The ion beam may also contain adduct ions (for example, $^{12}CH_2^-$ and $^{13}CH^-$) which are formed in the source from sputtered elemental carbon ions and atmospheric hydrogen (McNichol and Aluwihare, 2007). These adducts are able to pass through previous analysis steps undetected and can only be destroyed in the electron stripper.

1.2.6. Electron stripper

The electron stripper in both high energy and low energy systems typically comprises a canal filled with argon gas located at the high voltage terminal in

acceleration tube or unit. The diameter of the canal is 8 to 10 mm and represents the smallest constriction in the accelerator tube (Tikkanen *et al.*, 2004). The number of electrons removed from a specific ion depends upon its velocity when colliding with stripper gas atoms (Barker and Garner, 1999). The most common charge in high energy systems is C^{4+}, though between 2 and 5 electrons can be lost (Vogel *et al.*, 1995). Electron stripping in low energy systems produces C^{+} ions due to the lower terminal voltage of the accelerator unit (Synal *et al.*, 2004). The electron stripper enables contaminant adduct ions that had passed through previous analysis steps to be dissociated and removed from the ion beam (McNichol and Aluwihare, 2007).

1.2.7. Tandem accelerator tube and magnetic analysers

The positively charged ion beam generated in the electron stripper is repelled by the positive V_T at the electron stripper canal and is directed into the second part of the tandem accelerator tube/unit. The tube is maintained at high energy, causing the ion beam to be attracted to the ground potential applied at the exit aperture (Hellborg and Skog, 2008). After leaving the accelerator tube/unit the beam encounters a lens which focuses the trajectory of the ion beam into an analysing magnet to remove any residual contamination (Fifield, 1999; Synal *et al.*, 2004). It is advantageous for the final analysing magnet to have a large radius (ca. 1 m) and a large exit aperture to allow separate trajectories for ^{12}C, ^{13}C and ^{14}C ion beams to be maintained (Tikkanen *et al.*, 2004). The distance between the isotope beams allows detection of ^{12}C and ^{13}C in Faraday cups that are situated away from the ^{14}C beam trajectory (Synal *et al.*, 2004; Tikkanen *et al.*, 2004). Separate detection of stable isotopes is necessary as they create background noise that hinders the detection of radiocarbon (Calcagnile *et al.*, 2004; Tikkanen *et al.*, 2004).

1.2.8. Electrostatic analysers

The isolated radiocarbon ion beam passes through an electrostatic analyser to remove any remaining contaminant ions that were transmitted by the magnetic analyser and which have the incorrect energy to charge ratios to be radiocarbon (Elmore and Phillips, 1987). After this final separation ^{14}C is detected.

1.2.9. Common Detectors for Radiocarbon

Silicon surface barrier detectors comprising semi conductor p–n junctions (Pell, 1960) can be used to detect radiocarbon. Lithium ions (Li^+) act as electron acceptors and create holes within a p–type silicon barrier. The use of two surface barriers creates an instrument with a limit of detection (LOD) low enough to discern ^{14}C, and was first reported as a detector for AMS by Nelson *et al.* (1977). The first barrier gives information on ionisation energy as the positively charged radiocarbon ions accept electrons from silicon (Nelson *et al.*, 1977). The addition of the signals from barrier one and two gives total energy of the ions and the total number of ions detected can be found by plotting ionisation energy against total energy (Nelson *et al.*, 1977). A limitation of the detector is that radiation from ^{14}C decaying to ^{14}N and high intensity beams can cause damage to the silicon semiconductor (Hellborg and Skog, 2008).

The use of a gas ionisation chamber detector for AMS was reported by Bennett *et al.* (1977). Radiocarbon ions enter the detector by passing through a Mylar (polyester) window of a few µm thickness (Shapira *et al.*, 1975). Modern detectors use silicon nitride (Si_3N_4) windows which were introduced to reduce energy loss and improve resolution (Dobeli *et al.*, 2004; Jull and Burr, 2006). The ions enter a chamber filled with isobutene gas, which reduces their velocity, causing free electrons to be produced. Due to an orthogonal electric field, the free electrons travel towards the upper part of the chamber for detection by an anode whereas ions drift towards the bottom of the detector where they are collected by a cathode (Shapira *et al.*, 1975). The free electrons produce the detection signal (Fifield, 1999) with two positively biased plates providing information on both energy loss and the residual energy of the ions (Shapira *et al.*, 1975).

1.2.10. AMS measurements

During analysis by AMS single ions are detected, thus radiocarbon is measured as a ratio (R) with stable carbon isotopes either $^{14}C/^{12}C$ or $^{14}C/^{13}C$. The ratio of $^{14}C/^{12}C$ is generally used and it must be corrected for isotopic fractionation corresponding to $\delta^{13}C$ of - 25 ‰ which occurs during biosynthesis as plants preferentially up take ^{12}C over heavier isotopes (McNichol and Aluwihare, 2007).

Once corrected the ratio only reflects the decay of radiocarbon (R_{sn}). The corrected ratio is determined from equations 2 and 3 below. From the corrected sample ratio the portion of modern carbon in the sample known as fraction modern (*fm*) can be determined (equation 4). The radiocarbon content ($\Delta^{14}C$) of a sample (‰) is thus determined from its fraction modern, the decay constant for radiocarbon and its date of collection minus radiocarbon year 0 (1950) (McNichol and Aluwihare, 2007), as shown in equation 5. The calendar year 1950 was chosen as radiocarbon year 0 due to atomic weapons testing that occurred in the late 1950's and 1960's. Atomic testing led to a large increase of radiocarbon in the atmosphere as neutrons released from nuclear reactions interacted with atmospheric nitrogen to form ^{14}C and consequently $^{14}CO_2$ which entered the carbon cycle (Currie, 2004). The increased availability of radiocarbon in the carbon cycle gave biomass from this period a much younger radiocarbon age than expected. The radiocarbon age of a sample in years before present (yr $_{BP}$) is determined using the Libby radiocarbon half life of 5568 years with 8033 (activity per gram) as the atmospheric concentration of ^{14}C independent of time (Stuiver and Polach, 1977) and the natural log of the fraction modern of the sample (equation 6).

$$\delta^{13}C = \left[\frac{{}^{13}R_{sample}}{{}^{13}R_{\text{standard}}} - 1 \right] x1000 \qquad 2$$

$$R_{sn} = R_s \left[\frac{1 + 0.001x(-25)}{1 + 0.001x\delta^{13}C_s} \right]^2 \qquad 3$$

$$fm = 0.01(pM) = R_{sn} / R_m \qquad 4$$

$$\Delta^{14}C = 1000\left[fm \exp^{-\lambda(y-1950)} - 1 \right] \qquad 5$$

$$Age = -8033 \ln fm \qquad 6$$

R = ratio, subscript *s* = sample, subscript *n* = normalised, subscript *m* = modern, pM = percent modern, *fm* = fraction modern, $\lambda = 1.201 \times 10^{-4}$ the decay constant for ^{14}C, y = the year the sample was collected or the year of growth.

1.3. Structures and functions of chlorophylls and bacteriochlorophylls

Chlorophyll *a* (chl *a*; structure **1**, Figure 2) is a light-capturing pigment present in all plants, algae and cyanobacteria (Table 1). It comprises four pyrrole rings joined to form an aromatic macrocycle, with a magnesium ion complexed to the pyrrole nitrogens (Scheer, 1991). A five-membered cyclopentanone ring (ring E, see for example chl *a* (**1**)) distinguishes chls from all other biosynthetic tetrapyrroles (Scheer, 1991). A phytyl chain is coupled to $C17^3$ via an ester link. Although most chls are based on a chlorin structure (**2**) (i.e. having a saturated carbon-carbon bond between C17 and C18), chl *c* (**3**) is a porphyrin (**4**) as it contains an unsaturated bond in ring D in place of the saturated C17–C18 bond (Falkowski and Raven, 1997). All photosynthetic bacteria (except cyanobacteria) use bacteriochlorophylls (bchls) during photosynthesis (Table 1). Bchl *a* (structure **5**, Figure 2) biosynthesised by purple sulfur bacteria, is based on a bacteriochlorin (**6**) structure and differs from chl *a* in two places: the former contains a ketone in place of the C3 vinyl group and it has a saturated bond in ring B. Bchls *c*, *d* and *e* (structures **7**, **8** and **9**, Figure 2) are also based on a bacteriochlorin structure are biosynthesised by green sulfur bacteria. These compounds have a secondary alcohol at C3 in place of the ketone in bchl *a* and bchl *e* has an aldehyde group at C7 in place of the methyl group of bchl *a*, *c* and *d*. Bchls *c* and *e* have a methyl group at C20 that is not present in bchls *a* and *d*. Bchls *c*, *d* and *e* have other possible peripheral configurations at C8 (R1 = Me, Et, *n*-Pr, *i*-Bu, *neo*-Pent (bchl *d* only)) and C12 (R2 = Me, Et).

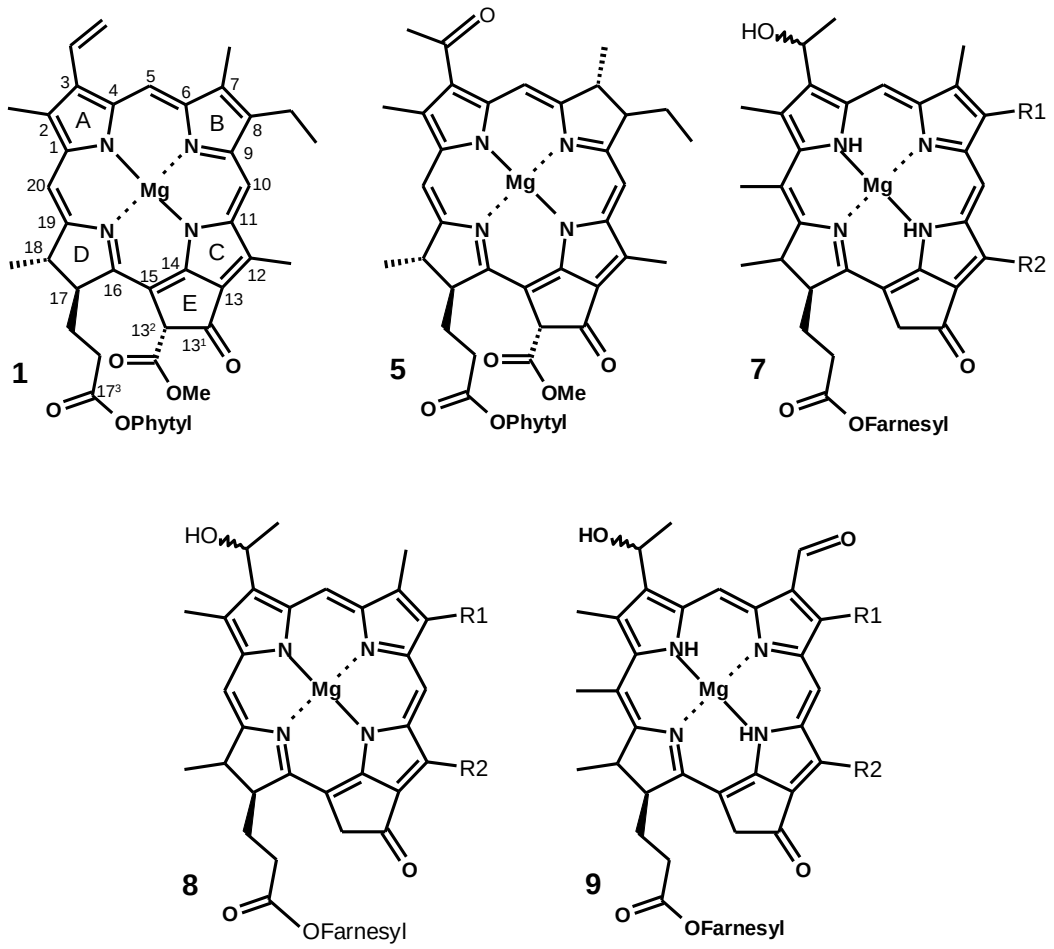

Figure 2. Molecular structures of chl *a* (**1**), bchl *a* (**5**), bchl *c* (**7**), bchl *d* (**8**) and bchl *e* (**9**), R1 = Me, Et, *n*-Pr, *i*-Bu, *neo*-Pent (bchl *d* only) and R2 = Me, Et.

During the oxygenic photosynthesis, performed by eukaryotes and cyanophyta, chls are used in the conversion of inorganic carbon (CO_2) into organic products (for example sugars) to enable growth, reproduction and to provide stores of energy (Table 1) (Foyer, 1984). The process occurs by the following reaction where water is split into its component parts:

$$6CO_2 + 6H_2O \xrightarrow{\text{sunlight}} C_6H_{12}O_6 + 6O_2.$$

Oxygen is toxic to all but one form of photosynthetic bacteria (Table 1), therefore prokaryotes cannot use H_2O as an electron donor to synthesise sugars. Thus, both green and purple sulfur bacteria photosynthesise using hydrogen sulfide (H_2S) as an electron donor (Hall and Rao, 1999) by following the reaction:

$$12H_2S + 6CO_2 \xrightarrow{\text{sunlight}} C_6H_{12}O_6 + 6H_2O + 12S^o$$

Table 1. Occurrences of pigments and type of photosynthesis used by primary producers (modified from Scheer (1991)).

Pigment	Occurrence	Photosynthesis
Chl *a*	All oxygenic photoautotrophs	Aerobic
Chl *b* (**10**)	Green plants and algae	Aerobic
Chls *c*	Brown algae, Dinoflagellates, diatoms	Aerobic
Bchl *a*	Photosynthetic bacteria (mainly purple sulfur bacteria)	Anaerobic
Bchl *c*, *d*, *e*	Green sulfur bacteria (for example chlorobiaceae)	Anaerobic

1.4. Transformation reactions of chlorophylls

In lacustrine environments the majority of chlorophyll in micro algal remains and heterotrophic faecal clusters is destroyed by photo-oxidative processes within days (Carpenter *et al.*, 1986). These processes are associated with cellular decomposition that takes place during senescence. Photo–oxidation reactions (termed type II reactions) destroy the tetrapyrrole macrocycle to form linear chains followed by degradation to monopyrrole maleimides (see reviews, Hendry *et al.*, 1987; Keely, 2006). Degradation is limited once chlorophylls and their derivatives are incorporated into sediments as they are protected from light. The degradation rate is further decreased if anoxic conditions prevail in the bottom waters (Hurley and Armstrong, 1990). Type II photo-oxidation reactions occur in

well lit oxic environments, whereas type I reactions involve enzymatic breakdown, which preserve the macrocycle, can occur in both oxic and anoxic environments.

1.4.1. Type I degradation reactions of chlorophylls

Type I reactions involve the peripheral side groups of the macrocycle and can occur in the water column and surface sediments. These reactions are generally caused by enzymatic action, for example, chlorophyllase causes the loss of the $C17^3$ phytyl esterifying alcohol (**11**) from chl *a* to form chlorophyllide *a* (**12**) and Mg dechelatase removes the central magnesium atom to form phaeophytin *a* (**13**) and phaeophorbide *a* (**14**) derivatives (Matile *et al.*, 1996; Matile *et al.*, 1999). Pyro-derivatives, for example pyrochlorophyll *a* (**15**) and pyrophaeophytin *a* (**16**), are formed by decarbomethoxylation reactions of the substituent group at $C13^2$. The reaction steps described form essential parts of the Treibs scheme linking chlorophyll precursors to fossil alkyl porphyrins found in ancient sediments and oils. The scheme, introduced by Alfred Treibs in the 1930's, has been modified by subsequent researchers (see for example Keely, 2006 and references cited therein). Common water column and surface sediment reactions are shown in Figure 3.

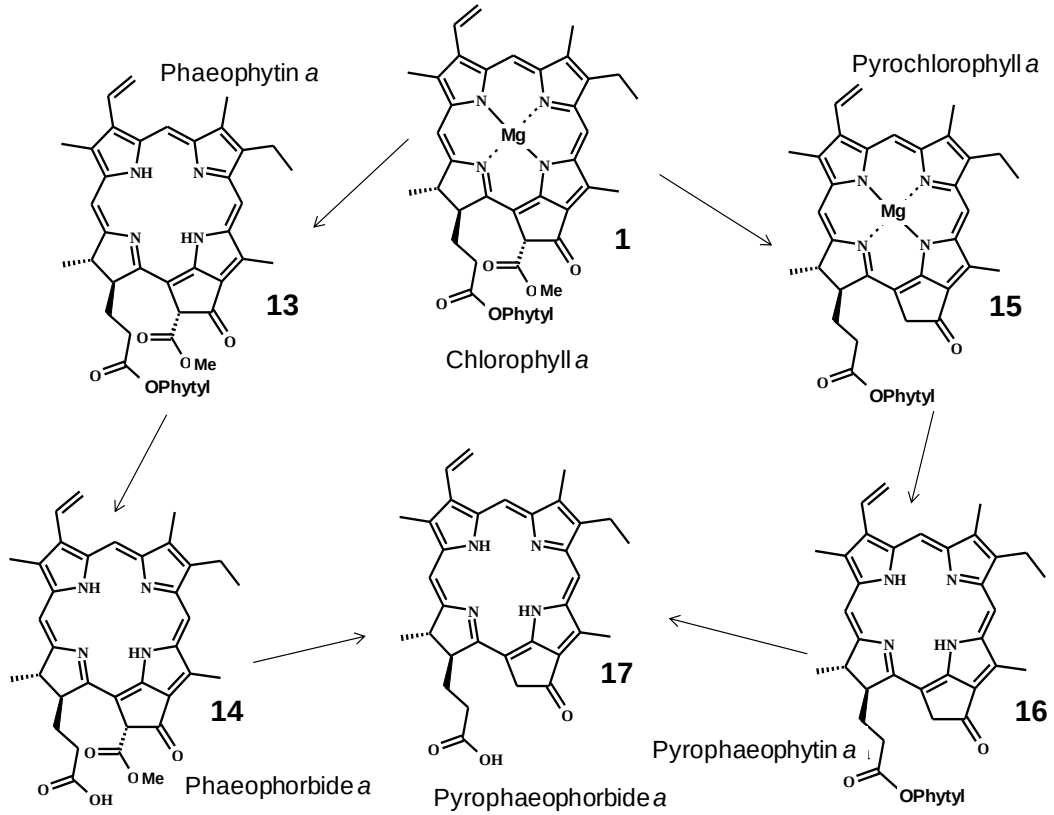

Figure 3. Transformation reactions of chlorophyll (formulated for chl *a*) which are known to occur during algal senescence and/or in aquatic sediments.

1.4.2. Pigments in aquatic environments and sediments

Most aquatic systems support communities of photoautotrophic organisms. The most widespread of these, eukaryotes (for example algae) and cyanophyta (a distinct phylum of bacteria) are mainly oxygenic photoautotrophs (see Table 1). In highly productive aquatic environments, the oxygenic photoautotrophic community is often accompanied by an underlying community of anoxygenic photoautotrophic prokaryotes, for example green and purple sulfur bacteria (see Table 1). Systems with abundant oxygenic primary production can also support heterotrophs, for example zooplankton which do not photosynthesise but graze on photoautotrophs for their energy requirements. Sedimentary pigment signatures can be used both to identify precursor photoautotrophs and assign certain conditions within the system at the time of sedimentation. For example, phaeophytin *a* and pyrophaeophytin *a* are often identified in sediments and are indicative of the presence of algae (Airs *et al.*, 2001; Itoh *et al.*, 2003). The

identification of oxidised chlorophyll derivatives such as hydroxyphaeophytin *a* suggests that sediments were oxygenated at the time of deposition (Walker *et al.*, 2002).

Sedimentary pigments can be used to identify periods of stratification within lacustrine environments. In temperate regions lakes and ponds generally have two periods of mixing: spring and autumn, during which complete overturn of the water occurs (Killops and Killops, 2005). During summer and winter the waters in these dimictic systems tend to be static, allowing the formation of distinct stratified layers. In summer thermal stratification can occur during which the upper layer, consisting of warm oxygenated water, is separated from the cold and oxygen-depleted bottom layer by a narrow transition zone known as the thermocline (Killops and Killops, 2005). Oxidative degradation reactions of organic matter further limit the presence of oxygen in bottom waters (Baird, 1995), leading to the development of anoxic conditions in which bacterial communities can develop. Another cause of summer stratification is high primary productivity within the water column, for example during the development of algal blooms. The presence of high levels of photosynthetic cells in the upper portion of the water column restricts the full spectrum of light from reaching lower depths (Killops and Killops, 2005), thus limiting photosynthesis to photoautotrophs such as purple sulfur bacteria which can utilise low level and wavelength-restricted light. Thus, the detection of sedimentary bacteriochlorophylls (for example bchls *a*, *c*, *d* or *e* or their derivatives) provides evidence of the occurrence of photic zone anoxia and stratification of the water column during the growth of their source organism (Squier *et al.*, 2002). Modifications of the C8 and C12 substituent groups during biosynthesis of bacteriochlorophylls *c*, *d* and *e* are dependent on conditions within the water column (Bobe *et al.*, 1990; Borrego *et al.*, 1997). Greater alkylation at C8 and C12 allows the organism to utilise longer wavelengths of light (red shifted) (Bobe *et al.*, 1990), thus the identification of these homologues in sediments reveals that light was restricted in the lake at the time of the source organisms' growth (Wilson *et al.*, 2004). Light restriction can also be identified through changes in production of bchl *c* versus bchl *d* over time. As bchl *c* absorbs longer wavelengths of light than bchl *d*, a shift in production to bchl *c* can occur as light becomes restricted (Bobe *et al.*, 1990), this occurrence has been identified in an Antarctic lake sediment by Wilson (2004).

Sedimentary pigments can be used to indicate the existence of populations of heterotrophs which graze the algal community, for example steryl chlorin esters (SCEs) of pyrophaeophorbides, which are formed in the gut of zooplankton, can be used to infer grazing of algal biomass (Harradine *et al.*, 1996). SCEs identified in sediment can reflect the sterol compositions of the grazed photoautotroph, which form SCEs with sterol carbon numbers of C_{28} and C_{29} (Harradine *et al.*, 1996). Dietary sterols of zooplankton, originating from algae, can be metabolised to form cholesterol and esterified to pyrophaeophorbide to form SCEs, thus dominance of C_{27} sterol-containing SCEs (Figure 4) indicates that zooplankton are not receiving enough cholesterol through their diet (Talbot *et al.*, 1999). SCEs may reflect more accurately the sterol composition of source organisms than free sterols which are degraded more readily in sediment (Pearce *et al.*, 1998; Talbot *et al.*, 1999). 4–methyl sterols from dinoflagallates (a type of zooplankton) are an exception as they have been found in higher abundance as free sterols than bound as SCEs in both marine and lacustrine sediments (Pearce *et al.*, 1998), thus SCEs may not be used to constrain population estimates. If analysis of sedimentary pigments reveals the occurrence of SCEs, and hence the presence of zooplankton, this provides evidence that the system was productive and supported organisms of a higher trophic level than primary producers.

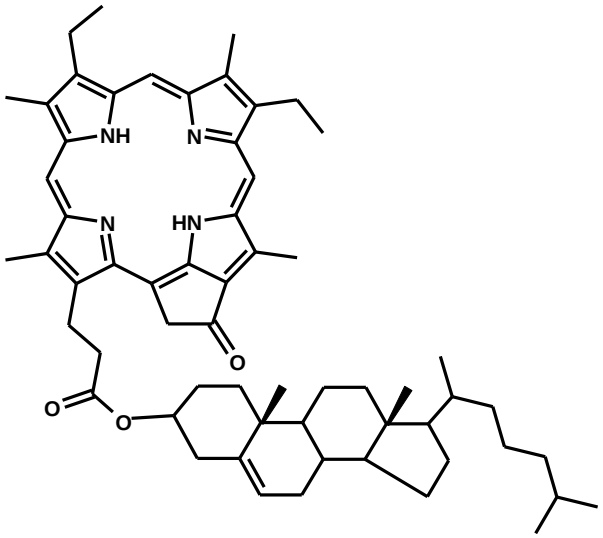

Figure 4. Structure of pyrophaeophorbide *a* C_{27} sterol chlorin ester (**18**).

1.5. Compound specific radiocarbon analysis

Compound specific radiocarbon analysis (CSRA) targets individual chemical compounds to establish the ages of environmental samples. The technique avoids the use of bulk samples which may be contaminated with carbon from multiple sources, both allochthonous and autochthonous, which can compromise the determination of radiocarbon age (Eglinton *et al.*, 1996; Ingalls *et al.*, 2010). An important factor when considering the suitability of a compound for CSRA is its fundamental source organism. Previously reported targets for radiocarbon analysis have suffered from limitations resulting from multiple biological sources or undefined origins of the carbon. For example, fatty acids (FA) have previously been isolated from Ross sea sediments for radiocarbon analysis (Ohkouchi *et al.*, 2003). FA however, suffer from the limitation that they are biosynthesised by both heterotrophs and photoautotrophs. The carbon supply for heterotrophs originates from grazing and possible sources include: photoautotrophs (both oxygenic and anoxygenic), organic debris and other heterotrophs. Thus, the carbon of FA can be derived from mixed and undefined sources. Similarly, tetraether lipid cores, markers for Archaea, have also been radiocarbon dated (Smittenberg *et al.*, 2002; Shah *et al.*, 2008). Glycerol dibiphytanyl glycerol tetraethers (GDGTs) derived from marine sediments have been targeted for CSRA by Smittenberg *et al.* (2002) and Shah *et al.* (2008). Compounds isolated include GDGT-0 (Figure 5, structure A), which is produced by numerous Archaea, and crenarchaeol which is produced by Thaumarchaeotal (Smittenberg *et al.*, 2002) (Figure 5, structure B).

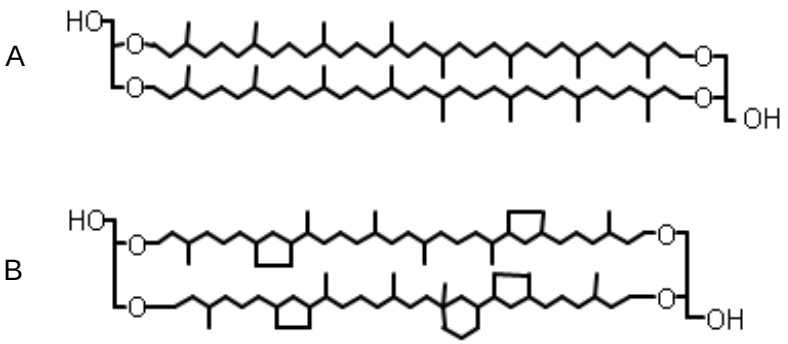

Figure 5. Structures of GDGT-0 (A) and crenarchaeol (B).

Specific archaeal sources for many GDGTs are undefined, and since Archaea include both heterotrophic and autotrophic organisms the origins of the carbon in the lipid cores cannot be known precisely. Archaea tend to have very similar distributions of core lipids, hence the specificity for source organism is low, limiting the information that GDGTs can provide.

1.5.1. Chlorophyll pigments as CSRA targets

Chlorophyll pigments of algae are excellent alternative targets for CSRA of sediments for several reasons. Firstly, they are biosynthesised by oxygenic photoautotrophs which utilise carbon derived mainly from CO_2 sourced from the atmosphere. Thus, chlorophyll pigments reflect the concentration of atmospheric ^{14}C at the time of their formation. Secondly, pigment signatures can be preserved over long periods of geological time, for example in Progress Lake Antarctica phaeophytin *a* was detected in sediments which exceeded the limit of detection for radiocarbon analysis (Hodgson *et al.*, 2006). These sediments were dated by thermoluminescence to > 100 ka BP which corresponds to the last interglacial age (Hodgson *et al.*, 2006). Thirdly terrestrially produced chlorophyll pigments do not influence the lacustrine signal as they are exposed to light and oxygen which promotes degradation. Terrestrial pigments degrade within days of senescence to form colourless compounds which do not retain the tetrapyrrole macrocycle (see review, Hendry *et al.*, 1987). Chlorophyll pigments produced in aquatic environments are protected from light once they are deposited in sediments, thus they are preserved over longer timescales.

During the preparation of this work a study by Kusch *et al.* (2010) was published which described CSRA and stable isotope analysis of chlorophyll *a* and its derivatives phaeophytin *a*, pyrophaeophytin *a* and 13^2,17^3 cyclopheophorbide-*a*-enol (**19**). These measurements were used to determine the date of formation of the pigments and to track their subsequent transport and deposition in Black Sea sediments (Kusch *et al.*, 2010). Sedimentary pigments isolated from three wholly marine influenced sampling sites were determined to be enriched in radiocarbon derived from atomic weapons testing, thus indicating the pigments were modern. Pigments recovered from two sampling points located near the Danube river mouth contained ca. 150‰ less radiocarbon than co-occurring bivalve shells

(Kusch *et al.*, 2010). It was hypothesised that when the Danube delta region flooded radiocarbon depleted terrestrial chlorophyll contained within leaf fragments was washed into the river mouth, thus influencing the signature of recently synthesised marine pigments (Kusch *et al.*, 2010). The study therefore shows that chlorophyll *a* and its derivatives can be utilised for CSRA but also shows that sediments can be contaminated by terrestrial matter.

1.5.2. Radiocarbon reservoir effect

An important consideration when subjecting components in lacustrine or marine sediments to radiocarbon dating is the reservoir effect. A reservoir effect can be caused by one or more event (see, Macdonald *et al.*, 1991 and references there in) for example:

- Stratification of lacustrine environments: CO_2 from the atmosphere dissolves in surface water but does not circulate to the lake bottom (see Chapter 1, Section 1.4.2).

- Microbial decomposition of organic compounds in sediments can release carbon as CO_2. Carbon depleted in ^{14}C contained in the sediment can be liberated in this way and fixed by photoautotrophs during photosynthesis.

- Dissolved bedrock containing calcium carbonate (e.g. limestone or chalk) can leach into aquatic systems releasing radiocarbon dead carbon into the water.

- Glacial bodies can gather ^{14}C depleted organic material during their movement over land, which can be deposited into lacustrine environments when the ice melts.

Organisms which contain ^{14}C depleted carbon provide artificially old radiocarbon ages (Macdonald *et al.*, 1991). As bacterial primary production generally occurs lower in the water column than algal primary production, bchls are more likely to be influenced by radiocarbon dead CO_2. This can be exploited as comparison of

bchl ages determined by AMS with those determined for chls has the potential to reveal the reservoir effect of the system.

Owing to stratification, glacier movement and dissolution of bedrock plants and organisms living within the sediment appear to be older than other contemporaneous oxygenic aquatic and terrestrial organisms due to the uptake of radiocarbon depleted carbon (Madeja and Latowski, 2008). Several approaches have been used to quantify the reservoir effect, for example museum specimens such as shells and animals recovered live with known collection dates have been radiocarbon dated (Zale, 1994). The reservoir effect (R), is determined by comparing the actual calendar date of when a contemporaneous sample died or was collected with the radiocarbon age determined by AMS (Ascough *et al.*, 2005). Dating museum artefacts is only applicable for determining the reservoir effect before the increase of radiocarbon in the atmosphere from atomic weapons testing as the spike in radiocarbon abundance was not immediately recorded in marine environments (Ascough *et al.*, 2005). Thus, terrestrial and marine samples cannot be easily compared. Tephra deposition (ash originating from erupting volcanoes) simultaneously collects over land and water, thus it can be used to determine R, assuming aquatic sediments are not rapidly mixed. Terrestrial and aquatic materials are generally proven to be contemporaneous due to their proximity to the tephra layer, thus R is determined from the difference between the terrestrial and aquatic radiocarbon age (Eiriksson *et al.*, 2000).

In highly productive aquatic environments, the oxygenic photoautotrophic community is often accompanied by an underlying community of anoxygenic photoautotrophic prokaryotes. Owing to their requirement for low or zero oxygen concentrations, bacterial communities are situated in or below the chemocline (the interface between oxygen rich upper waters and anoxic bottom waters), which can vary in its position in the water column. Dissolved gases in the hypolimnion (oxygen poor bottom waters) do not undergo gaseous exchange with the atmosphere, and thus the carbon bacteria use in photosynthesis can be influenced by the reservoir effect. Thus comparison of radiocarbon ages determined for contemporaneous photosynthetic pigments derived from oxygenic

and anoxygenic organisms (for example chlorophyll and bacteriochlorophyll) can determine the reservoir effect.

1.6. Analysis of pigments

1.6.1. High performance liquid chromatography

Photosynthetic pigments extracted from plant leaves were first separated by Twsett in 1906 who pioneered the technique of liquid chromatography using a glass column packed with powdered sugar (Hall and Rao, 1999). Liquid chromatography has evolved into the modern technique of high performance liquid chromatography (HPLC). Modern HPLC columns are commercially packed with silica particles of uniform size, typically between 3 and 5 µm. This type of packing is known a normal phase (NP) stationary phase. Reversed phase (RP) columns are packed with non-polar hydrocarbon chains (typically C18) bonded to silica particles. Both NP and RP columns are capable of separating complex mixtures of components. Solvents used for the elution of analytes are selected based on the type column used. Non-polar solvents (such as hexane) are used for NP columns, and polar solvents (such as methanol and water buffers) are used for RP columns. Generally solvents are pumped through analytical columns at flow rates between 0.5 and 2 mL min^{-1} to separate analytes from sample injections of 10 to 40 µL. Retention of components in RP mode is dependent on hydrophobic interactions between analytes and the stationary phase (Vailaya and Horvath, 1998). There are two hypotheses for this process: the partition model in which analytes transfer from the aqueous phase into the organic phase adjacent to the stationary phase and the adsorption model in which analytes transfer from the mobile phase to absorb onto the surface of the stationary phase (Vailaya and Horvath, 1998). It is likely that in practice a combination of these two hypotheses occurs. Elution of analytes from the column is based on their affinity for the stationary phase, thus in RP mode relatively non-polar analytes are retained more strongly. A constant solvent composition over the chromatographic run, known as isocratic elution, can be used to elute analytes. Another type of elution is gradient elution which uses solvent compositions that change during the course of the run. When using gradient elution in RP-HPLC the solvent composition typically changes from a polar starting composition to a less polar

composition at the end of the run to elute the least polar components from the sample.

RP-HPLC is commonly used for the analysis of chlorophylls as it can be operated over the wide range of polarities needed to separate the complex distributions of photosynthetic pigments which are present in environmental samples. Airs *et al*. (2001) developed an RP-HPLC method with gradient elution to separate samples with up to 64 photosynthetic pigment components extracted from a lake sediment and a microbial mat. A RP-HPLC method to improve the separation of bacteriochlorophyll derivatives extracted from lake sediments was developed by Wilson *et al.* (2003). Good separation of individual pigments is essential to enable their identification, which can be achieved by online photodiode array (PDA) analysis and/or mass spectrometry.

1.6.2. Detection of chlorophylls, bacteriochlorophylls and their derivatives

Owing to their aromatic character, chlorophylls, bacteriochlorophylls and their derivatives can be analysed using liquid chromatography with UV/visible detection (HPLC with PDA detection). Chl *a* does not absorb light throughout the visible region of the electromagnetic spectrum, but predominately in two regions which results in its green colour. Chl *a* has a main absorption band in the blue region of the spectrum at ca. 430 nm known as the Soret band, caused by 3 rapid decays of electrons from an excited energy singlet band to the lowest energy singlet band (Falkowski and Raven, 1997). The second important absorption for chlorins, known as the Q_y band, occurs in the red region of the spectrum at ca.650 nm. Electrons in ring D transition from the $\pi \rightarrow \pi^*$ orbital which results in a redistribution of electrons around the aromatic macrocycle allowing the Q_y absorption (Falkowski and Raven, 1997). Porphyrins have a more symmetrical structure than chlorins due to the unsaturated bond in ring D, which causes the Q_y band to be weak. Although chl *c* is based on a porphyrin structure, it has a weak Q_y band due to the presence of ring E which decreases its symmetry (Falkowski and Raven, 1997). The saturated bond in ring B of bchls alters their absorption spectrometry; they have a maximum absorption band at ca. 770 nm rather than the chl *a* band of 650 nm, so the Soret band of bchls is blue shifted

compared with chlorophylls with a maximum absorption observed at ca. 350 nm (Hendry *et al.*, 1987). Both of these features result in bchl *a* appearing to be weakly coloured (Hendry *et al.*, 1987).

1.6.3. Mass spectrometry

Sir J. J. Thomson was instrumental in developing mass spectrometry, first by discovering the electron and determining its mass to charge ratio in 1897 and then by assembling the first mass spectrometer with which he detected negative and multiply charged ions (de Hoffmann and Stroobant, 2007). A mass spectrometer (MS) separates ions based on mass to charge ratio (*m/z*) and comprises: a sample introduction system, ion source, mass analyser and a detector. Mass spectrometers have been coupled together with other instruments forming hyphenated techniques to provide online separation and detection of samples containing a mixture of components. Gas chromatography (GC) separates analytes in the gas phase and thus GC–MS is a natural coupling as mass spectrometry also requires analytes to be in the gas phase.

1.6.4. Liquid chromatography - mass spectrometry (LC-MS)

HPLC is used to separate relatively polar non-volatile analytes in the liquid phase using both organic and aqueous solvent. The attributes of HPLC provide difficulties for coupling the technique to mass spectrometry. An interface is required to resolve the incompatibilities of the techniques to enable LC-MS. The interface must evaporate eluent solvent, which may contain water and to transfer non–volatile components into the gas phase. Two major types of ion sources have been developed to provide an interface and generate gas phase ions from an HPLC eluent. Briefly, electrospray ionisation (ESI) involves applying a voltage to HPLC eluent to form charged droplets. Gas ions are formed as the solvent evaporates (de Hoffmann and Stroobant, 2007) and coulombic explosions cause the droplet to breakdown. Atmospheric pressure chemical ionisation (APCI) is another source used to couple HPLC and MS.

1.6.5. Atmospheric pressure chemical ionisation (APCI)

APCI is a soft ionisation technique which produces molecular ions and singly charged ions that are either positive or negative depending on its mode of operation (a schematic diagram of the source is shown in Figure 6). It is used for polar analytes (up to maximum molecular masses of 1500 Da) eluting from HPLC at flow rates up to 2 mL min^{-1} (de Hoffmann and Stroobant, 2007). The eluent containing the analytes flows from a capillary into a pneumatic nebuliser where it is converted into a fine mist of droplets by nitrogen sheath gas. The mist passes into a heated chamber to evaporate solvent from the analytes; the sheath gas carries the gaseous analytes past the corona discharge needle which ionises the molecules. In positive ionisation mode the sheath gas is ionised to form positive nitrogen radicals known as primary ions. These primary ions can interact with gaseous solvent molecules to form secondary ions (for example H_3O^+) which can transfer protons to analyte molecules by colliding with them to form protonated molecules $[M + H]^+$.

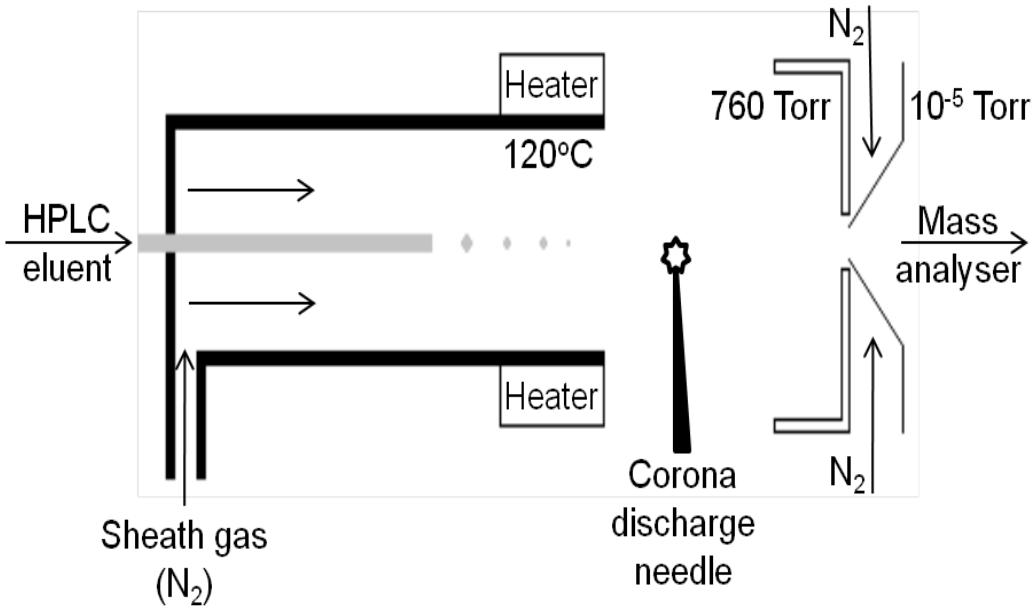

Figure 6. Schematic diagram of an APCI source (modified from de Hoffmann and Stroobant, 2007).

1.6.6. Ion trap mass spectrometry

The quadrupole ion trap was first reported by Paul and Steinwedel (1960) and it was developed for commercial use by Stafford *et al.* (1984). An ion trap

comprises a circular ring electrode, to which an oscillating rf (radiofrequency) potential is applied, and two hyperboloidal end cap electrodes which are held at ground potential (Figure 7). Ions enter the trap through a perforation in the end cap and oscillate in figure of 8 trajectories caused by the application of direct and oscillating voltages which form a quadrupolar field. The frequency of oscillations is known as the ion secular frequency, which is proportional to the frequency of the rf potential of the ring electrode. Helium gas is maintained at a constant pressure (ca. 0.13 Pa) within the trap to remove excess energy from ions (gained from ion-ion repulsions) which would otherwise cause them to strike the walls of the ion trap. Ions are focussed into the centre of the trap by the alternating positive and negative ring electrode rf potential and the grounded end caps. A repulsive rf potential focuses ions into the centre of the trap on the radial axis and it is followed by an attractive potential on the radial axis which destabilises ions towards the walls of the trap. Concurrently, in the axial direction the ion is defocused towards the end cap electrode and then it is focussed towards the end cap. Thus, the alternating potentials focusing and defocusing ions in both axial and radial directions keeps ions stable (Figure 7).

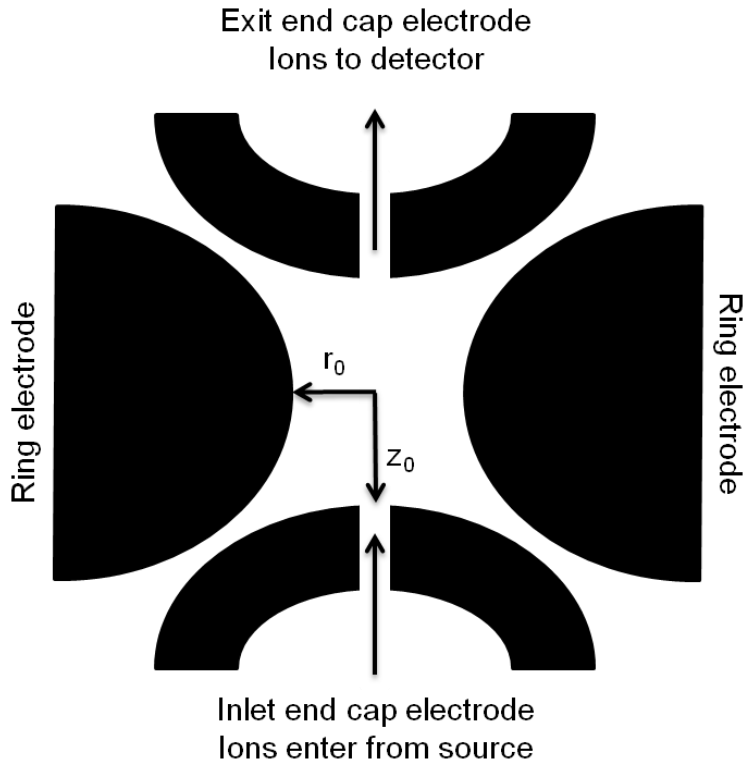

Figure 7. Schematic diagram of a quadrupole ion trap with radial (r_0) and axial (z_0) dimensions of the trap, modified from de Hoffmann and Stroobant (2007).

The Mathieu equations can be used to determine regions of stability for ions in the trap. Motion can occur in three dimensions within the trap but, due to the cylindrical symmetry, radial (r) and axial (z) dimensions can be used. As ions are ejected from the trap through the perforations in the end caps by defocusing in the axial direction, the relevant Mathieu solutions are in the axial (z) direction (equations 6 and 7). From the solutions a diagram showing the regions of stability for ions oscillating in a quadrupolar field can be constructed (Figure 8). During operation, the end cap electrodes are held at ground potential ($a_z = 0$), thus, ions are arranged along the q_z axis (Figure 8) and only vary in their q_z value. Ions which have the highest *m/z* ratios have the lowest q_z values.

$$a_z = \frac{-16zeU}{m(r_0^2 + 2z_0^2)\omega^2} \qquad (6)$$

$$q_z = \frac{8zeV}{m(r_0^2 + 2z_0^2)\omega^2} \qquad (7)$$

a_z and q_z = stability parameters of axial dimension
m and z = mass and charge of the ion
e = elementary charge
U = amplitude of applied DC potential
V = amplitude of the fundamental rf potential
ω = oscillating frequency of the fundamental rf potential
z_0 = half the axial distance between end cap electrodes
r_0 = radius of ring electrode

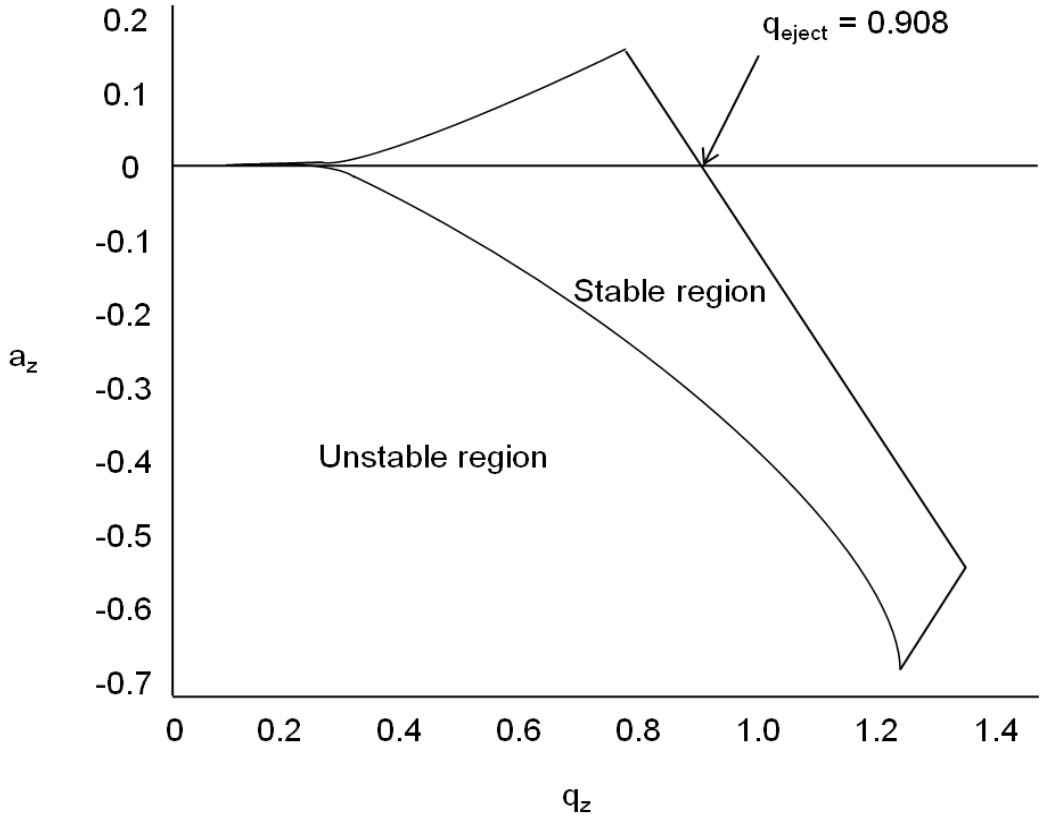

Figure 8. Stability diagram for ions in a quadrupolar field from solutions to the Mathieu equations modified from Stafford *et al.* (1984).

Increasing the amplitude of the fundamental rf potential causes the amplitude of oscillation in the axial direction and q_z value to increase. Ions are ejected from the trap when their amplitude of oscillation in the axial direction reaches q_{eject} which is equal to 0.908 (this value is constant for commercial traps which have the same dimensions). Ions with high *m/z* ratios cannot reach q_{eject} without electrical arcing occurring due to the high rf potential required, thus a small potential with the same oscillating frequency as the target ions secular frequency is applied to the end cap electrodes. This causes the amplitude of the ions' oscillations in the axial direction to increase until it is ejected from the trap, a process known as resonance ejection. Ions can be ejected from the perforations both end caps but only one cap is connected to the detector (typically an electron multiplier) thus half of the ions from the trap are lost.

1.6.7. Tandem and multistage mass spectrometry

Tandem MS (MS/MS) is comprised of four stages: mass analysis, selection and isolation of an ion from the mass analysis (precursor ion), fragmentation of the precursor ion and a second stage of mass analysis of the products from the precursor ion. Triple quadrupole mass spectrometers perform MS/MS in space with one quadrupole acting as the first mass analyser; the second acting as a collision cell inducing fragmentation of the precursor ion and the third acting as the second mass analyser (Figure 9).

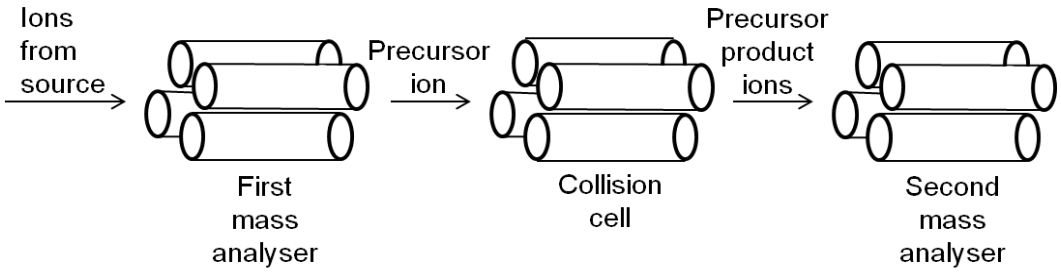

Figure 9. Schematic diagram of a triple quadrupole mass spectrometer modified from de Hoffmann and Stroobant (2007).

Tandem MS in ion trap mass spectrometers has to occur temporally rather than spatially as there is only one ion trap. Firstly, resonance ejection is used to remove all but the precursor ion (or ions) from the tap. Then an oscillating supplementary rf potential is applied to the end cap electrodes with the same frequency as the ion's secular frequency, but with insufficient amplitude to cause ejection of the precursor ion from the trap. The precursor ion gains kinetic energy from the supplementary potential and thus strikes the helium gas which is within the trap. These collisions convert some of the ion's kinetic energy into internal energy, thus causing the precursor ion to fragment, a process termed collision induced dissociation (CID). As the fragment ions do not have the same secular frequency as the precursor ion, they are focussed into stable oscillations and not fragmented further, so they can then be sequentially ejected from the trap to the detector. Ion traps can be used for multistage MS (MS^n) by isolating a product ion in the trap and subjecting it to CID, as described above. This process can be continued until the precursor ion fails to dissociate or the product ions create an insufficient signal in the detector.

APCI LC-MS^n has been used to profile sedimentary photosynthetic pigment in several studies (Airs *et al.*, 2001; Squier *et al.*, 2002; Walker *et al.*, 2002; Airs and Keely, 2003), and Wilson *et al.* (2004; 2005) used MS^6 to identify specific bacterial pigment homologues. The combination of traditional identification methods of pigments by UV/vis or online PDA detection with APCI LC-MS^n provides robust identification of environmental photosynthetic pigments.

1.7. Summary and aims

Sedimentary photosynthetic pigments can originate from aquatic photoautotrophic organisms, thus they are excellent compounds to investigate the history of current or former aquatic systems. Certain chlorophyll and bacteriochlorophyll derivatives can be used as indicators of the environmental conditions within the system at the time of their source organism's growth and specific chlorophyll derivatives can also be used to indicate the presence of organisms of a higher trophic level. The origin of chlorophyll pigments has important consequences when considering their use for radiocarbon dating. As they are derived from oxygenic photoautotrophs, chlorophyll pigments reflect atmospheric concentrations of ^{14}C thus making these compounds suitable candidates for CSRA. Bacteriochlorophylls derived from anoxygenic primary production influenced by radiocarbon dead CO_2 provide a means to explore the reservoir effect by CSRA.

The main aim of the work in this thesis was to use photosynthetic pigments as a means to investigate the past. Accordingly, Chapter 2 focuses on the use of sedimentary pigments as a novel way of confirming the presence of former water features in archaeological sites. Through the identification of pigments the primary producer communities living within the water column can be revealed along with information relating to the productivity and environmental conditions such as stratification and the availability of oxygen. By profiling pigments and their abundance in several layers of sediment the evolution of the water feature through time can revealed. Chapters 3 and 4 are concerned with the use of photosynthetic pigments as targets for CSRA. Chapter 3 proposes an experimental plan for the isolation of individual sedimentary pigments and aims to validate the instrumentation chosen to recover individual pigments. Sedimentary

pigments from Kirisjes Pond, a coastal lake in Antarctica, have previously been intensively profiled (Squier *et al.*, 2002; Wilson *et al.*, 2004; Wilson *et al.*, 2005). Through the identification of specific pigment derivatives it has been established that there was a past incursion of marine water into the pond. Radiocarbon analysis of bulk material has previously been carried out which provided an estimate of the timing of the incursion (Hodgson *et al.*, 2001). Thus, Chapter 4 focuses on the application of CSRA dating methods to constrain the timing of the marine incursion.

Chapter 2. Photosynthetic pigments in archaeological water features

2.1. Background

Water features that serve both functional and aesthetic roles have been created in English gardens for thousands of years (Currie, 1990). During medieval times (ca. 1066 to 1600), ponds were common features in high status properties, for example bishop's estates (Currie, 1990), where they provided an important source of nutrition through fish farming. By the latter half of the eighteenth century, ponds became mainly decorative features as domestic fish production diminished (Currie, 1990; Felus, 2006). The lack of channels to drain water in ponds constructed in the later period provides evidence for the increasing ornamental view of water features, as fish could not be efficiently collected (Currie, 1990). The presence and location of former water features has been recognised through both archive-based and physical approaches. Construction plans, surveys/maps and contemporary magazine articles have been used to determine the positions of ponds and lakes in parks and notable private gardens during restoration works and historical research (Laurie, 1985). In addition, these significant archaeological features have been located using geophysical techniques (Holden *et al.*, 2002).

Organic material, and specifically lipids, found in archaeological remains can provide valuable information regarding its source, thus the use of geochemical methodology is on the increase in the field of archaeology (Evershed, 2008). To determine the primary constituents of bulk organic material in soil samples, CHNS elemental analysis and total organic carbon measurements are generally used (Bull *et al.*, 1999). Elemental analysis can indicate the presence of lipid material if samples have high carbon and hydrogen contents. Gas chromatography (GC) has been used to analyse complex mixtures of lipid components (Evershed, 1993), and comparisons with known standards can be used to identify components from environmental samples in GC chromatograms.

2.1.1. Aims

The aim of this work was to analyse sediments from archaeological sites to construct their pigment profiles, thus confirming or disproving their identification as archaeological water features. Interpretation of the sources of pigment

derivatives present in sedimentary profiles would also be examined to reveal changes in the conditions within the features during the period of their use. Sediment samples were collected from: Beningbrough Hall, North Yorkshire, UK, Hall Garth, Bolton, UK and Cawood Castle, North Yorkshire UK (see section 6.1.3, Chapter 6).

2.2. Results and Discussion

2.2.1. Beningbrough Hall

A 23 cm long sediment core was collected from sampling point B starting at a depth of 41 cm from ground level in an area thought to have been formerly occupied by a fish pond. The sediment was very dry and compacted with a uniform mid brown colour and contained charcoal flecks. The sediment from the putative fish pond had TOC contents between 1.0 and 1.2%, which falls in the range of those typically measured for soils (Bull *et al.*, 1998; Bull *et al.*, 1999). The TOC contents determined were much lower than those reported for a eutrophic lake (average of ca. 10 wt. %) (Woszczyk *et al.*, 2011), thus it may be inferred that sediment from sampling point B could correspond to a water feature that is poor in nutrients (oligotrophic). HPLC analysis did not reveal any photosynthetic pigments or their derivatives; hence no evidence was found that the sediment originated from a former fish pond.

Auger samples were collected from sampling point C which was within a trench-like feature thought to mark an area formerly occupied by a canal. Samples were collected at three depths (Figure 10) (the measurement recorded denotes the maximum depth of the sample). TOC contents of sediment from sampling point C increase from 1.0% at the greatest depth, to 2.3% at the shallowest depth (Figure 10). The latter is consistent with a water body that has sufficient nutrients to support life but not to sustain high levels of primary production (mesotrophic) as samples with generally greater than 5 wt. % TOC content were reported for a eutrophic lake (Woszczyk *et al.*, 2011). The TOC contents show a noticeable increase as the depth decreased (Figure 10), which could relate to increased photoautotrophic productivity in the canal over time.

Photosynthetic pigments were identified in the uppermost (144 cm depth) and middle (168 cm depth) samples from their online UV/vis and LC-MS^n spectra. Pigment distributions were very similar at both depths and comprised chl *a* derivatives: phaeophytin *a* and pyrophaeophytin *a,* and the chl *b* derivative, pyrophaeophytin *b* (peaks 20, 23 and 21, respectively, for example, Figure 11). Chl *a* and *b* derivatives can be easily identified by online PDA detection, for example pyrophaeophytin *b* (**20**) which has absorption maxima at 438 and 649 nm and pyrophaeophytin *a* which has absorption maxima at 410 and 666 nm. The online UV/vis spectra and structures of both compounds are shown in Figure 12. All of the components identified in the HPLC chromatogram of the sample from 144 cm depth are listed in Table 2. The presence of chl *a* and *b* derivatives must be attributed to aquatic photosynthetic communities within the canal, as chlorophyll pigments originating from terrestrial organic matter degrade within weeks in senescent leaves and thus do not accumulate in soils (see review, Hendry *et al.*, 1987). LC-MS^n analysis of the extract from 144 cm depth revealed the presence of hydroxyphaeophytin *a* (**21**), an oxidative transformation product of chl *a*, which indicates oxygenated conditions in the water feature (Walker *et al.*, 2002). HPLC analysis revealed the presence of pyrophaeophorbide *a* sterol ester (peak 25, Figure 11), and LC-MS^n enabled the esterifying sterol to be identified as having carbon numbers of $C_{29.}$ Furthermore the sensitivity of MS allowed the identification of SCEs containing sterols with carbon numbers of C_{27} that were could not be observed in the PDA chromatogram. For example, the C_{29} steryl ester of pyrophaeophorbide *a* was identified at 144 cm depth. C_{29} sterols are endogenous components of selected algal primary producers and are also found in terrestrial plants (Volkman *et al.*, 1999). SCEs containing sterols with carbon numbers of C_{27}, native to zooplankton (Talbot *et al.*, 1999), were also identified at 144 cm depth, thus providing further evidence of the aquatic nature of the sampling site.

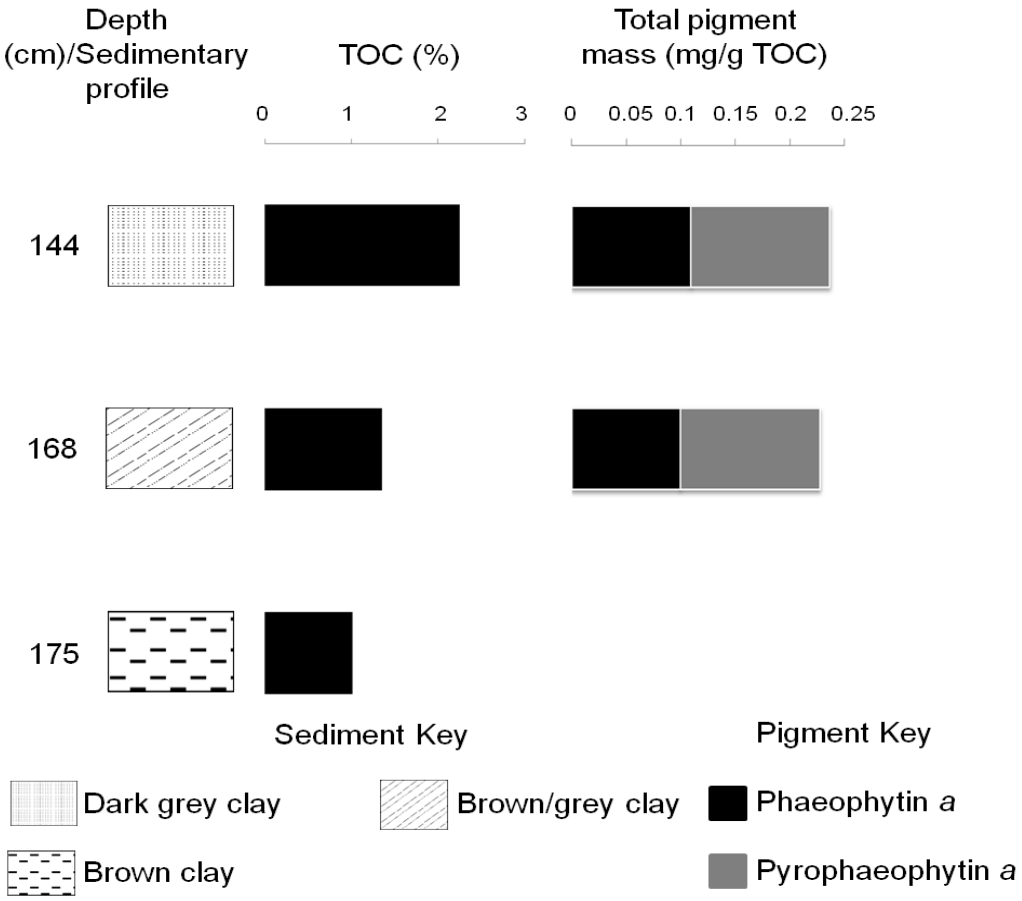

Figure 10. Beningbrough Hall sampling point C sedimentary profile, TOC contents and total pigment masses (depth denotes maximum depth collected).

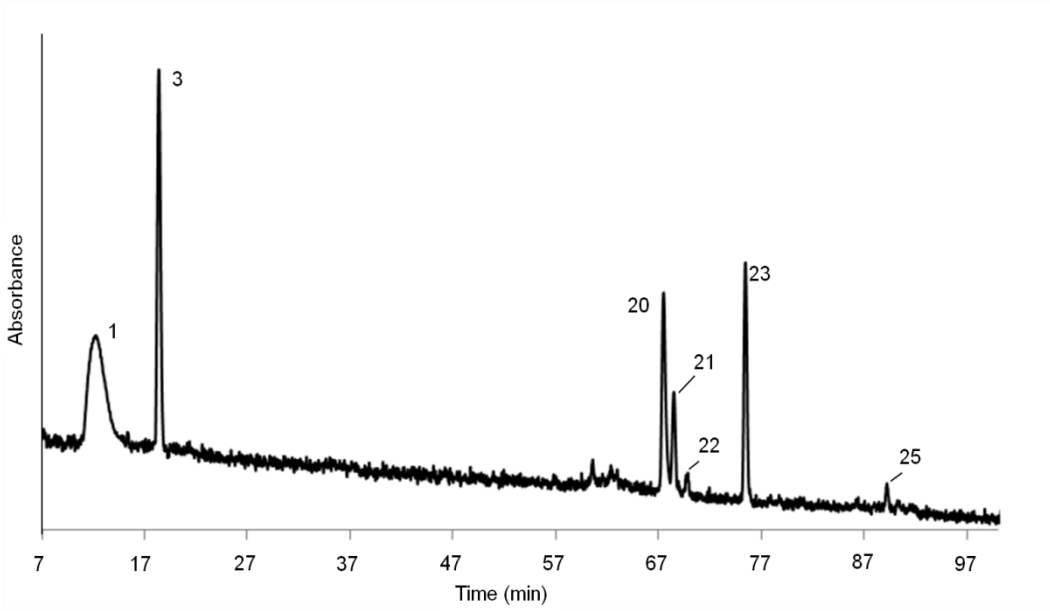

Figure 11. Partial RP-HPLC-UV/vis chromatogram (350-800nm) of Beningbrough Hall sampling point C, 144 cm depth.

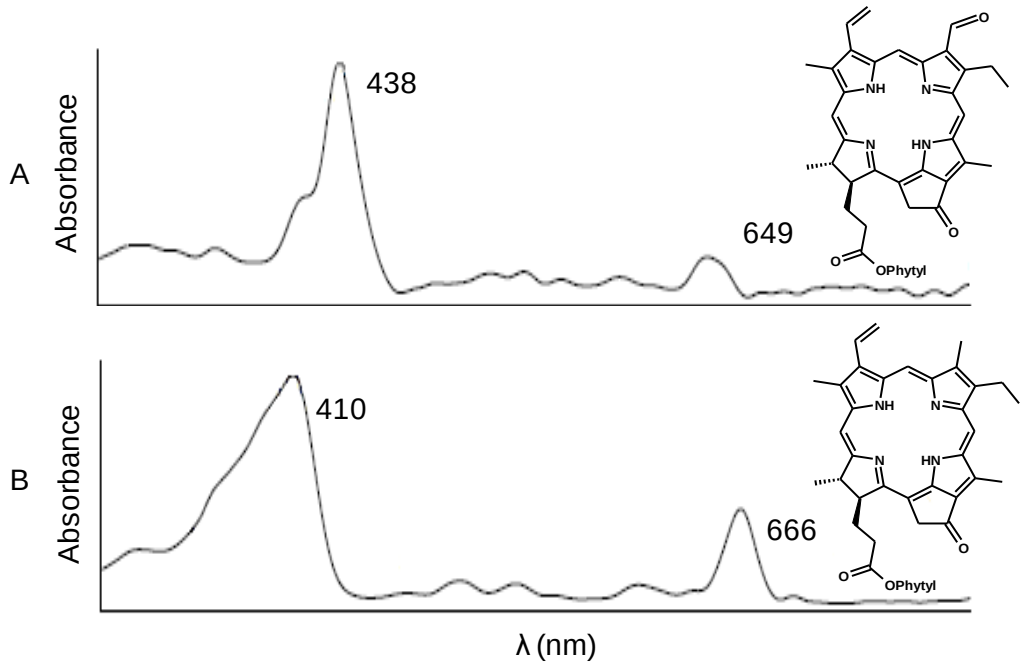

Figure 12. Online UV/vis spectrum (350 to 800 nm) and structures of pyrophaeophytin *b* (A) and pyrophaeophytin *a* (B).

Table 2. Identification of peaks detected during HPLC analysis of Beningbrough Hall, Cawood Castle and Hall Garth sampling points (peak identifications made with reference to Airs *et al.*, 2001).

Peak	Retention Time (min)	Main UV/vis absorption bands (nm)	$[M+H]^+$ (*m/z*)	Assignment
1	9.7	450, 470		Carotenoid
2	10.8			Unidentified
3	19.5			Unknown
4	36.9	447		Carotenoid
5	37.5	446, 473		Unidentified
6	47.2	432, 665	871	Chl *a*
7	53.3	413, 452, 467		Unidentified
8	55.2	410, 660	777	Bacteriophaeophytin *c* hexahydrofarnesol ester
9	57.2	357, 526, 745	889	Bacteriophaeophytin *a*
10	60.3	436, 657		Unidentified
11	60.6	356, 525, 741	889	Bacteriophaeophytin *a* epimer
12	61.7	436, 649	885	Phaeophytin *b*
13	63.3	409, 660	819	Bacteriophaeophytin *c* C17 ester
14	63.5	408, 673		Unidentified
15	64.2	426, 658		Unidentified
16	64.8	407, 667	887	Hydroxyphaeophytin *a*
17	65.1	413, 651		Unidentified
18	65.8	357, 525, 653, 751	831	Pyrobacteriophaeophytin *a*
19	67.1	414, 678		Unidentified
20	68.8	408, 665	871	Phaeophytin *a*
21	70.3	438, 649	827	Pyrophaeophytin *b*
22	71.1	408, 670	871	Phaeophytin *a* epimer
23	77.4	410, 666	813	Pyrophaeophytin *a*
24	87.9	410, 669	901	Pyrophaeophorbide *a* sterol ester
25	89.2	410, 669	915	Pyrophaeophorbide *a* sterol ester
26	90.3	411, 668	903	Pyrophaeophorbide *a* sterol ester
27	91.3	411, 670	917	Pyrophaeophorbide *a* sterol ester
28	92.0	409, 665	931	Pyrophaeophorbide *a* sterol ester
29	94.2	406, 668	919	Pyrophaeophorbide *a* sterol ester

The most abundant derivatives identified by HPLC were normalised to TOC to determine the comparability in pigment contents between the two samples (Figure 10). The mass of pigment in both sample layers was comparable (Figure 10) suggesting that productivity was stable during the time period covered by the sediments examined.

Sediments were collected by an auger from a second sampling point within the trench-like feature thought to mark an area formerly occupied by a canal (sampling point E). Samples were collected at seven depths (Figure 14) and the measurement recorded denotes the maximum depth of the sample. The TOC at

sampling point E increased from 0.5% at 162 cm depth to 1.9 % TOC at 157 cm depth and remained of similar magnitude in the remaining sections (Figure 14). As for sampling point C the higher TOC values are consistent with a mesotrophic aquatic system. The TOC content at 162 cm depth, 0.5 %, is likely to correspond to a period where little primary productivity occurred. Photosynthetic pigments were identified at all but the lowest and highest depths (Figure 14). Phaeophytin *a* occurred in all pigment-containing samples and pyrophaeophytin *a* was present at all depths except 157 cm. The most abundant compound at 120, 142 and 157 cm depth was phaeophytin *a*, whereas similar proportions of phaeophytin *a* and pyrophaeophytin *a* were identified at 133 (Figure 15) and 154 cm depth (all of the components revealed in the HPLC chromatogram of 133 cm depth are listed in Table 2). Phaeophytin *a* can be formed both by enzymatic degradation during algal senescence and by zooplankton herbivory (Owens and Falkowski, 1982). Pyrophaeophytin *a* is also formed by enzymatic degradation (Schoch *et al.*, 1981). Thus, because pyrophaeophytin *a* levels are lower, it appears that zooplankton had a greater influence on pigment degradation at 120, 142, and 157 cm depth than enzymatic degradation. The chl *a* derivatives detected provide evidence of algal communities that lived in the water feature at the time of sediment deposition. Sediment from 133, 142 and 154 cm depth revealed the greatest abundance of total pigments (Figure 14) suggesting these layers correspond to the most productive period within the canal. The carotenoids alloxanthin (**22**) and monadoxanthin (**23**), both derived from cryptophyta (Jeffrey *et al.*, 1996; Itoh *et al.*, 2003) a type of algae, were identified at 142 cm depth. The sediment from 133 cm depth (Figure 15) contained a series of pyrophaeophorbide *a* steryl ester derivatives. The sterol carbon numbers were identified by LC-MS^n to comprise C_{27}, native to zooplankton (Figure 13) and C_{28}, and C_{29} native to algae (Talbot *et al.*, 1999; Soma *et al.*, 2005).

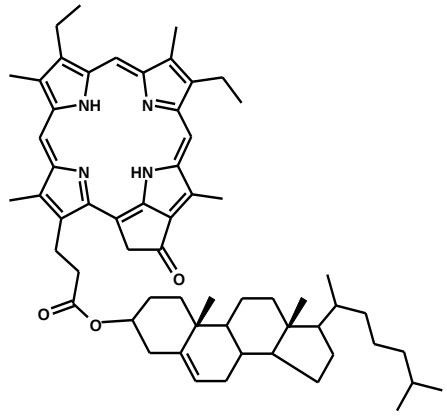

Figure 13. Structure of pyrophaeophorbide *a* C_{27} sterol chlorin ester.

SCEs containing C_{28} sterols are more specific to algae than C_{29} SCEs, as C_{29} sterols are common in higher plants, and therefore provide good evidence that the sediment was derived from an aquatic environment (Volkman *et al.*, 1998). The identification of SCEs at sampling point E reveals that the canal was a productive environment which supported both primary producers and zooplankton.

Thus, due to the identification of chl pigment derivatives associated with algal primary production and derivatives that imply the presence of zooplankton, it can be concluded that the sediment collected from sampling points C and E were deposited in a water feature, interpreted from its lateral continuity to represent a canal.

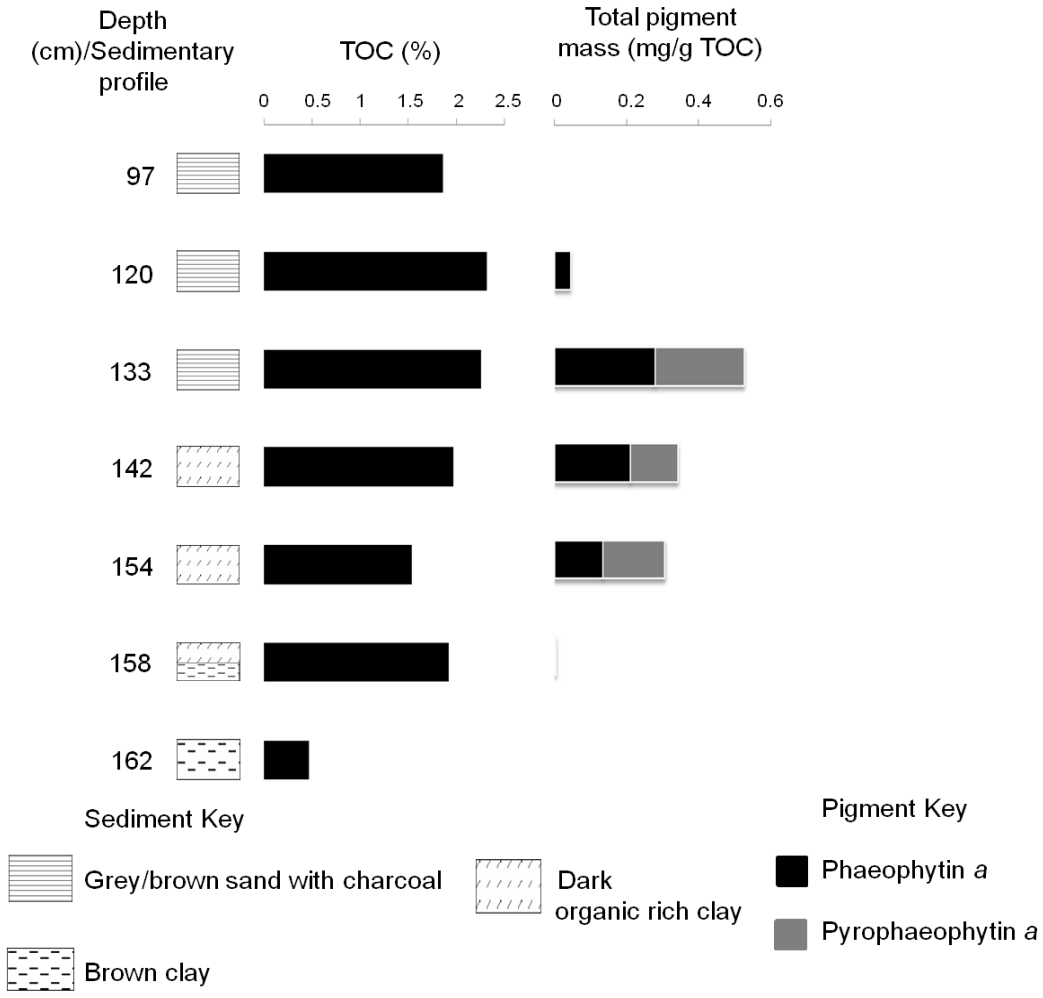

Figure 14. Beningbrough Hall sampling point E sedimentary profile, TOC contents and total pigment masses.

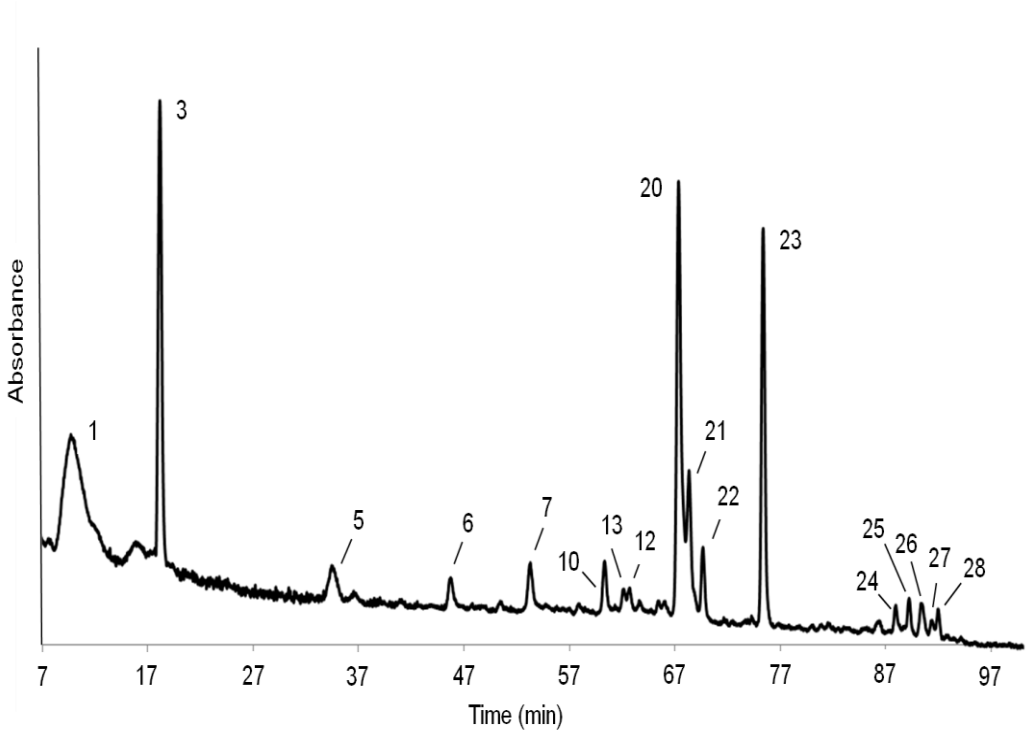

Figure 15. Partial RP-HPLC-UV/vis chromatogram (350-800nm) of Beningbrough Hall sampling point E, 133 cm depth.

2.2.2. Hall Garth

A 25 cm long sediment core was collected from a depth of 17 cm within the area previously designated as a fish pond (sampling point C); the sediment was uniform sandy silt. The sediment sampling point C had TOC contents that were variable (between 0.9 and 3.6%). Sample depths with TOC contents between ca. 1 to 2% could correspond to sediment originating from a mesotrophic environment, except 29 cm depth which had the highest TOC content (3.6%) and 33 cm depth which had the lowest (0.9%). HPLC-PDA analysis revealed only one sample (28 cm depth) to contain photosynthetic pigments (phaeophytin *a* and pyrophaeophytin *a*) above the limit of detection (LOD). As photosynthetic pigments were only detected in one layer, the TOC values alone do not provide enough evidence to support the hypothesis that the sediment analysed originated from a water feature.

A second 26 cm long sediment core was collected at Hall Garth from a depth of 23 cm from the dried moat area (sampling point E). The sediment was silty with a uniform dark brown/black colour (Figure 16). High TOC contents were detected

throughout sampling point E which displays highly variable abundances with the greatest TOC content (15.2%) at 36 cm depth and the lowest (6.9%) at 37 cm depth (Figure 16). TOC values of this magnitude are similar to those reported by Woszczyk *et al.* (2011) for a eutrophic system, or could result from inputs of exogenous organic matter.

Bacteriophaeophytin *a* (**24**), phaeophytin *a* and pyrophaeophytin *a* were identified in every layer of the sediment core by online UV/vis detection (for example 28 cm depth, Figure 17). All components revealed in the chromatogram are listed in Table 2. Bacteriophaeophytin *a* (Figure 18) has a very distinctive UV/vis spectrum with absorption maxima at 357, 526 and 745, thus allowing it to be easily identified from other components. Algal pigments phaeophytin *a* and pyrophaeophytin *a* were the most abundant components in the core (Figure 16). The deepest layers, 42 to 49 cm depth, contain higher levels of bacteriophaeophytin *a* (derived from purple sulfur bacteria) than the rest of the core, thus anoxic conditions had been established in the moat before it became more oxygenic (Figure 16). Other commonly identified compounds throughout the core were chl *b* derivatives, phaeophytin *b* (**25**) and pyrophaeophytin *b* which are attributable to algae (Figure 17) (Scheer, 1991). The identification of algal pigments provides evidence that photoautotrophic communities were present throughout the period of sediment deposition represented by the core and that the structure was indeed a moat. The highest pigment contents, and hence highest levels of productivity, correspond to 26 and 31 cm depth (Figure 16). The lowest levels of pigment were identified in moat samples loose top core sediment (LTS) and at 43 and 48 cm depth (Figure 16) indicating periods of lower productivity.

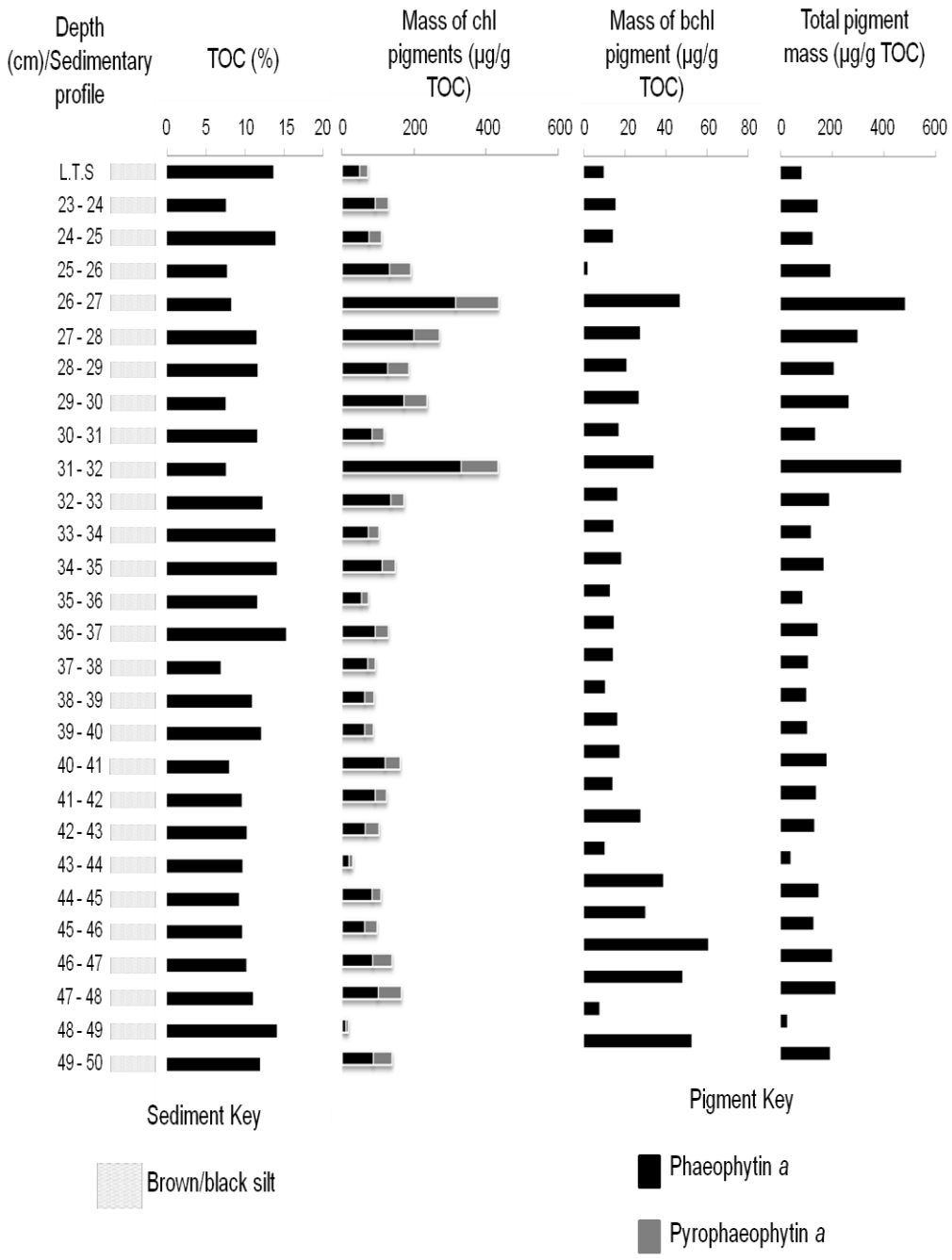

Figure 16. Hall Garth sampling point E sedimentary profile, TOC contents and total pigment masses.

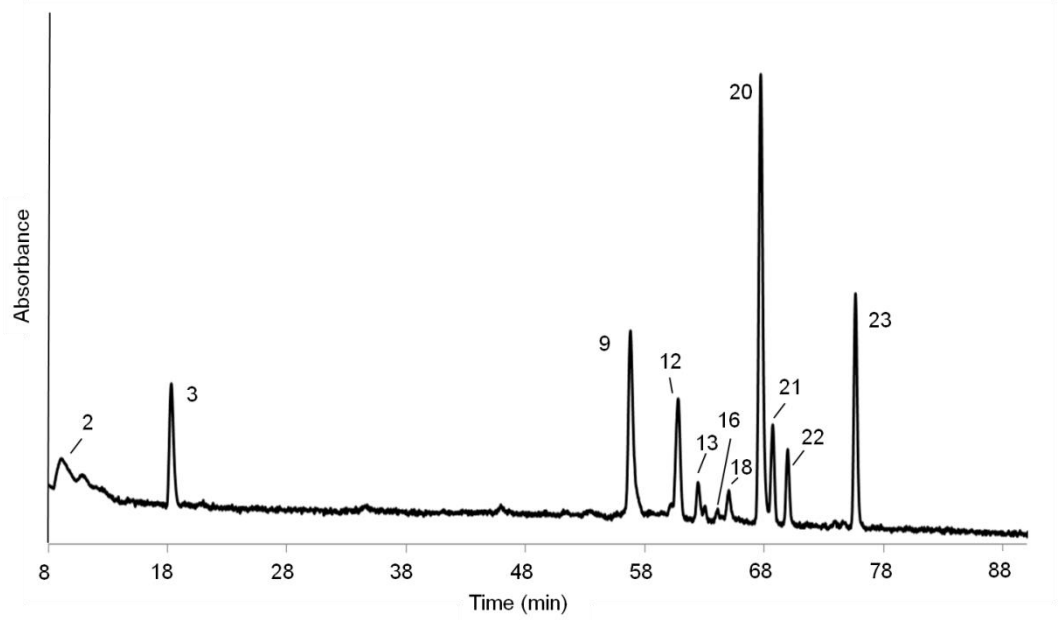

Figure 17. Partial RP-HPLC-UV/vis chromatogram (350-800nm) of Hall Garth sampling point E, 28 cm depth.

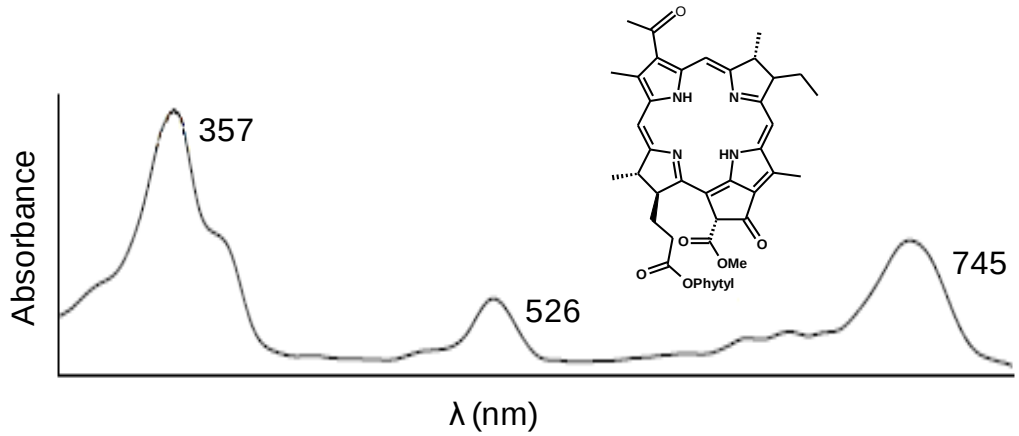

Figure 18. Online UV/vis spectrum (300 to 800 nm) and structure of bacteriophaeophytin *a* from Hall Garth sampling point E, 28 cm depth

2.2.3. Cawood Castle sampling point G

A 23 cm long sediment core (Figure 19) was collected from a depth of 45 cm from an area thought to have been occupied by a fish pond (sampling point G). The sediment collected from sampling point G had low to high TOC contents at the top and bottom of the core (0.5 to 10.0%), and extremely high contents in the middle layers, ca. 40.0% (Figure 19). The lowest TOC values could be attributed to an oligotrophic system and the moderate values to a eutrophic system (Woszczyk *et al.*, 2011), allochthonous organic material could have also

contributed to the carbon content of the sediment. The very high TOC values between 50 and 54 cm depth may be due to extensive algal blooms caused by fertilisation of the water or from the presence of exogenous carbon. Further investigation is required to determine the source of the organic carbon from this region of the core.

Photosynthetic pigments were detected throughout the sediment core, with bacteriophaeophytin *a*, phaeophytin *a* and pyrophaeophytin *a* being identified in all layers. Bacteriophaeophytin *a* was the most abundant component in the upper most layer and between 54 to 55 cm depth (for example, see 55 cm depth Figure 20), and was a prominent component at depths 51, 56 to 57 and 60 cm, the rest of the core was dominated by algal pigments (Figure 19). All components revealed in 55 cm depth (Figure 20) are listed in Table 2. Pyrobacteriophaeophytin *a* (**26**) was identified at all depths except 53 and 64 – 68 cm. The significant contribution from bacteriochlorophyll derivatives throughout the core (except the bottom two layers) suggests that photic zone anoxia was strongly developed in the water column and anoxygenic photoautotrophic productivity occurred during the time period represented by the core. The total masses of pigments determined for the layers between 50 and 54 cm depth (Figure 19) do not support the hypothesis that high TOC contents were caused by extensive algal blooms. The C_{27} steryl ester of pyrophaeophorbide *a* was detected by LC-MS^n between 48 and 50 cm depth, and at the bottom of the core (58 to 64 - 68 cm). The C_{29} steryl ester of pyrophaeophorbide *a* was also detected at 47 to 50 cm depth, and in the bottom layers, 58 to 63 cm, of the core. The C_{28} steryl ester of pyrophaeophorbide *a* was identified at 61 to 63 cm depth. SCE derivatives of chl *b* were detected at 50 cm depth (carbon numbers of C_{27} and C_{29}) and 63 cm depth (carbon numbers of C_{27}). Similar ratios of SCEs attributable to algae (C_{28} and C_{29} SCEs of pyrophaeophorbide *a*) and those attributable to zooplankton (C_{27} SCEs of pyrophaeophorbide *a*) were identified in all depths where SCEs were present. The abundances of the SCEs detected were lower than the parent pigment compounds, showing that zooplankton-mediated modifications of pigments was not the main degradation pathway for chlorophylls in the fish pond.

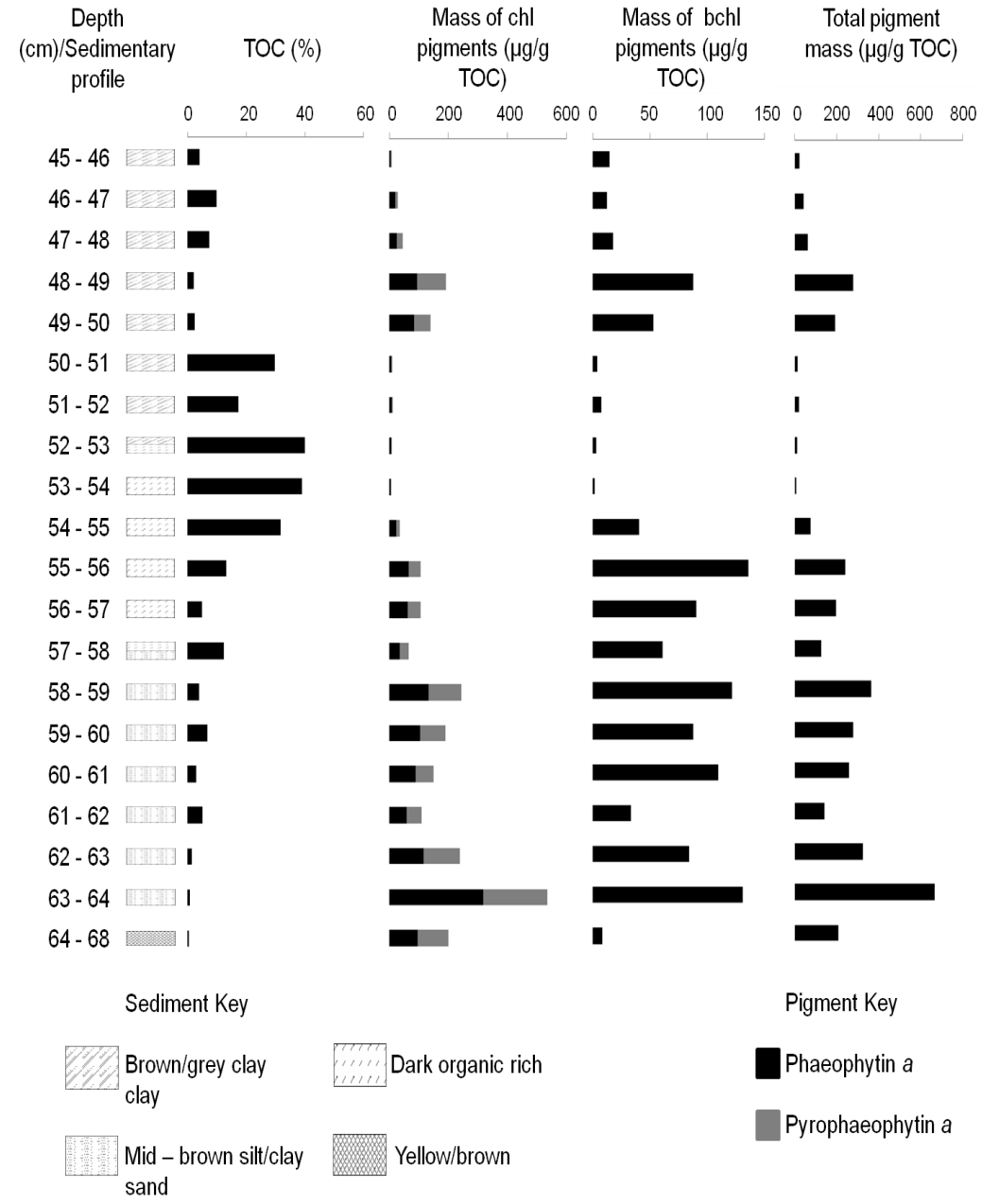

Figure 19. Cawood Castle sampling point G sedimentary profile, TOC contents and total pigment masses.

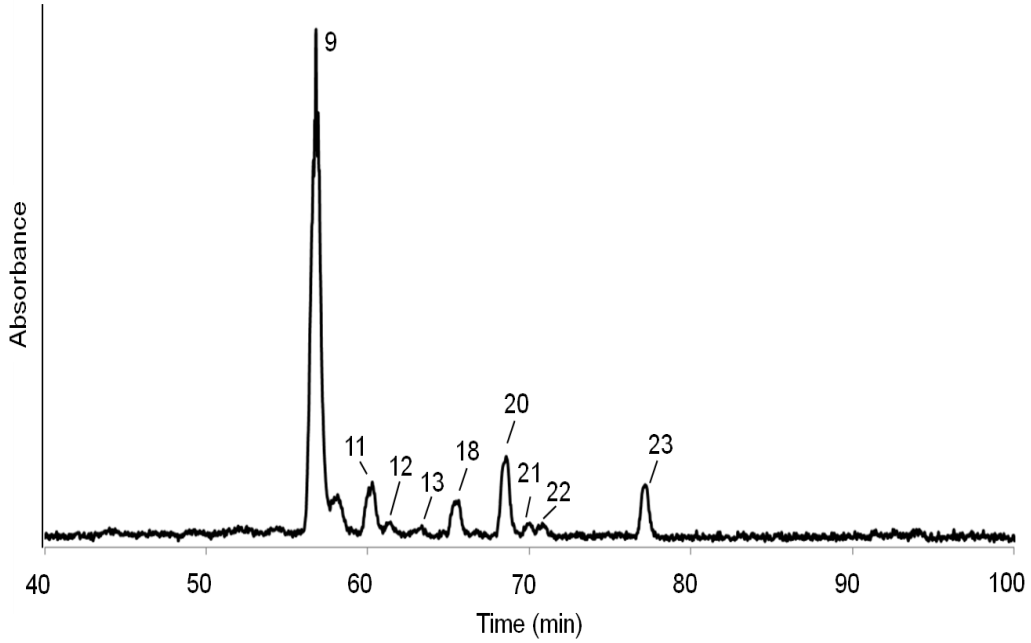

Figure 20. Partial RP-HPLC-UV/vis chromatogram (350-800 nm) of Cawood Castle sampling point G, 55 cm depth.

2.2.4. Lipid analysis of Cawood Castle sampling point G

The pigments in the core show significant differences in abundance between the lower section and the horizon between 50 and 54 cm depth, contrasting with the TOC contents determined for these sections (Figure 19). In order to examine the significance of these variations more closely, sediment between 50 and 54 cm depth (zone B) and in the layers above 46 and 49 cm depth (zone C) and below 57, 59 and 60 cm depth (zone A) were subjected to lipid analysis to determine if the organic carbon was from an exogenous source. Sediments were extracted using ASE with 9:1 DCM:methanol (Brothwell *et al.*, 2001) and reduced to dryness, followed by reconstitution in DCM to achieve a concentration of 5 mg/mL for lipid analysis by GC-FID (Brothwell *et al.*, 2001). A standard mixture comprising fourteen components (Table 4) was subjected to GC-FID and was used to identify components in sample chromatograms by retention time comparisons. The mass of lipids extracted from the samples varied with zone B containing the layer with the highest mass extracted (53 cm depth and 18.15 mg) and the layer with the second lowest mass (50 cm depth and 4.67 mg) (Table 3). Zones A and C had generally lower masses of extracted lipids than zone B (Table 3).

Table 3. Masses of lipids extracted from Cawood Castle sampling point G 46, 49 to 54, 57 and 59 to 60 cm depth.

Zone	Depth (cm)	Mass of extractable lipid (mg)
C	46	8.49
C	49	7.32
B	50	4.67
B	51	9.71
B	52	6.93
B	53	18.15
B	54	15.72
A	57	13.73
A	59	7.11
A	60	4.66

Layers in which TOC was low and pigment abundance was high had a lower total abundance (based on total GC peak area and accounting for sample dilution) of lipids than zone B, see for example 60 cm depth from zone A (Figure 21) and 49 cm depth from zone C (Figure 23) versus 51 cm depth from zone B (Figure 22). Zone B had high TOC contents and low pigment abundance coupled with high total lipid content (based on total GC peak area) compared with zones A and C.

Table 4. Compounds present in lipid standard used to identify components in lipid samples.

Retention time (min)	Compund
17.5	C16 HC
23.5	Phenanthrene
26.0	C16:0 FAME
29.8	C18:3 FAME
30.0	C18:2 FAME
30.1	C18:1 FAME
31.0	C18:0 FAME
34.5	C23 HC
36.5	Phenylhexadecane
44.0	C28 HC
47.5	C30 HC
50.9	C32 HC
59.0	C36 HC
64.5	C38 HC

In zones A and C prominent early eluting components at t_R = 25.5 and 30.5 min in the lipid distributions were C16:0 and C18:0 fatty acids (FA) analysed as their methyl esters (FAMEs), for example see chromatograms typical of zone A and C (peaks 1 and 2 Figure 21 and Figure 23). By contrast, the C16:0 and C18:0 FAMEs exhibit low relative abundances in the lipid profiles within Zone B (peaks 1 and 2 Figure 22). Bacteria and plants are both sources of C16:0 and C18:0 FAMEs (Zelles, 1997) and would be expected to have contributed to the organic matter of sediments which correspond to periods of high productivity by photosynthetic organisms. A series of long chain fatty acids (C24 to C30) were identified. These compounds show highest relative abundances in zone B (for example 51 cm depth; Figure 22), for which the C28 FA component is the most abundant. Sediments from zones A and C also contain C24 to C30 FAs, both zones had C24 as the most abundant FA (for example Figure 21, 60 cm depth and Figure 23 49 cm depth). C24 to C30 FAs are derived both from epicuticular leaf waxes and from algae (Rezanka, 1989). C24 FAs were the most dominant in Zone A followed by a predominance of C28 FAs in zone B, subsequently zone C showed a return to C24 as the most dominant FA. These shifts indicate different plant sources dominated in the pond at during the time period corresponding to zone B and zones A and C (Rezanka, 1989). The samples also contain a series

of C24 to C30 *n*-alkanols which are also major components of plant leaf waxes (Eglinton and Hamilton, 1967). The predominance of the C24 to C30 FAs and *n*-alkanols in layers with low pigment concentration suggests they have a terrestrial source and that the high TOC contents within Zone B derive from leaf litter collecting in the fish pond. All peaks revealed in 60, 49 and 51 cm depth are identified in Table 5.

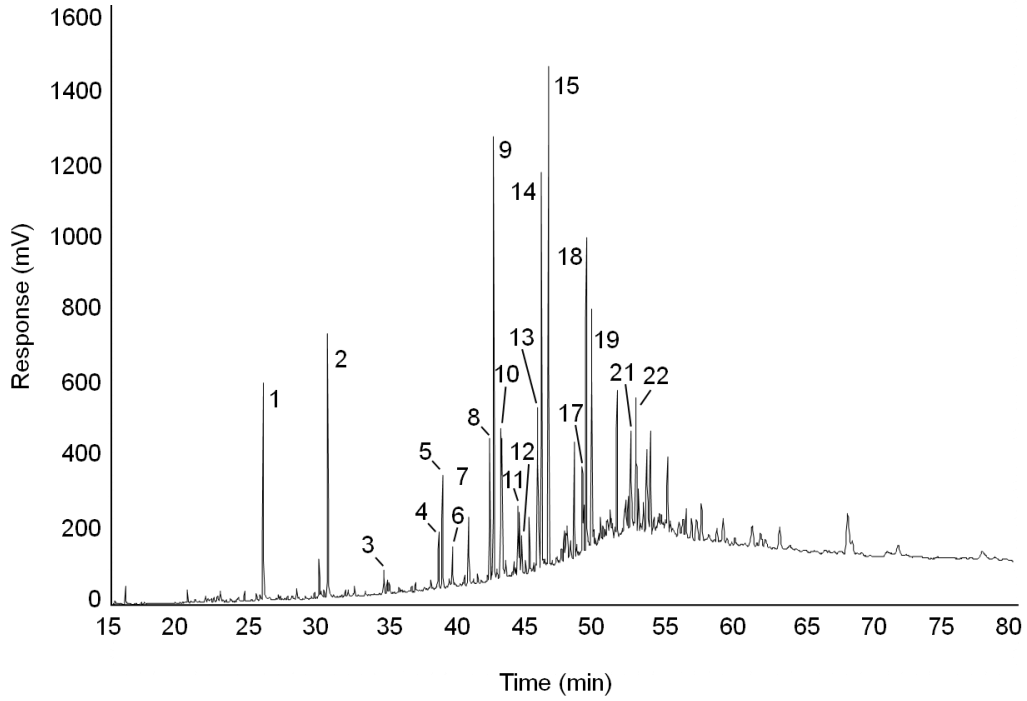

Figure 21. Partial GC FID chromatogram of Cawood Castle sampling point G zone A 60 cm depth, peak identities are detailed in Table 5.

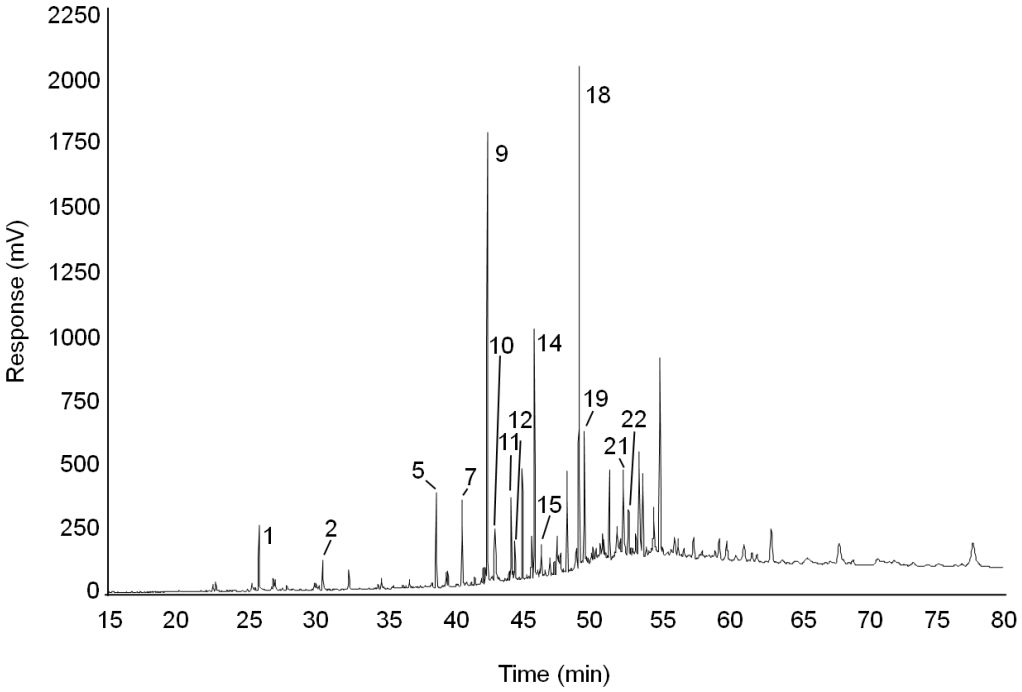

Figure 22. Partial GC FID chromatogram of Cawood Castle sampling point G zone B 51 cm depth, peak identities are detailed in Table 5.

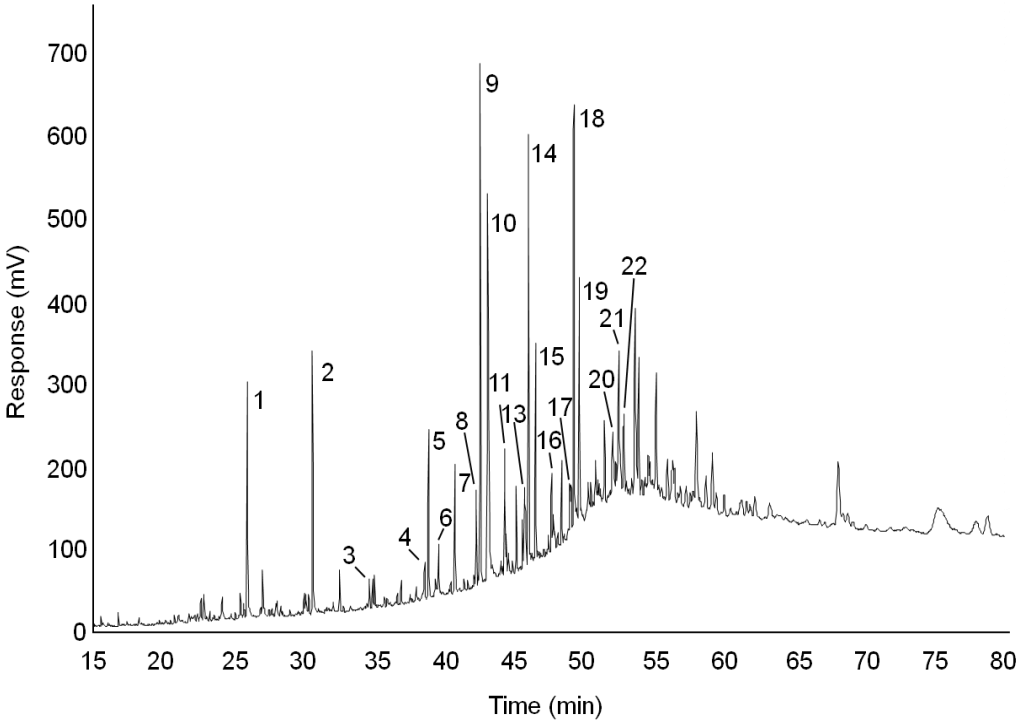

Figure 23. Partial GC FID chromatogram of Cawood Castle sampling point G zone C 49 cm depth, peak identities are detailed in Table 5.

Table 5. Identification of peaks from lipid analysis of Cawood Castle core G (FAME = fatty acid methyl ester, HC = hydrocarbon, OH = alcohol).

Peak	Identity
1	C16:0 FAME
2	C18:0 FAME
3	C20 FAME
4	C19 HC
5	C22 FAME
6	C22 OH
7	C23 FAME
8	C27 HC
9	C24 FAME
10	C24 OH
11	C25 FAME
12	C25 OH
13	C29 HC
14	C26 FAME
15	C26 OH
16	C27 FAME
17	C31 HC
18	C28 FAME
19	C28 OH
20	C33 HC
21	C30 FAME
22	C30 OH

Based on the sedimentary pigment evidence, the feature has previously contained water and was highly productive. The identification of chl and bchl pigment derivatives confirms that it supported both oxygenic and anoxygenic photoautotrophic communities and zooplankton (inferred from the presence of steryl chlorin esters).

2.2.5. Cawood Castle sampling point C

Three depths of sediment (Figure 24) were collected using an auger from a second location at Cawood Castle. Sediments were sampled from within a trench-like area interpreted to have been within the limits of the moat (sampling point C). The TOC contents of the sediments from sampling point C increased from 2.0% at 117 cm depth to 3.2% for 111 and 75 cm depths (Figure 24), these

values could reflect a mesotrophic system. Photosynthetic pigments were detected at all three depths. Chl *a* derivatives, phaeophytin *a* and pyrophaeophytin *a,* were identified at all three depths and were the most abundant components (Figure 24). The Chl *b* derivative, pyrophaeophytin *b,* was identified at 111 (Figure 25) and 117 cm depth, providing further evidence of oxygenic photoautotrophic communities. Sediment from 111 (Figure 25) and 117 cm depth contained bacteriophaeophytin *a* and pyrobacteriophaeophytin *a*, indicating the presence of anoxygenic primary producers and therefore photic zone anoxia in the water column. Carotenoid pigments were also identified at all three depths: lutein (**27**) derived from green algae and/or higher plants (Itoh *et al.*, 2003) was identified at 75 and 111 cm depth, and alloxanthin from cryptophyta (Itoh *et al.*, 2003) at 75 and 117 cm depth. All components revealed at 111 cm depth are listed in Table 2. Sediments from 117 and 111 cm depth contain similar total pigment contents, with a sharp decrease in content at 75 cm depth (Figure 24). Sediment originating from 111 cm depth (Figure 25) contained C_{27} steryl esters of pyrophaeophorbide *a* (identified by LC-MS^n) which are endogenous to zooplankton. Thus the moat environment was productive with both photoautotrophic and zooplankton communities established in the water during the time period covered by the deepest two sediment samples.

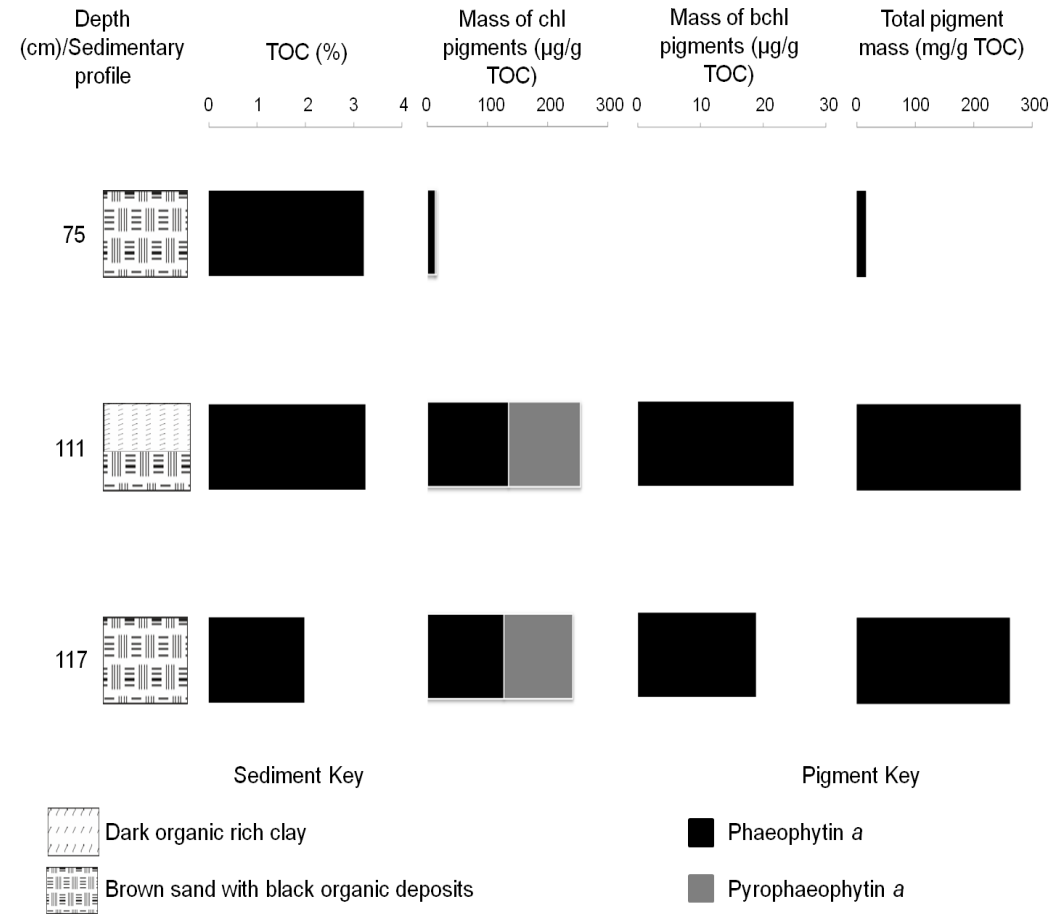

Figure 24. Cawood Castle sampling point C sedimentary profile, TOC contents and total pigment masses.

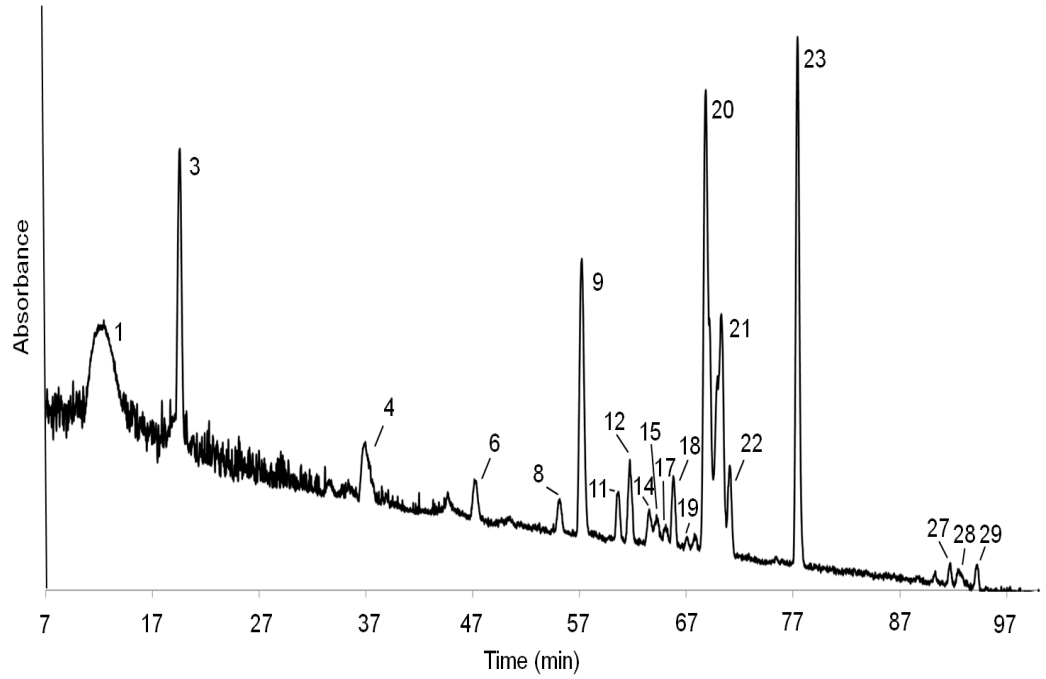

Figure 25. Partial RP-HPLC-UV/vis chromatogram (350-800 nm) of Cawood Castle sampling point C, 111 cm depth.

2.3. Conclusions

The detection in sediments of compounds that are exclusively derived from aquatic environments provides clear evidence for the existence of archaeological water features. Most of the sediments analysed contained phaeophytin *a* and pyrophaeophytin *a* which are derived from algal primary producers (Keely, 2006). The identification of bchl *a* derivatives in Cawood Castle (fish pond and moat) and Hall Garth (moat) sediment not only confirms that the sediment was that of an aquatic feature but that the water was stratified, with anoxic conditions existing in the photic zone. Sediment from Cawood Castle fish pond provides evidence that the productivity in the water feature had a significant contribution from anoxygenic primary production which is indicative of a highly productive system. Sediment collected from Beningbrough Hall (canal, sampling points C and E) and Cawood Castle (fish pond and moat) contained SCEs which are formed by zooplankton grazing primary producers. The identification of SCEs provides definitive evidence that archaeological structures were formally water features as they indicate high primary production and existence of heterotrophic communities comprising zooplankton. Lipid analysis of Cawood Castle fish pond showed that zone B had a predominance of C24 to C30 FAs. As zone B has a low

abundance of photosynthetic pigments it is likely that these FA are derived from epicuticular leaf waxes, thus terrestrial material had accumulated in the pond during the formation of this sediment. Analysis of sediment from sites of suspected fish ponds at Beningbrough Hall (sampling point B) and Hall Garth (sampling point C) provided no evidence that these areas were part of archaeological water features, and calls into question the reliability of currently used identification methods.

Chapter 3. Methods for the isolation of chlorophyll pigments for CSRA

3.1. Introduction

Compound specific radiocarbon analysis was developed to avoid the contamination issues inherent in bulk samples (Eglinton *et al.*, 1996). The technique suffers, however, from limitations relating to the abundance of single compounds in sediment samples and the addition of exogenous carbon from pre-treatment and isolation procedures (Ingalls *et al.*, 2010). Thus, procedures chosen to isolate single compounds must provide high yields and add a minimum amount of exogenous carbon.

3.1.1. Preparative capillary gas chromatography

The concept of using single compounds for AMS analysis was developed by Eglinton *et al.* (1996), who used preparative capillary GC (PCGC) with cooled auto-injection and cryo-trapping as a means to isolate components for CSRA. Their work encompassed radiocarbon dead samples (petroleum derived alkanes), modern samples from biomass (alkanes from *C. argentea* and FA and sterols from *A. americana*) and a known age sample dated to 1498 BC (FA from an Egyptian vase). Following extraction, samples containing FA and alcohols were subjected to pre-treatment to esterify FA to form methyl esters and silylate alcohols (Eglinton *et al.*, 1996), rendering the components amenable to GC analysis. To assess the contribution of carbon from PCGC isolation, blank eluent was collected, and it was estimated that < 5 µg of C was added to samples comprising up to 200 µg of carbon (Eglinton *et al.*, 1996). AMS measurements of petroleum alkanes gave radiocarbon ages of 39300 to 46170 yr $_{BP}$ with errors up to 7610 yr (Eglinton *et al.*, 1996). These ages are close to the limit of radiocarbon dating of ca. 50,000 years (McNichol and Aluwihare, 2007). Once corrected for the added carbon during pre–treatment, the measurement of FA and sterols from *A. americana* and FA from the Egyptian oil agreed with the ages hypothesised: modern for the plant remains and 1498 BC for the Egyptian oil (Eglinton *et al.*, 1996). The alkane *n*–C_{31} isolated from *C. argentea* was subjected to three radiocarbon measurements providing ages between 1530 to 1750 yr $_{BP}$ with errors of up to 70 yr, which did not correspond to the expected modern ^{14}C content (Eglinton *et al.*, 1996). A plausible explanation for the anomalous measurements was that *C. argentea* had been exposed to

radiocarbon dead CO_2 during its growth. The source of the old carbon was identified as a natural gas fuelled heater used in the greenhouse in which the plant had been grown (Eglinton *et al.*, 1996).

3.1.2. Preparative high performance liquid chromatography

Preparative HPLC has been used to isolate compounds for CSRA that are not amenable to GC, for example amino acids, tetraether lipids and cellulose (Hodgins *et al.*, 2001; Ingalls *et al.*, 2004; Shah *et al.*, 2008). Pre-treatment of samples might be required before they can be subjected to preparative HPLC. Hodgins *et al.* (2001) investigated the use of acid hydrolysis and enzymolysis for the degradation of cellulose to glucose monomers while studying the Chelford Log (Early Devensian period). Both procedures have advantages; for example mineral acids which do not contain carbon can be used and enzymes can specifically produce glucose monomers. Drawbacks include the lack of specificity for acid hydrolysis reactions and the possible addition of modern carbon from enzymes, respectively. The yield of glucose from acid hydrolysis was low, ca. 5% of the starting mass (Hodgins *et al.*, 2001). Online analysis and isolation was achieved by high pH anion exchange chromatography with online pulsed amperometric detection (PAD), followed by membrane desalting, UV detection and fraction collection (Hodgins *et al.*, 2001). PAD analysis of the acid hydrolysed cellulose revealed that hydrolysis had been incomplete as it was deduced that oligosaccharides were present (Hodgins *et al.*, 2001). Before its use, the enzyme was initially ultrafiltered with a membrane to remove any glucose contamination. Enzymolysis using the purified enzyme provided a yield of ca. 30% by mass from cellulose (Hodgins *et al.*, 2001). Glucose was identified as the major component in the hydrolysate using the same online analysis and isolation system as employed with the acid hydrolysis product (Hodgins *et al.*, 2001). A greater mass of glucose-derived carbon was recovered from the enzymolysis reaction than from the acid hydrolysis reaction (310 µg versus 42 µg). AMS measurement showed it to comprise 5.8 ± 0.3% modern carbon compared with 21.5 ± 0.3% modern carbon for glucose by acid hydrolysis (Hodgins *et al.*, 2001). Thus, enzymolysis with online analysis and employing the isolation procedure described above was suggested as the direction for future study (Hodgins *et al.*, 2001).

Another example of sample pre–treatment before preparative isolation was the extraction of organic matter (OM) from diatom frustules as an alternative to dating calcium carbonate derived from foraminifera shells (Ingalls *et al.*, 2004). The study investigated three sites in the Southern Ocean; sediment from each location was extracted to remove unbound OM, followed by dissolution of diatom frustules by hydrofluoric acid to liberate the bound OM (Ingalls *et al.*, 2004). The OM recovered was subjected to RP-HPLC with online MS analysis and isolation (1% of the eluent diverted to MS and the remaining amino acids were isolated by fraction collection) (Ingalls *et al.*, 2004). Carbon from several sources can be added to samples during preparative HPLC. These include the elution solvent, column packing material and co–eluting contaminants (Shah and Pearson, 2007). Methods for determining the contribution of carbon from preparative HPLC were investigated by Ingalls *et al.* (2004): blank eluent was collected at different points during the gradient elution and after differing numbers of blank injections. The masses of carbon collected (< 7 µg of C) were too small to be subjected to AMS analysis. Based on the blank eluent collected, it was estimated that the minimum carbon contribution from HPLC would be 2.67 µg of C (Ingalls *et al.*, 2004). An alternative method used to establish the blank contribution was to subject a modern and a radiocarbon dead standard to the preparative procedure and compare the measurement with material not subjected to preparative isolation (Ingalls *et al.*, 2004). AMS analysis of the modern standard subjected to preparative HPLC gave measurements of +79 ‰ $\Delta^{14}C$ and the radiocarbon dead standard had a radiocarbon content of between –949 to 982 ‰, showing that preparative HPLC can alter the radiocarbon content of samples (Ingalls *et al.*, 2004). Polyamines and amino acids isolated from the bound OM of the diatoms were subjected to AMS. CSRA dates of diatom lipids from only one site corresponded to foraminifera measurements: 10,800 to 11,400 ^{14}C years versus 9340 ^{14}C years from foraminiferal $CaCO_3$ (Ingalls *et al.*, 2004). The radiocarbon ages from isolated amino acids and from $CaCO_3$ at the other two sites do not correspond. Explanations for this discrepancy include: differing depositional processes for diatoms and foraminifera and diatoms suffering from greater post-depositional movement (Ingalls *et al.*, 2004).

A study by Shah and Pearson (2007) investigated the addition of exogenous carbon during the preparation of ultra micro scale (5 to 25 µg of C) samples of

tetra-ether lipids for CSRA. They found the carbon added by the preparative HPLC system used was proportional to the volume of eluent collected (Shah and Pearson, 2007). The measurement of carbon added during preparative HPLC was determined from blank injections and thus it is unknown if the amount of added carbon would remain the same during the isolation of samples.

3.1.3. Isolation of chlorophyll *a* derivatives for CSRA

Isolates of chlorophyll *a*, phaeophytin *a*, pyrophaeophytin *a* and $13^2, 17^3$-cyclophaeophorbide-*a*-enol from Black sea sediments were radiocarbon dated by Kusch *et al.* (2010) (see Introduction). Briefly, their procedure involved solvent extraction with acetone followed by liquid–liquid extraction of the pigments using a water/hexane bilayer and subsequent partitioning into DMF (dimethylformamide) for HPLC analysis. Pigment extracts were subjected to two stages of preparative HPLC each using a different C18-based stationary phase and elution program. The mobile phase of the first preparative isolation comprised acetonitrile (ACN)/pyridine (100:0.5) (A) and ethyl acetate (EtOAc)/pyridine (100:0.5) (B). The mobile phase for the second preparative step comprised solvent composition A and 2–butanone/pyridine (100:0.5) (C). The elution gradients used in the preparative HPLC isolation are shown in Figure 26 and Figure 27. The first half of both elution programs are very similar and only differ the addition of ethyl acetate or 2-butanone, thus any early eluting co–elutants will be observed in both preparative HPLC stages and only later eluting components will be affected by the altered section of the gradient.

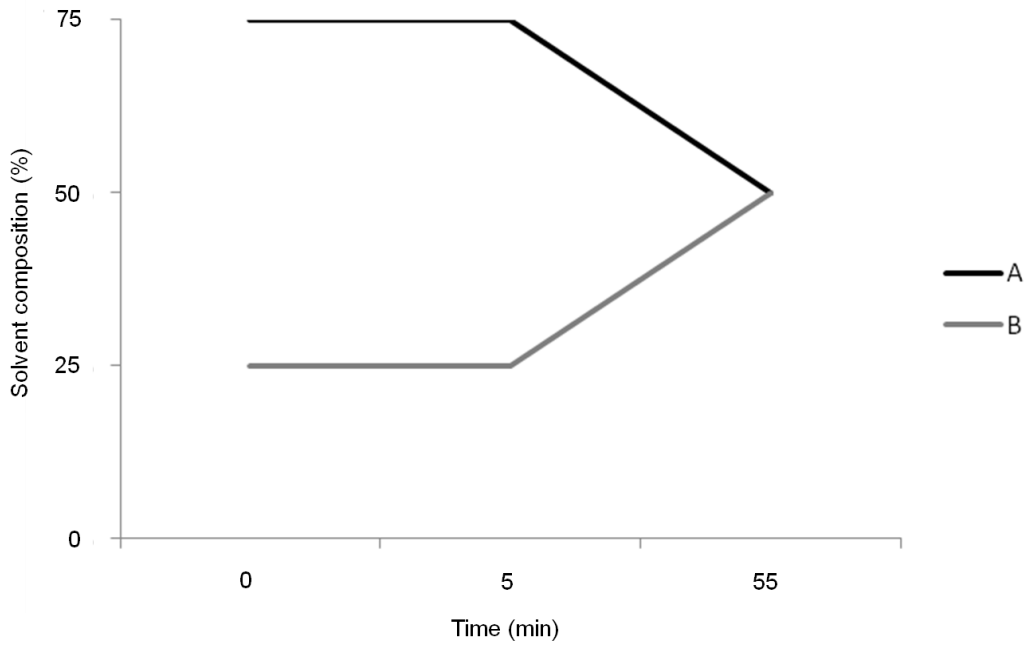

Figure 26. Elution program used in the first preparative HPLC isolation by Kusch *et al.* (2010).

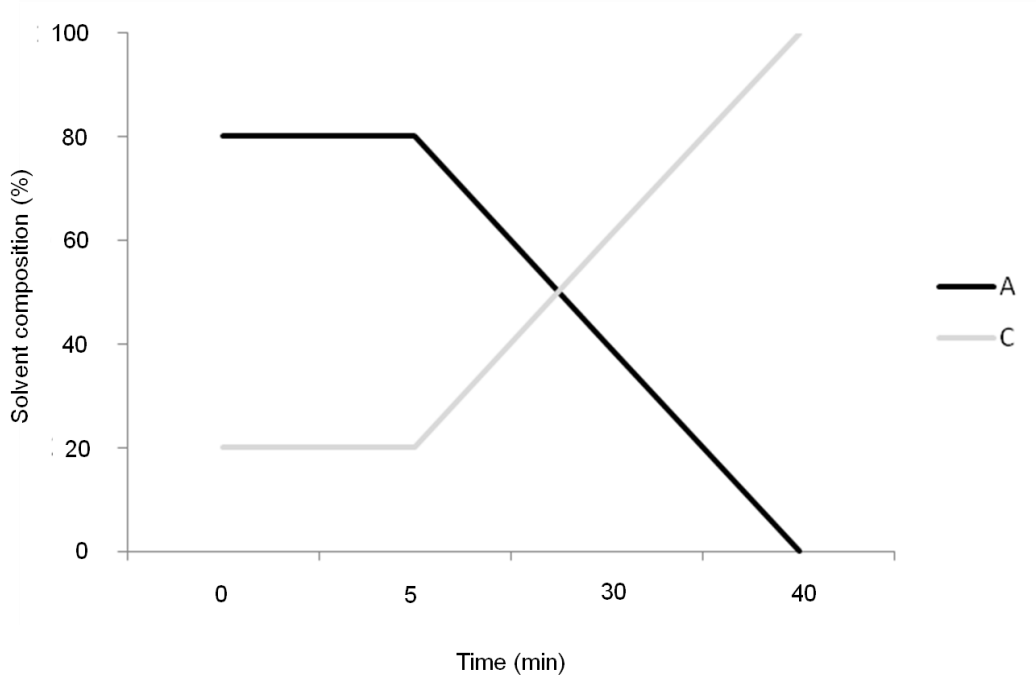

Figure 27. Elution program used in the second preparative HPLC isolation by Kusch *et al.* (2010).

The extraction and isolation procedures of Kusch *et al.* (2010) suffer two potentially limiting factors. Firstly, the use of water and hexane during extraction

will cause sample losses as they cause chlorophylls and their derivatives to aggregate and precipitate out of solution. Secondly, the use of similar stationary phases during preparative isolation will not affect the separation of co-eluting impurities thus isolated fractions may be contaminated.

The contribution of carbon from the preparative HPLC system used in the study was assessed by collecting effluent from blank injections. The carbon added was radiocarbon dead and the mass ranged from 0.8 to 2.5 µg (Kusch *et al.*, 2010). Blank eluent will not model the effects that preparative HPLC has on samples as it is possible that the elution of samples causes greater column bleed.

3.1.4. Implications from previous studies

Previous studies have shown that compounds for CSRA can be subjected to pre–treatment if the carbon added is accounted for during the determination of radiocarbon age. For example, Hodgins *et al.* (2001) used an enzyme, comprising modern carbon, to degrade cellulose into monomer units, and Ingalls *et al.* (2004) added carbon through derivatisation procedures. Preparative isolation can add carbon to compounds isolated for CSRA (Eglinton *et al.*, 1996; Shah and Pearson, 2007). This is an important consequence of using preparative systems to isolate and purify target compounds and the determination of the preparative blank must be incorporated into such work. Ingalls *et al.* (2004) showed that standards of a similar molecular structure to targets for CSRA are useful for establishing the preparative HPLC blank.

3.2. Aims

The aim of the work described in this chapter was to create a robust approach for isolating sedimentary photosynthetic pigments for CSRA.

3.3. Results and discussion

3.3.1. Experimental plan

The experimental plan outlines the strategy adopted to isolate material in sufficient abundance and purity to enable reliable radiocarbon dates to be

obtained from single chlorophyll-derived compounds. Creation of a robust method is reliant on several processes which are outlined schematically in Figure 28. Firstly, and most importantly, sediments with adequate abundance levels of photosynthetic pigments are required as, otherwise, CSRA would not be possible. A high yielding extraction method is essential to recover sedimentary pigments and a method is required to profile the sedimentary extract. As complex distributions of chl and bchl derivatives are often present in natural environments, a means to simplify the distributions is required. Following simplification, individual compounds must be isolated and purified.

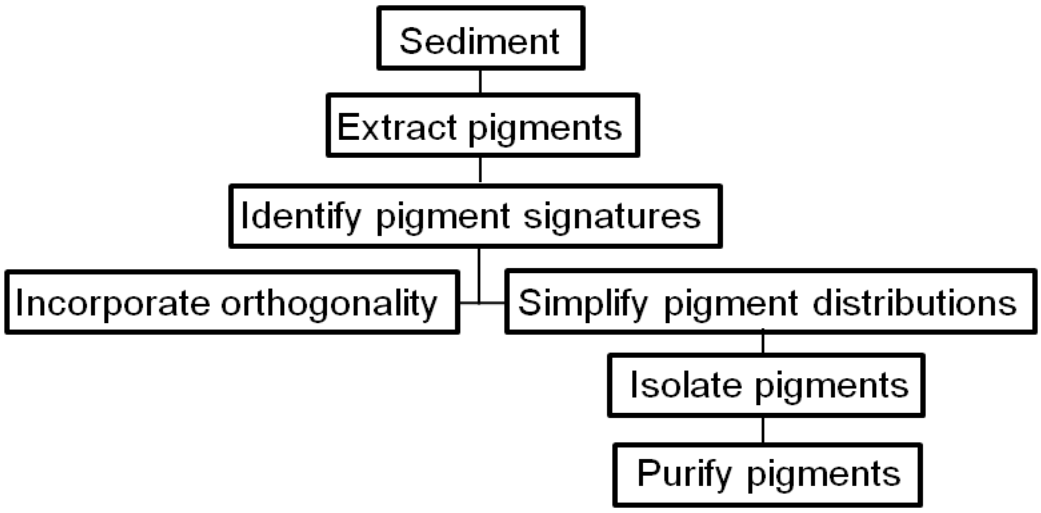

Figure 28. Experimental plan

The methods used in this study (Figure 29) were selected on the basis that they were likely to provide a high yield of pigment derivatives and introduced aspects of orthogonality to produce pure isolates of single compounds. The methods chosen must, however, be validated, which can be achieved through the use of a suitable standard.

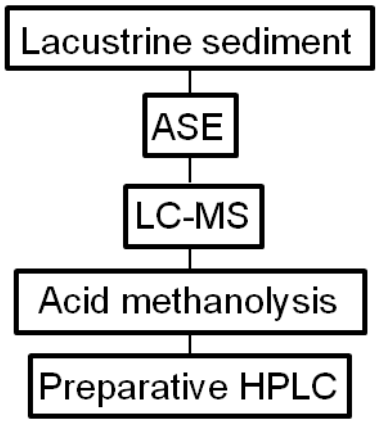

Figure 29. Methods selected for the isolation of sedimentary pigments

3.3.2. Extraction of pigments from sediment

Lake Chiprana, Spain which has been shown to have a productive water column (Vila *et al.*, 2002) (see Chapter 4) and Kirisjes Pond, Antarctica (see Chapter 4) which has pigment-rich sediments (Squier *et al.*, 2002) were selected to undergo preparation for CSRA. Accelerated solvent extraction (ASE) was used to extract pigments from sediments as it is a rapid method that provides high yields of extracts (Richter *et al.*, 1996). The technique uses organic solvents at high pressures and temperatures in order to improve their efficiency for extraction, and decreases the amount of solvent required for extraction (Richter *et al.*, 1996). High pressures increase the diffusion rate of solvent into matrix pores and improve the solubilising power of solvents for analytes and water trapped in the pores (Richter *et al.*, 1996). High temperatures lower the activation energy for desorption of analytes by interrupting non-bonding interactions between analytes and the matrix (Richter *et al.*, 1996). Acetone was used to extract pigments, as both chl and bchl derivatives are readily solubilised. Acetone does not cause the degradation of tetrapyrrole pigment derivatives (Mantoura and Llewellyn, 1983) which is an advantage over the solvents (hexane and water) used by Kusch *et al.*(2010). A temperature of 70°C was used to extract sediment samples; this parameter was previously determined to be the most suitable to extract chlorophyll pigments during an optimisation study (N. Saesaengseerung, personal communication).

3.3.3. Acid methanolysis of pigment derivatives

The ability to target individual sedimentary compounds for CSRA is dependent on their abundance in natural environments. Complex distributions of photosynthetic pigment derivatives (for example those that have been formed via type I degradative processes) are often found in sediments (Keely, 2006). A method was required to simplify pigment distributions and provide an aspect of orthogonality in the separation of the target analytes. Acid methanolysis was chosen as it can meet both of these requirements. Acid methanolysis de-metallates Mg-containing pigments, transforming chls and bchls into their phaeophytin derivatives (Wilson *et al.*, 2003). It also trans-esterifies the $C17^3$ ester of chls and bchls to form the corresponding methyl esters, thus converting phaeophytins into phaeophorbide derivatives (Wilson *et al.*, 2004). During methanolysis, several chl or bchl derivatives can be defunctionalised to yield the same product; hence simpler distributions are formed from an array of related components. For example, chl *a* and its derivatives phaeophytin *a* and phaeophorbide *a* are converted to Me phaeophorbide *a* (**28**) and pyro-derivatives pyrochlorophyll *a* and pyrophaeophytin *a* are converted to Me pyrophaeophorbide *a* (**29**) (see Figure 30). Me phaeophorbide derivatives are not present in nature, thus providing the first aspect of orthogonality.

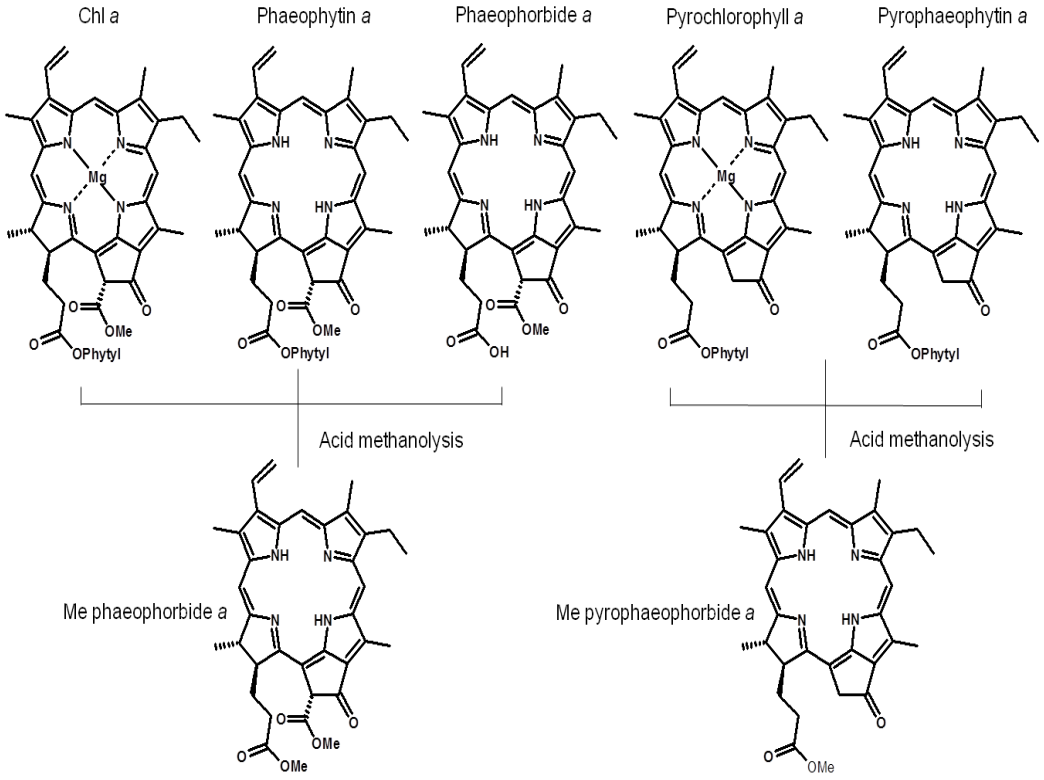

Figure 30. Conversion of chl *a* derivatives into Me phaeophorbide *a* and Me pyrophaeophorbide *a* by acid methanolysis.

A further benefit of acid methanolysis is that it enables separation of chlorophyll pigments from non-chlorophyll compounds of similar polarity. During acid methanolysis, chl pigments and their derivatives are protonated to form dications, and thus become soluble in aqueous solvent. Components which cannot be protonated (for example tetrapyrrole-devoid compounds such as carotenoids and straight chain lipids) remain in the organic solvent and are thus removed from the extract during solvent partitioning. The aqueous layer is then washed with water to increase the pH, thus neutralising the dications and transferring chls and bchls into the organic solvent, leaving polar compounds in the aqueous phase. Accordingly, the experimental plan incorporates an important aspect of orthogonality in the separation as target compounds are isolated from contaminant components by two distinctly different methods.

3.3.4. Analysis of the products of acid methanolysis

The sediments selected for CRSA have previously been extensively profiled using a combination of HPLC and LC-MS^n techniques (Squier *et al.*, 2002; Wilson

et al., 2003; Wilson *et al.*, 2004; Wilson *et al.*, 2005). Thus, analysis via both techniques was incorporated into the experimental plan after acid methanolysis. The acid methanolysis products were subjected to analytical HPLC to identify the methyl phaeophorbide-derivatives formed and to measure their abundance. HPLC method B (Airs *et al.*, 2001) was chosen to analyse samples containing predominantly chl derivatives given that it is appropriate (and was indeed developed) for the rapid analysis of extracts containing relatively simple distributions of components. A HPLC method developed specifically for the analysis of bacteriophaeophorbide methyl esters (BPMEs), method M3 (Wilson *et al.*, 2003), was chosen to analyse samples with predominately bacterial signatures, as it allows greater separation of BPME derivatives.

3.3.5. Preparative HPLC

Preparative HPLC was selected as the method to isolate and purify individual compounds from the products of acid methanolysis as the technique adds a further aspect of orthogonality to the separation. It can be used to recover targeted components based on UV/vis detection at a specific wavelength or at a specific retention time, thus purifying compounds of contaminants with different retention times or UV/vis spectra. Depending on the derivatives present in the samples, as determined by previous studies (Squier *et al.*, 2002; Wilson *et al.*, 2004; Wilson *et al.*, 2005), either Method B (chosen for chl containing samples) or M3 (chosen for bchl containing samples) (Airs *et al.*, 2001; Wilson *et al.*, 2003) was selected for use in preparative HPLC.

3.3.6. Method validation

It was essential to validate the experimental plan for the preparation of sedimentary pigments for CSRA. Thus, it proved necessary to create a stock of pure standard material. An outline of methods used for the preparation the standard is shown schematically in Figure 31.

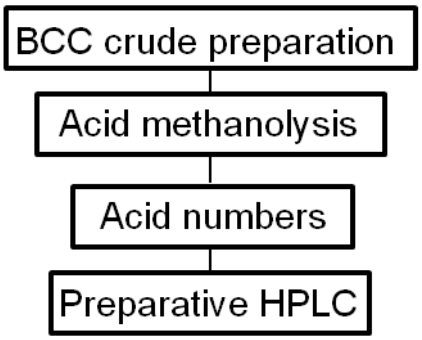

Figure 31. Experimental plan used for the creation of a stock of pure standard material from British chlorophyll company crude material.

The targets of this study, chl pigments, are large, relatively non–polar molecules which are most soluble in polar organic solvents such as acetone or diethyl ether. Chls are degraded by exposure to high light intensities and oxygen, which each had to be taken into consideration during the handling and storage of pigments and their derivatives. The standard was required to be of similar chemical composition to chls in order to be able to subject it to the same preparation procedures as the samples destined for CSRA. Pure pigment standards were prohibitively expensive for this work, hence Me pyrophaeophorbide *a* was selected as an alternative as it can be prepared relatively easily from a British Chlorophyll Company (BCC) crude preparation containing predominately pyrophaeophytin *a* (Naylor, 1997). The BCC preparation is a bulk extraction product which also contains other photosynthetic pigments, including carotenoids and various lipids which do not possess a chromophore and are not detected by UV/vis. Milligram amounts of Me pyrophaeophorbide *a* were required to provide sufficient material for method validation. The BCC crude preparation was subjected to acid methanolysis to convert pyrophaeophytin *a* to Me pyrophaeophorbide *a* and to purify it from other lipid components (see Section 3.3.3 Chapter 3). The acid methanolysis product was subsequently subjected to acid numbering, a liquid–liquid extraction technique using diethyl ether and aqueous HCl (Smith, 1975). The acid numbering technique, due to its simplicity and ability to extract ca. mg quantities of pigment, was used as a means of purifying the acid methanolysis product of the BCC preparation to produce a single compound as a standard. Acid numbering purifies pigments by using specific concentrations of HCl to extract individual tetrapyrroles into an aqueous phase. The concentration of the acid used is dependent both on the basicity of

the compound and its ether–water partition coefficient (Smith, 1975). The solubility of pigments in ether is largely affected by the nature of the C17[3] esterifying group (Smith, 1975). Given that the standard was subjected to acid methanolysis, all components are esterified with methanol. Thus, the main control on solubility is the basicity of the pyrrole nitrogens, which is strongly affected by the presence and structure of ring E. For example, Me phaeophorbide *a*, in which ring E is intact, is less basic than its pyro-derivative. Peripheral electrophilic substituents, for example acetyl (bchl *a*) and formyl (chl *b*) groups, also affect basicity as they draw electron density away from the pyrrole nitrogen atoms, rendering them less basic (Smith, 1975). Acid numbering could not be applied to sediment extracts intended for CSRA due to the complexity of their pigment distributions, as each compound to be purified would have required a separate acid number extraction. Thus the acing numbering process would be very time consuming and therefore impractical for sediment samples.

3.3.7. Preparative HPLC of samples for AMS analysis

Preparative HPLC was used to isolate and purify compounds for radiocarbon analysis. Compounds can be affected by isotopic fractionation during liquid chromatography. A study by Baumann *et al.* (1992) used an amino acid (leucine) labelled with one ^{14}C atom to determine if fractionation occurred during ion exchange HPLC. The authors showed that isotopic fractionation had occurred as the front of the leucine peak was isotopically light compared to the tail (23.57 ± 2.3 versus 29 ± 1.1 counts per minute/nmol of leucine) (Baumann *et al.*, 1992). They also carried out a retention time comparison study of natural leucine and leucine labelled with one ^{13}C atom. The ^{13}C labelled leucine was found to elute 0.033 min later than standard leucine (Baumann *et al.*, 1992). O'Connell and Hedges (2001) reported that RP-HPLC analysis of amino acids causes minimal fractionation; glycine, an amino acid which is susceptible to fractionation, had only a 0.5‰ difference in $\delta^{13}C$ across the peak (O'Connell and Hedges, 2001). The low isotopic fractionation was explicitly attributed to the use of RP-HPLC instead of ion exchange HPLC, and it was suggested that the technique could be used to separate amino acids prior to AMS. Thus, it can be inferred that the carbon isotopes are not significantly fractionated (O'Connell and Hedges, 2001).

The Me pyrophaeophorbide *a* standard was used in the current study to check if isotopic fractionation had occurred during preparative RP-HPLC on the column used (Jones Chromatography APEX ODS II). If fractionation were to occur on the column, it could be exacerbated further through the limitations of the fraction collector (for example if the instrument did not collect the entire peak).

3.3.8. Validation of AMS measurement

Good precision for AMS radiocarbon measurements is dependent on low statistical uncertainty and high reproducibility (Fifield, 1999). Standards are commonly used during radiocarbon analysis by AMS to check for instrument drift and to account for its effect on the measurement of samples (Pearson *et al.*, 1998; Santos *et al.*, 2007). Precision can be improved by quantitatively correcting for any drift through repeated measurements of an appropriate standard during a sample sequence. Oxalic acid dehydrate OX I and II, from the National Bureau of Standards (now NIST), are commonly used standards for determination of radiocarbon age (Cavallo and Mann, 1980). The radiocarbon age of OX II was verified by 16 laboratories (Mann, 1983) and was given the date 1950 AD, which represents modern in ^{14}C AMS measurements (Currie, 2004). Radiocarbon analyses are often reported as fraction of modern (see Section 1.2.10, Chapter 1). Fm is calculated to be 0.95 of the value of OX I which corresponds to its radiocarbon activity in 1950, and the fm of OX II is fm_{OXII}/fm_{OXI} (Pearson *et al.*, 1998; McNichol and Aluwihare, 2007).

Isotopic fractionation may occur during the graphitisation procedures used to prepare AMS targets (Fifield, 1999). Use of a standard with known radiocarbon signature can be employed to quantify this effect. Standards can also be used to determine if the carbon signature of samples is altered by preparation techniques, for example during chemical purification or preparative HPLC. Thus, the Me pyrophaeophorbide *a* standard could be used to correct for procedural changes in isotopic signature as well any instrument effects during CSRA sample measurements.

3.3.9. Sample size requirements for AMS

CSRA measurements are limited by sample size: large uncertainties are associated with AMS measurement of small samples. For example, measurement of samples comprising 5 µg of carbon can yield errors in excess of 30‰ (Shah and Pearson, 2007). Measuring the process blank is critical for samples comprising between 5 to 25 µg of carbon, as this is the main source of uncertainty (Shah and Pearson, 2007). By contrast, the largest uncertainty for samples of > 25 µg of carbon derives results from graphitisation procedures. Carbon in the processing blanks can originate from modern carbon added when samples are combusted to CO_2, during graphitisation reactions which require catalysts and/or from the background level of ^{14}C inherent in the AMS instrument (Pearson *et al.*, 1998).

The use of a gas source avoids graphitisation reactions which can add contamination to samples (Bronk and Hedges, 1987), and samples containing as little as 2 µg of carbon have been measured through use of such sources (Ruff *et al.*, 2010). A constant blank of 55 ng of carbon (50% modern) derived from multiple sources, which were likely to include contamination from sample ampoules and preparation steps, was reported by Ruff *et al.* (2010) for samples containing between 8 and 40 µg of carbon derived from various sources such as aerosol filters and ice cores. A further source of error in gas source measurements originates from the titanium target in the source which can produce background currents from imbedded carbon (Kjeldsen *et al.*, 2008).

Photosynthetic pigments are not wholly composed of carbon and this must be taken into account when assessing sample requirements for CSRA. Balancing the desire for robust AMS measurements and the mass of sediments available for this study, it was decided to base preliminary calculations on a requirement of 20 µg of C. Carbon accounts for 74.5% of the formula mass of the Me pyrophaeophorbide *a* standard. Therefore, one analysis requires 26.85 µg of Me pyrophaeophorbide *a* and three replicate measurements require 80.54 µg. Thus, total recoveries of ca. 0.1 mg per target pigment were required from the extracts of sediments for the study.

3.4. Preparation of the standard

3.4.1. Preparation of standard and validation of isolation approaches

Me pyrophaeophorbide *a* was chosen as the standard to validate the experimental plan because it was of similar structure to the target compounds. Thus it could be subjected to the same pre-treatment, chromatographic and isolation methods as it is likely to react in the same way as the target compounds. The standard was sourced from a BCC crude preparation which contains chlorophyll pigment derivatives, the most abundant of which is pyrophaeophytin *a* (Naylor, 1997).

3.4.2. Acid methanolysis

The acid methanolysis product of the BCC crude preparation was analysed by RP-HPLC with PDA detection using method B (Airs *et al.*, 2001) on an analytical column (two coupled Waters Spherisorb ODS II columns) (Figure 32).

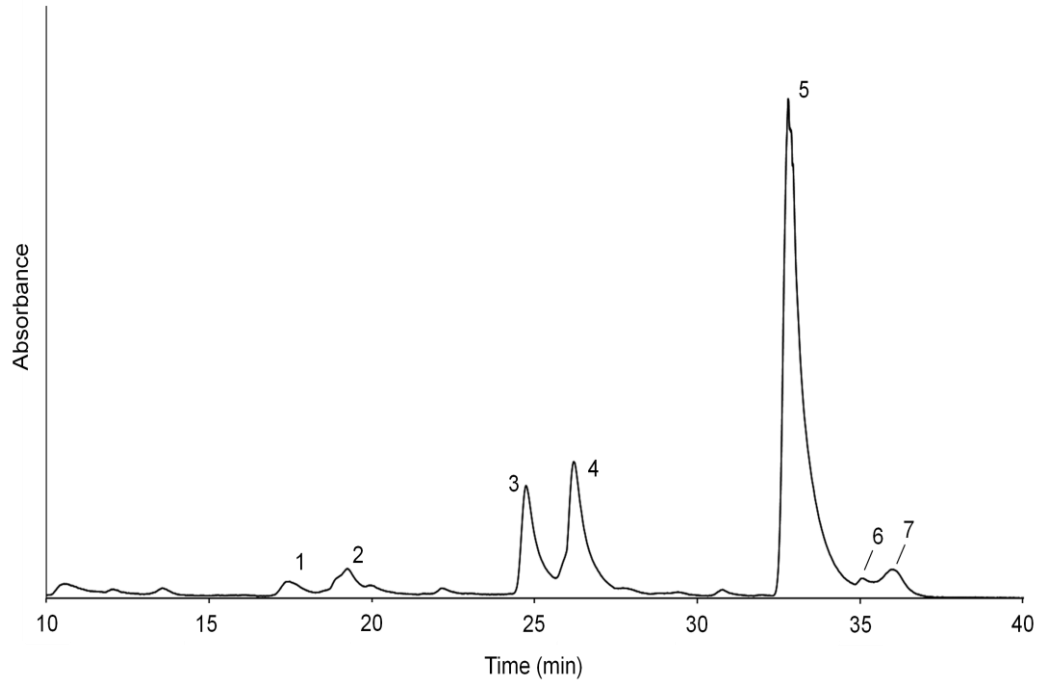

Figure 32. Partial RP-HPLC-UV/vis chromatogram (350-800 nm) of BCC crude preparation after acid methanolysis.

The chromatogram (Figure 32) revealed the presence of several components, the most abundant of which (peak 5; retention time (t_R) = 33 min) gave an online UV/vis spectrum with maximum absorbances at 409 and 666 nm, attributable to Me pyrophaeophorbide *a* Soret and Q_y bands. A direct injection positive mode APCI MS spectrum of the acid methanolysis product revealed the most abundant ion was at *m/z* 549, which corresponds to the protonated molecule of Me pyrophaeophorbide *a* (Figure 33).

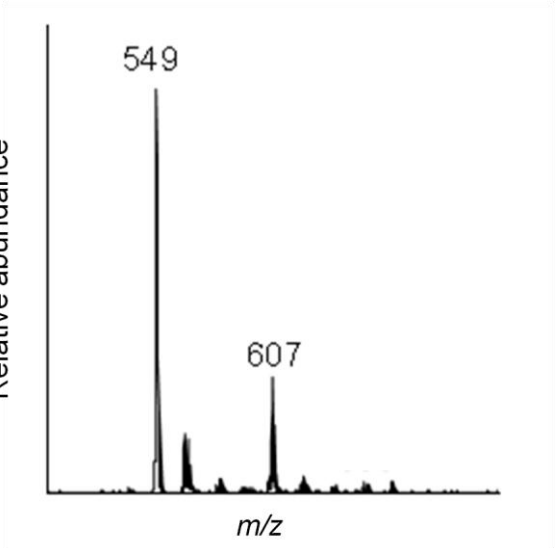

Figure 33. Partial APCI positive mode mass spectrum of the direct injection analysis of BCC preparation subjected to methanolysis.

Three other prominent components were detected in the HPLC chromatogram, including peak 3 (t_R = 25 min, Figure 32) which gave maximum absorbances at 411 and 664 nm, attributable to Me phaeophorbide *a*. The identification of Me phaeophorbide *a* was confirmed from its protonated molecule (*m/z* 607) in the direct injection MS spectrum (Figure 33). Peak 4 (t_R = 26.5 min, Figure 32) gave maximum absorbance at 437 and 660 nm, attributable to Me pyrophaeophorbide *b* (**30**). Peaks 1, 2, 6 and 7 (t_R =17.5, 19, 35 and 36 min, Figure 32), minor components in the chromatogram, could not be identified but are likely to have a chlorin or porphyrin macrocycle origin due to their UV/vis spectra. Thus, HPLC and MS analysis of the acid methanolysis product from the BCC preparation revealed that further purification was required to isolate Me pyrophaeophorbide *a*.

3.4.3. Acid numbering

To obtain a stock of pure Me pyrophaeophorbide *a*, the acid methanolysis product was subjected to acid numbering, which can hypothetically purify 2/3 of the target compound if the starting material is subjected to two extractions (Smith, 1975). By the third extraction, the concentration of the target molecule has decreased sufficiently for the acid to protonate other tetrapyrroles, hence losing specificity for the target pigment derivative. Thus, the methanolysis product was purified twice using 13% (w/v) aq. HCl, the acid number for Me pyrophaeophorbide *a* which was experimentally determined by Naylor (1997). HPLC analysis of the acid number purification products by method B (Airs *et al.*, 2001) using the same analytical column revealed that the target compound Me pyrophaeophorbide *a* (peak 5, Figure 34) now only represented a minor component. An unexpected component, peak x (Figure 34), which was not observed in the chromatogram of the acid methanolysis products (Figure 32), was now the most prominent peak in the chromatogram. Peak x shares the same maximum absorbances as Me pyrophaeophorbide *a* (409 and 666 nm) but eluted much earlier, with direct infusion MS analysis required to identify the component. The most abundant ion in the positive mode APCI MS spectrum was at *m/z* 536, which corresponds to the protonated molecule of pyrophaeophorbide *a* free acid. The HPLC chromatogram also reveal the presence of a minor component (peak 6/7, t_R = 35.5 min, Figure 34) which partially co-elutes with Me pyrophaeophorbide *a*. Due to the apparently low abundance of peak 6/7, it was not possible to determine the identity of the component(s) responsible for the peak. However, based on comparable retention times, it is assumed that peak 6/7 corresponds to peaks 6 and 7 identified in the acid methanolysis product (Figure 32).

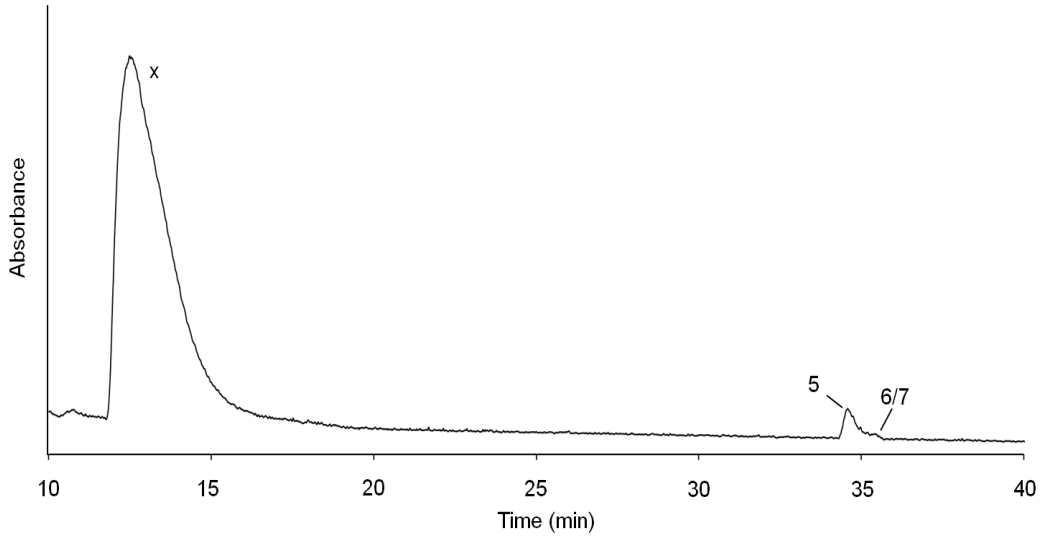

Figure 34. Partial RP-HPLC-UV/vis chromatogram (350-800 nm) of the acid methanolysis product subjected to acid numbering purification with 13 % (w/v) aq. HCl.

The identification of pyrophaeophorbide *a* in the acid numbers product suggests that Me pyrophaeophorbide *a* was de-esterified during purification, thus accounting for the low abundance of peak 5 (Figure 34) in the chromatogram. Theoretically, purification by acid numbering should only isolate Me pyrophaeophorbide *a* (Smith, 1975), hence the desired outcome was not achieved. The acid number of 13% (w/v) aq. HCl was evidently too high and caused the hydrolysis of the $C17^3$ methyl ester to form pyrophaeophorbide *a*. A lower concentration of HCl was considered as a means to avoid de-esterification whilst still affording Me pyrophaeophorbide *a* with sufficient purity. A second quantity of the BCC preparation was subjected to acid methanolysis followed by stepwise acid numbering, which was achieved by increasing the concentration of HCl. Several acid numbering reactions with differing concentrations of acid were carried out to identify experimentally when the majority of Me pyrophaeophorbide *a* was isolated from the methanolysis product with minimum de-esterification. It was found that sequential acid numbering extractions allow the use of less concentrated acid to achieve purification from the bulk acid methanolysis product without de-esterification. The optimum conditions were extraction with 8% (w/v) aq. HCl to remove the most polar compounds from the extract followed by 11% (w/v) aq. HCl to purify Me pyrophaeophorbide *a* from non polar components in

the extract. Acid numbering using two concentrations of HCl extracted Me pyrophaeophorbide *a* with the least contamination from other components (HPLC analysis by method B (Airs *et al.*, 2001), chromatogram in Figure 35). The method has the additional benefit of removing compounds that are both more polar and non-polar than Me pyrophaeophorbide *a*, adding further orthogonality to the standard preparation procedure. Thus, stepwise acid numbering purification with 8 and 11% (w/v) aq. HCl was chosen as the method to extract a quantity of Me pyrophaeophorbide *a* to form a stock of standard material. The standard was subjected to a final acid methanolysis step as a precaution to ensure all the pyrophaeophorbide *a* was present as the methyl ester.

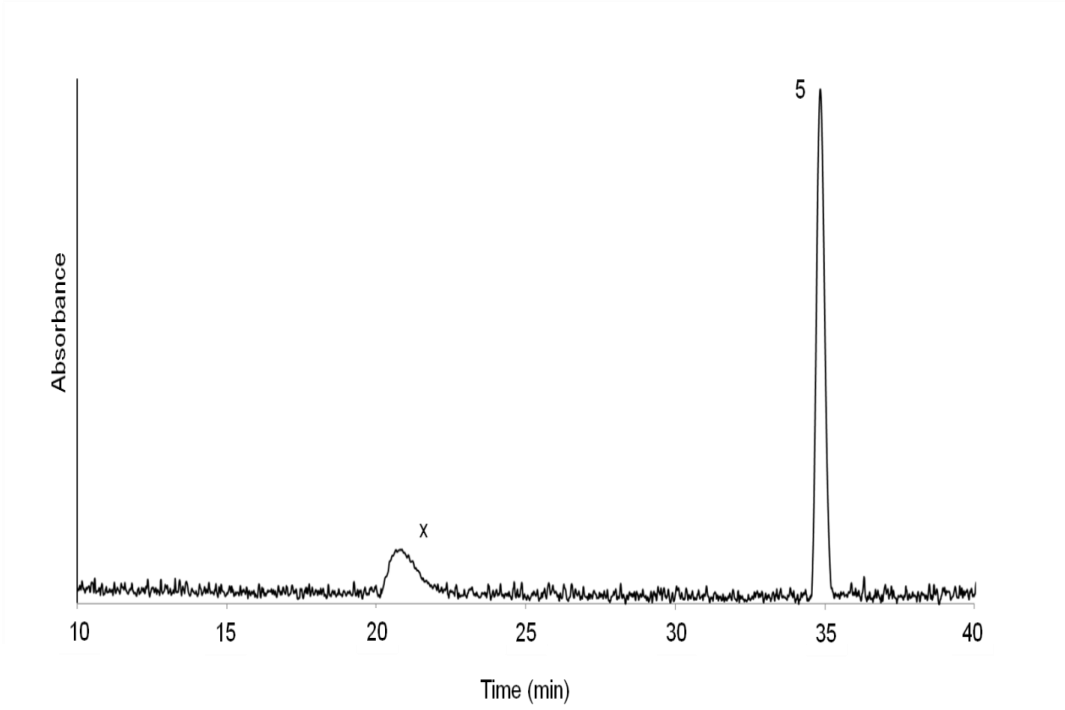

Figure 35. Partial RP-HPLC-UV/vis chromatogram (350-800 nm) of the BCC preparation acid methanolysis product subjected to acid numbering purification with 8 and 11% (w/v) aq. HCl.

3.4.4. Preparative HPLC of Me pyrophaeophorbide *a* standard

A final purification step of preparative HPLC was introduced because small contaminant components were observed in the chromatogram of the Me pyrophaeophorbide *a* standard, for example peak x in Figure 35. Two later eluting components were observed in the analysis of the acid methanolysis product (peaks 6 and 7, Figure 32) and a single component in some acid numbering purifications (Figure 36) but not in others (Figure 35). The t_R of Me

pyrophaeophorbide *a* and peak 6/7 had changed as a short binary elution HPLC method was used, see Table 6.

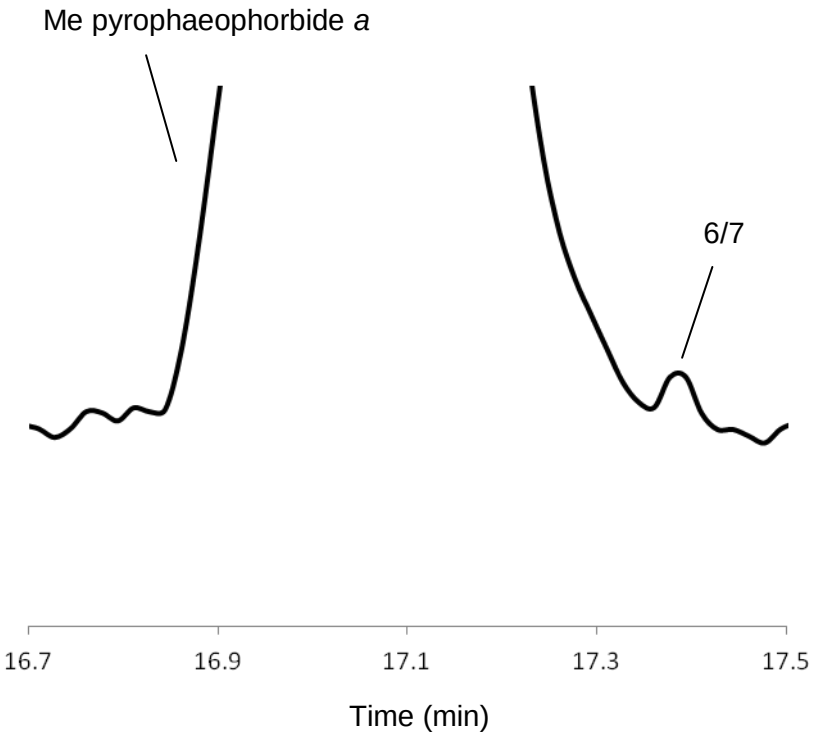

Figure 36. Expansion of a region of the RP-HPLC-UV/vis chromatogram (350-800 nm) of the BCC preparation acid methanolysis product subjected to 8 and 11% (w/v) aq. HCl acid numbering purification using the binary method.

Preparative HPLC also attempted to isolate Me pyrophaeophorbide *a* from any previously unidentified non–UV/vis active components by only collecting eluent during the trigger from the programmed wavelength. As the Me pyrophaeophorbide *a* standard contains a simple pigment profile (for example only one major component) by this state of purification, a shorter binary elution HPLC method (Table 6) was developed for the preparative HPLC instead of method B (Airs *et al.*, 2001), which is 85 min long. The use of the method accounts for the different retention times for Me pyrophaeophorbide *a* and peak 6/7 noted in Figure 36 compared to in Figure 32 and Figure 35.

During the development of the new HPLC method, the continued use of a quaternary elution program was critically evaluated: ammonium acetate assists in the retention and resolution of acidic chlorophyll derivatives (Zapata *et al.*, 1987).

The standard has no acidic tetrapyrrole ring substituents and has been neutralised as part of the acid numbering procedure, with methanol as the $C17^3$ esterifying alcohol. Thus, the 10 mM ammonium acetate buffer used in method B (Airs *et al.*, 2001) is not required in the eluent. Acetonitrile (ACN) is used in method B to improve the resolution of polar compounds (Airs *et al.*, 2001). As the standard only contains one major component and the resolution of Me pyrophaeophorbide *a* and the low abundance contaminant (peak 6/7) eluting after it is not significantly altered by the presence of ACN (see for example Figure 34, where the elution solvent contains ACN and Figure 36, where ACN is omitted), ACN was removed from the eluent. The 5 min isocratic period at the start of method B (Airs *et al.*, 2001) was designed to retain highly polar components on the column, this step was not necessary for the analysis of the standard as it does not elute early in the gradient program. Therefore, the isocratic period was omitted from the method. The time taken to reach the highest ethyl acetate composition was reduced from 81 min in method B (Airs *et al.*, 2001) to 20 min (Table 6), thus enabling early elution of Me pyrophaeophorbide *a* from the column. During preliminary tests, residual ethyl acetate left on the column following one analysis caused the standard not be retained in the next analysis. To address this issue, a four min isocratic period comprising the starting composition was added to the end of the method to recondition the column (Table 6). Thus, the preparative HPLC method developed in this study comprises a simple binary system of methanol and ethyl acetate, with gradient followed by isocratic elution for a total of 25 min (Table 6).

Table 6. Binary method for preparative HPLC of Me pyrophaeophorbide *a* standard.

Time (min)	Methanol (%)	Ethyl acetate (%)
0	95	5
20	40	60
21	95	5
25	95	5

The binary method (Table 6) was used for preparative HPLC purification of the Me pyrophaeophorbide *a* standard (Figure 37) on a Jones Chromatography APEX ODS II semi preparative HPLC column. The column used for preparative HPLC is shorter than the analytical HPLC column as samples subjected to

preparative HPLC have simple distributions of compounds due to acid methanolysis. Me pyrophaeophorbide *a* eluted from the semi preparative column at t_R = 17.1 min, an improvement of 17.5 min compared with method B (Airs *et al.*, 2001) on the Waters Spherisorb analytical column. A total of 0.68 mg (determined by UV/vis) of Me pyrophaeophorbide *a* was purified by many repetitive preparative HPLC runs using the binary elution program.

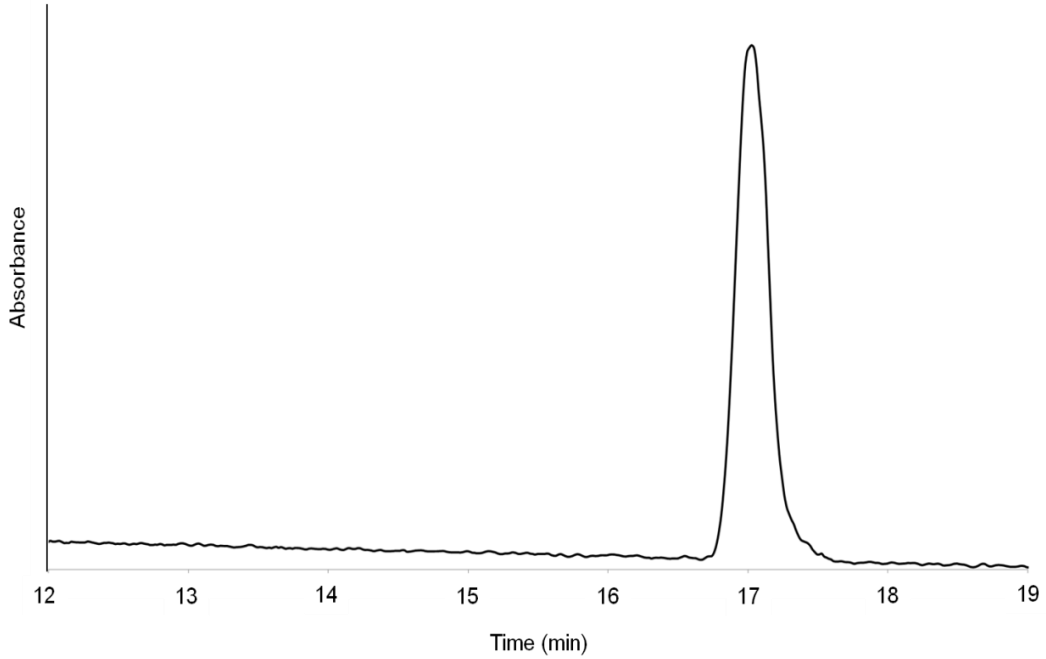

Figure 37. Partial RP-HPLC-UV/vis chromatogram (350-800 nm) of the Me pyrophaeophorbide *a* standard analysed by the binary method developed for preparative HPLC.

3.4.5. Elemental analysis of Me pyrophaeophorbide a standard

The standard was subjected to elemental analysis (EA) to quantify its purity. The carbon, nitrogen and hydrogen content determined for the sample is recorded in Table 7.

Table 7. Experimentally determined and theoretical values of the carbon, nitrogen and oxygen content of the Me pyrophaeophorbide *a* standard.

	Carbon (%)	Nitrogen (%)	Hydrogen (%)	Oxygen (%)
Theoretical	74.5	10.2	6.6	8.8
Measured by EA	61.5	8.1	5.7	not measured
Difference	-13	-2.1	-0.9	

The expected value of oxygen by mass balance from the EA measurement is 24.7%, which is greater than the theoretical value for Me pyrophaeophorbide *a* by 15.9%. The percentages of carbon, nitrogen and hydrogen were all lower than expected (Table 7). The chemical compositions of several potential contaminants (Table 8) were considered as the source of the discrepancy between the measured and theoretical composition of Me pyrophaeophorbide *a*. All contaminants considered; water, methanol, ethyl acetate and acetone could increase the oxygen and decrease the carbon content of the standard measurements. As none of the considered contaminants contain nitrogen, this would cause a decrease in the contribution of nitrogen to the mass of the standard. All of the solvents listed in Table 8 however would also cause an increase in the hydrogen content of the standard, which was not observed in EA. Hence the discrepancy in the EA of Me pyrophaeophorbide *a* and its theoretical composition was likely to have not been caused by exposure to the solvents listed in Table 8. Although possible sources of contamination have not been identified, EA analysis has shown the standard to be relatively pure.

Table 8. Carbon, nitrogen, hydrogen and oxygen composition of possible contaminants.

	Carbon (%)	Nitrogen (%)	Hydrogen (%)	Oxygen (%)
Water	N/A	N/A	11.1	88.9
MeOH	37.5	N/A	12.5	50.0
Ethyl acetate	54.5	N/A	9.1	36.4
Acetone	62.1	N/A	10.3	27.6

3.4.6. Analysis of a complex sample using the binary method

The binary method (Table 6) and semi preparative column was used to analyse a pigment-rich sediment from Lake Chiprana known to contain bacteria and algal pigments (Wilson, 2004). The sediment was acetone extracted using ASE and subjected to acid methanolysis, followed by HPLC analysis using the binary method. A chromatogram containing seven peaks was recorded (peak 1, BPME *d* [Et ,Et] (**31**); peak 2, Me phaeophorbide *b*; peak 3, BPME *c* [*n*-Pr, Et] (**32**); peak 4, Me phaeophorbide *a*; peak 5, Me phaeophorbide *a* epimer; peak 6, Me pyrophaeophorbide *b*; and peak 7, Me pyrophaeophorbide *a*; Figure 38). The same sample was also analysed using method A (Airs *et al.*, 2001) with the semi

preparative column (Figure 39) and a very similar result to the binary method was achieved. Only two major differences were observed; peaks 2 and 3 had greater resolution by method A (Airs *et al.*, 2001) and the co-eluting peaks 5 and 6 had slightly better resolution by the binary method. Thus, the binary method can also be used in the preparative HPLC of sediment samples containing a limited number of components.

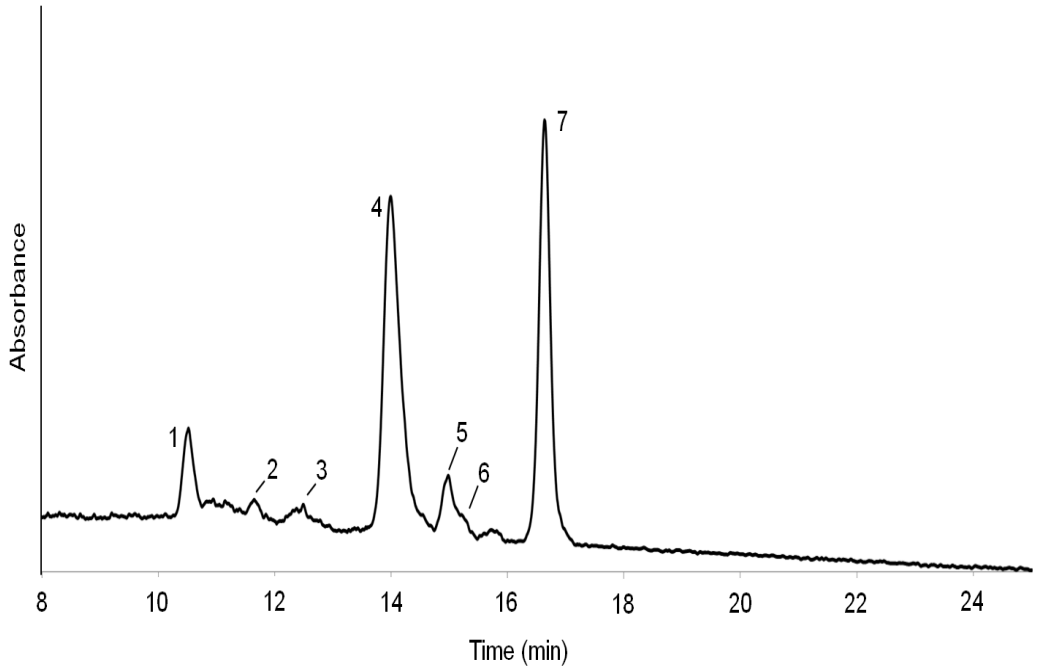

Figure 38. Partial RP-HPLC-UV/vis chromatogram (350-800 nm) of Lake Chiprana pigment extract subjected to acid methanolysis and analysed by the binary method developed for preparative HPLC.

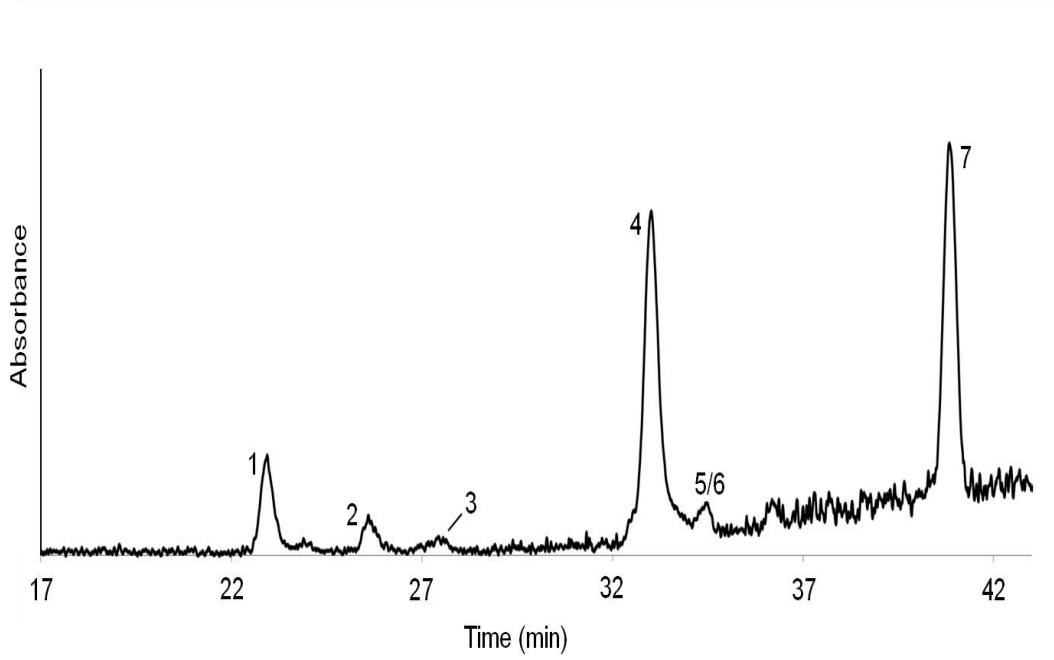

Figure 39. Partial RP-HPLC-UV/vis chromatogram (350-800 nm) of Lake Chiprana pigment extract subjected to acid methanolysis and analysed by method A (Airs *et al.*, 2001).

3.4.7. Preparative HPLC validation

The fraction collector available for this work collects fractions based on UV/vis output from the PDA detector. Based on experimental results, a threshold value for detector response was set as a trigger for collection to avoid collection of very minor components. The Me pyrophaeophorbide *a* standard was used to experimentally determine the collection threshold values of 0.079, 0.036, 0.026, 0.004 AU, which correspond in turn to fraction collector threshold collection parameters, levels 2, 3, 4 and 5 (arbitrary units). Level 3 (0.036 AU) was chosen as the threshold setting for isolation of components from complex samples as the majority of the peak is collected at this level and the collector does not respond to baseline noise (Figure 40).

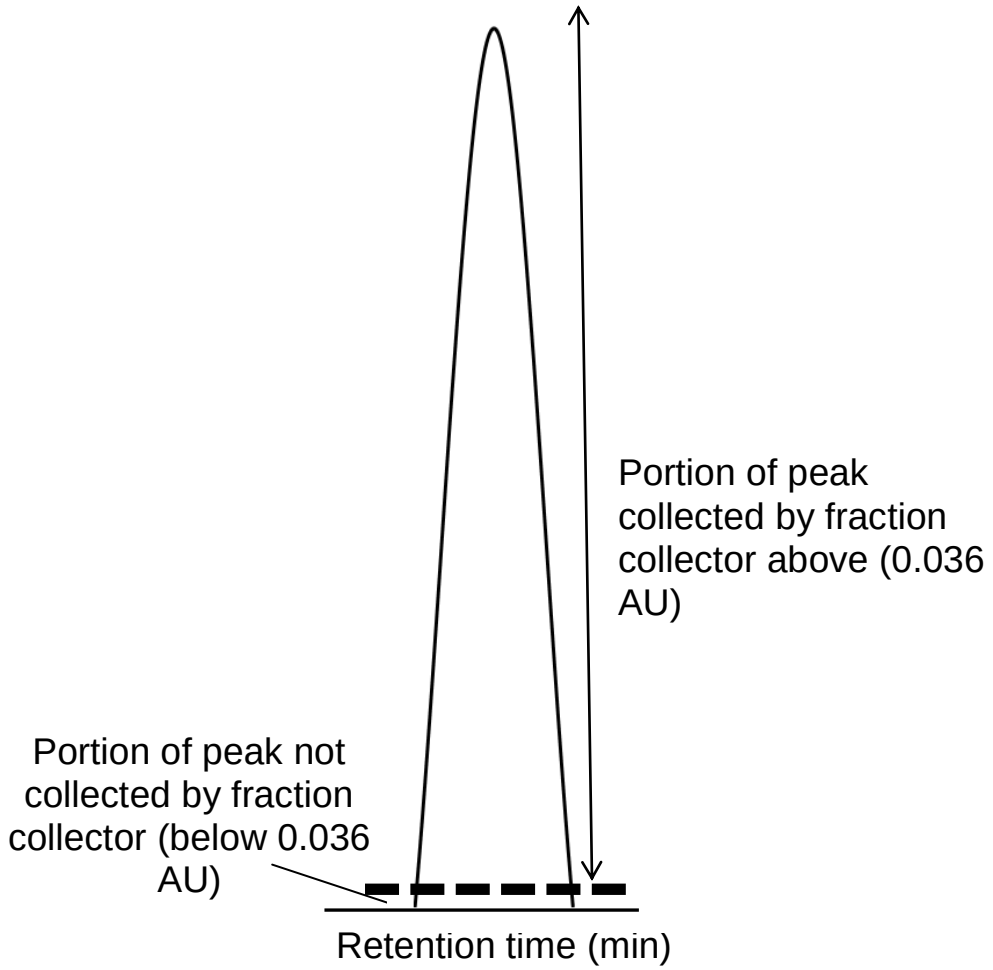

Figure 40. Model peak showing dashed line denoting response threshold of fraction collector formulated for level 3.

Prior to its use in preparative HPLC of samples for CSRA, the performance of the HPLC fraction collector was established by determining the recovery and repeatability of the collection of target compounds. A pigment rich sediment from Lake Chiprana was selected to verify the inter–batch repeatability and total recovery of compounds from the preparative HPLC system used in this study. The sediment was mixed to create a greater pool of available pigments, then extracted with acetone using ASE and subjected to acid methanolysis and analysed by HPLC with PDA detection using method A (Airs *et al.*, 2001) and the analytical column due to the complex distribution of pigments. The most abundant compounds, were carotenoids (labelled c, Figure 41), bacteriophaeophytin *a*, phaeophytin *a* and pyrophaeophytin *a* (peaks 6, 9 and 12,

Figure 41). All of the components were identified by their UV/vis spectrum and retention time with reference to Airs *et al.* (2001) and Wilson (2004), see Table 9.

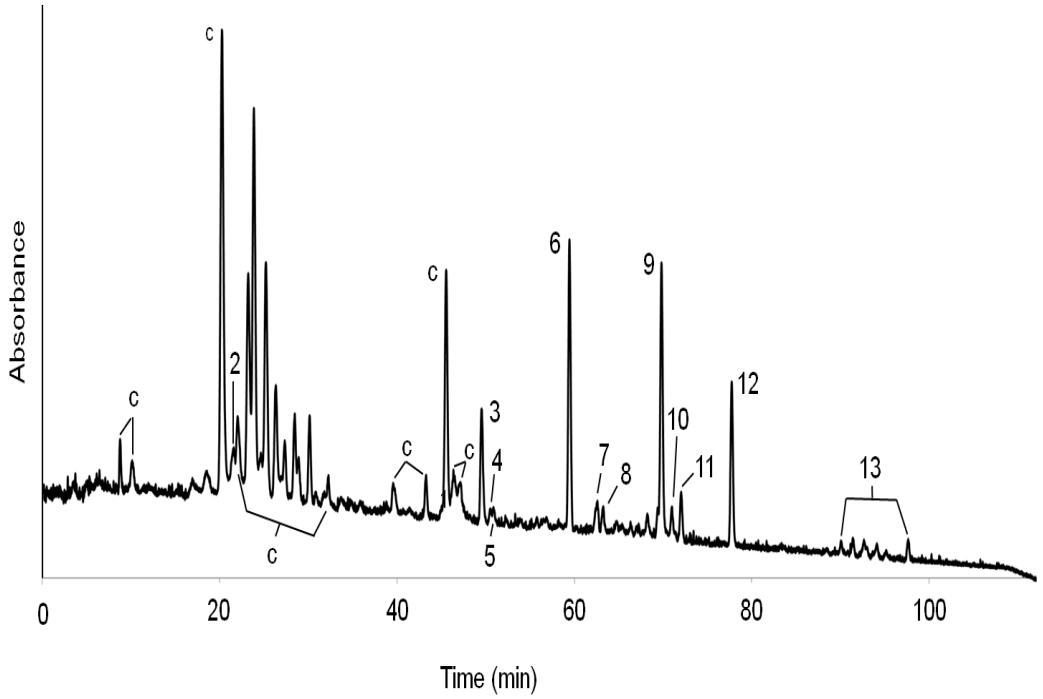

Figure 41. RP-HPLC-UV/vis chromatogram (350-800 nm) of mixed Chiprana sediment extracted by acetone and analysed with method A (chromatogram provided by N. Saesaengseerung).

Table 9. Assignment of components in mixed Lake Chiprana sediment acetone extract.

Extract Peak	Identification	UV/vis absorption (nm)
1	Carotenoids	-
2	Chlorophyllone (**33**)	610, 660
3	Chlorophyll *a*	431, 663
4	Bacteriophaeophytin	407, 661
5	Bacteriophaeophytin *c*	406, 659
6	Bacteriophaeophytin *a*	357, 523, 747
7	Bacteriophaeophytin *a* epimer	358, 523, 749
8	Phaeophytin *b*	436, 653
9	Phaeophytin *a*	409, 665
10	Pyrophaeophytin *b*	437, 660
11	Phaeophytin *a* epimer	407, 667
12	Pyrophaeophytin *a*	411, 667
13	SCEs	-

Following acid methanolysis of mixed Lake Chiprana sediment extract, the product was subjected to analytical HPLC analysis using method M3 (Wilson *et al.*, 2003). The distribution of compounds shows reduced complexity (Figure 42), with the carotenoids which dominated the early part of the chromatogram for the non-methanolysed total extract (Figure 41) having been removed. A component, BPME *d* [Et, Et] (peak 1, Figure 42), not identified in the non-methanolysed extract chromatogram, was revealed in the acid methanolysis product; it is likely that high abundance carotenoids had previously masked the component. Chlorophyll *a* is not present in Figure 42 because it has been demetallated and trans–esterified by the acid methanolysis procedure to form Me phaeophorbide *a*. The SCEs present in the total extract (Figure 41) are degraded during acid methanolysis and contribute to the Me pyrophaeophorbide *a* signature in the methanolysis products (Figure 42). The total extract showed a greater abundance of phaeophytin *a* (peak 9, Figure 41) than pyrophaeophytin *a* (peak 12, Figure 41). Due to the trans–esterification of several SCE compounds the yield of Me pyrophaeophorbide *a* was increased, resulting in the component having a similar abundance to Me phaeophorbide *a* in the acid methanolysis product (Figure 42). Bacteriophaeophytin *a* is a major component in the mixed Chiprana total extract (Figure 41), but the corresponding phaeophorbide, bacteriophaeophorbide *a*, was not identified amongst the methanolysis products. It is possible that bacteriophaeophorbide *a* was oxidised to form type II products as the acid methanolysis procedure was carried out in air. The assignments of the peaks identified in the acid methanolysis product of mixed Lake Chiprana sediment are listed in Table 10.

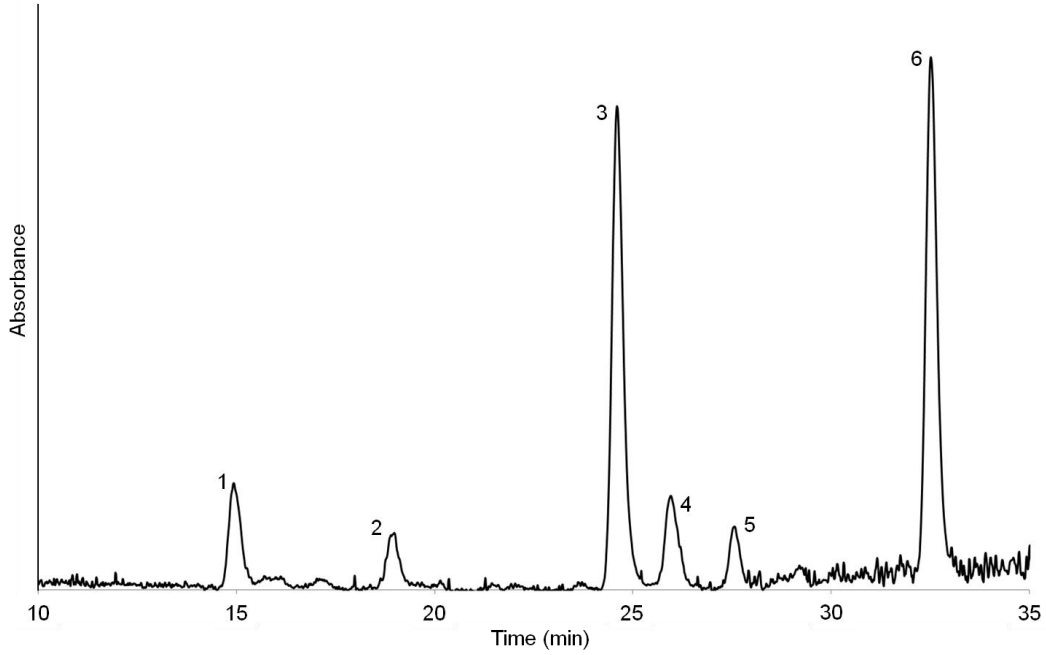

Figure 42. Partial RP-HPLC-UV/vis chromatogram (350-800 nm) of mixed Lake Chiprana sediment extracted by acetone then subjected to acid methanolysis and analysed with method M3 (Wilson *et al.*, 2003).

Table 10. Assignment of components in the mixed Chiprana sediment extracted by acetone and subjected to acid methanolysis.

Acid methanolysis Peak	Identification	UV/vis absorption (nm)
1	BPME *d* [Et,Et]	405, 653
2	Me phaeophorbide *b*	435, 650
3	Me phaeophorbide *a*	407, 664
4	Me pyrophaeophorbide *b*	406, 663
5	Me phaeophorbide *a* epimer	404, 662
6	Me pyrophaeophorbide *a*	409, 665

Preparative isolation of the mixed Lake Chiprana methanolysis products was carried out in batches of five 10 µL injections to assess the repeatability of the isolation of Me phaeophorbide *a* and Me pyrophaeophorbide *a* by the HPLC fraction collector using the binary method (Table 6). An optimum sample concentration of ca. 0.25 mg/ml had been previously established for preparative isolation using the Me pyrophaeophorbide *a* standard. The methanolysis products were dissolved in acetone to achieve a total concentration of 0.48 mg/mL, resulting in a concentration of 0.20 mg/mL for Me phaeophorbide *a* and

0.17 mg/ml Me pyrophaeophorbide *a* (determined by HPLC peak area by assuming the same molar extinction co-efficient for each derivative). Two fractions, corresponding to the most abundant components (peaks 3 and 6, Figure 42), were collected from each preparative analysis, with a total of eleven batches of Me phaeophorbide *a* and Me pyrophaeophorbide *a* being isolated. The repeatability of the system used in this study was determined by the amount of Me phaeophorbide *a* and Me pyrophaeophorbide *a* collected per batch both by UV/vis spectrophotometry and by HPLC peak area measurement. The recovery of analytes from the preparative HPLC system was determined by comparing the mass of Me phaeophorbide *a* or Me pyrophaeophorbide *a* in the methanolysis product with the total amount of each compound isolated during preparative HPLC.

3.4.8. Determination of inter-batch repeatability for Me phaeophorbide a

Similar masses were determined by UV/vis for Me phaeophorbide *a* in each of the isolated batches, except for batch 2, which had an anomalously high mass (11.9 µg) (Table 11). Batch 2 had the largest mass as it was contaminated with a small amount of Me pyrophaeophorbide *a* (27.7% of the total HPLC peak area) (Figure 43). The contamination is likely to be due to a one-off procedural error, rather than as a consequence of the methods used, because no other batches were contaminated. Discounting the contribution of the contaminant, the mass of Me phaeophorbide *a* is 8.60 µg for batch 2, which is comparable to the masses determined by UV/vis for the other batches (Table 11).

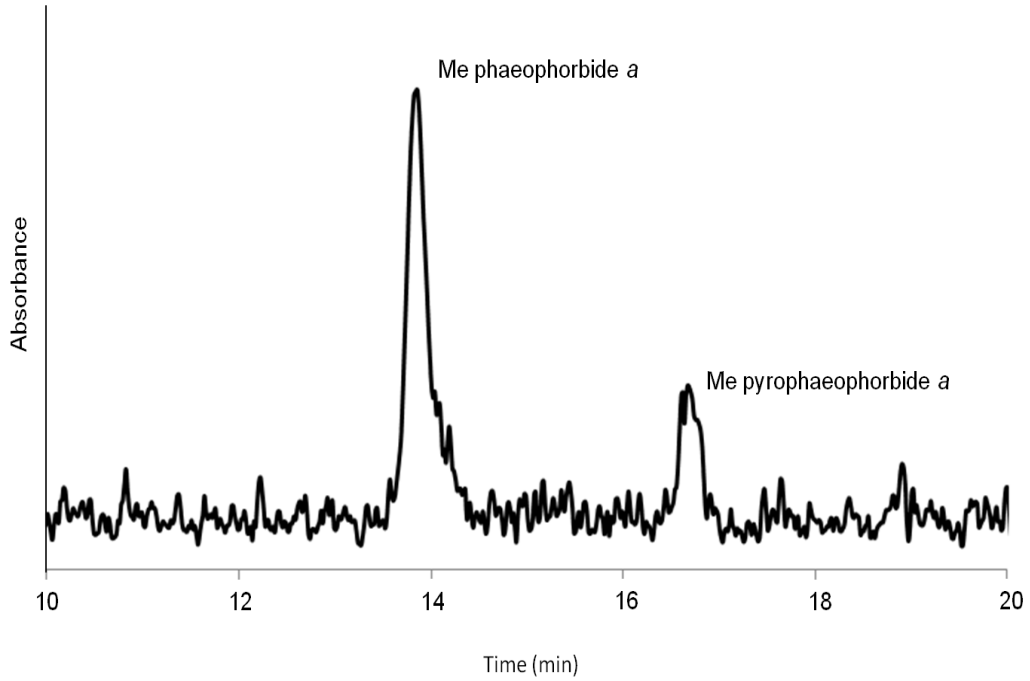

Figure 43. Partial RP-HPLC-UV/vis chromatogram (350-800 nm) of the contaminated Me phaeophorbide *a* fraction (batch 2) preparatively isolated from the mixed Lake Chiprana acid methanolysis products.

The masses determined for Me phaeophorbide *a* by HPLC peak area show a strong agreement for all eleven batches (Table 11). Batch 2 did not have an anomalous mass by HPLC peak area as only the peak area attributed to Me phaeophorbide *a* was measured and thus a corrected value was not required to be calculated (Table 11). From inspection of Table 11 the masses determined by UV/vis and HPLC peak area in batches 4, 8 and 9 were similar relative to one another. For example, batch 4 has the fifth largest mass by UV/vis and the fourth by HPLC. The relative standard deviation between mass measurements was ± 5.3% by UV/vis (corrected batch 2 mass was used) and ± 12.7% by HPLC measurement (Table 11), thus the inter-batch repeatability for phaeophorbide *a* was good.

Table 11. Determination of the inter–batch repeatability based on masses determined for Me phaeophorbide *a*.

Batch number	Mass (µg) by UV/vis	Mass (µg) by HPLC
1	7.06	5.72
2	11.90	4.32
2 (corrected)	8.60	N/A
3	7.75	4.16
4	7.55	4.47
5	7.45	5.21
6	7.80	5.07
7	7.65	4.10
8	8.03	5.50
9	7.23	4.64
10	7.60	6.01
11	7.09	5.41
Average	7.98	4.96
Std deviation	0.42	0.63
Relative standard deviation (%)	5.29	12.69

3.4.9. Determination of total recovery for Me phaeophorbide a

Me phaeophorbide *a* was estimated to represent 40.8% of the methanolysis product based on the total peak area of pigments detected by HPLC analysis (Figure 42). Thus, the concentration of Me phaeophorbide *a* to be subjected to preparative HPLC was 0.195 mg/mL (40.8% of the methanolysis product concentration of 0.48 mg/mL). The concentration of Me phaeophorbide *a* isolated was 0.180 mg/mL as determined by UV/vis, giving a value of injected on column to recovered Me phaeophorbide *a* of 87.4%. The recovery based on HPLC peak area was 91.9%, determined by comparing the HPLC peak area of Me phaeophorbide *a* collected to the theoretical value if no sample had been lost (peak area multiplied by the ratio of on column to recovered compound masses).

The mass of Me phaeophorbide *a* purified by preparative HPLC was 85.2 µg (determined by UV/vis), which was isolated from a starting mass of 107.2 µg (40.8% of the total mass of methanolysis product (263.4 µg)). The recovery

estimated by UV/vis was 79.5%, which is lower than the estimated recovery from HPLC peak area. This is due to the omission of batch 2 from the combined Me phaeophorbide *a* sample.

3.4.10. Determination of inter-batch repeatability and total recovery for Me pyrophaeophorbide a

The mass of Me pyrophaeophorbide *a* determined by UV/vis was similar for all eleven batches, with batches 7 and 8 having the greatest masses (6.86 µg) and batch 9 the lowest (4.73 µg) (Table 12). The masses of Me pyrophaeophorbide *a* determined by HPLC peak area are comparable to each other; batch 10 had the highest mass (5.72 µg) and batch 9 the lowest (3.48 µg) (Table 12). From inspection of Table 12 four batches (3, 8, 10 and 11) show good correspondences between the mass determined by UV/Vis and by HPLC peak area. For example, batch 8 has the tenth largest mass by UV/vis and the ninth by peak area. Inter-batch repeatability of Me pyrophaeophorbide *a* (Table 12) was determined in the same manner as for Me phaeophorbide *a*. The relative standard deviation in the mass of Me pyrophaeophorbide *a* recovered was ± 10.3% by UV/vis measurement and ± 14.4% by HPLC peak area (Table 12). Thus, the inter-batch repeatability for the isolation of Me pyrophaeophorbide *a*, whilst slightly lower than for Me phaeophorbide *a*, was acceptable.

Table 12. Determination of inter-batch repeatability based on masses determined for Me pyrophaeophorbide *a*.

Batch number	Mass (µg) by UV/vis	Mass (µg) by HPLC
1	5.85	5.38
2	6.51	5.46
3	6.12	4.85
4	6.26	3.71
5	6.10	4.95
6	6.63	4.84
7	6.86	4.77
8	6.86	5.42
9	4.73	3.48
10	6.66	5.72
11	5.32	4.22
Average	6.17	4.80
Standard deviation	0.63	0.69
Relative standard deviation (%)	10.29	14.44

The proportion of Me pyrophaeophorbide *a* in the mixed Lake Chiprana methanolysis product was calculated to be 34.4% (Figure 42), thus the recovery of Me pyrophaeophorbide *a* by HPLC peak area was determined to be 96.5%. The total mass of isolated material determined by UV/vis was 78.4 µg, which was isolated from a starting mass of 90.4 µg, thus the recovery estimated by UV/vis was 86.7%. The difference between recovery and repeatability determined by HPLC and UV/vis analysis could be the dilution volume used for each technique. For example sample batches were diluted in a much greater volume of acetone for UV/vis analysis (3 mL versus 0.5 mL for HPLC analysis), which provided a more accurate concentration.

The preparative HPLC system has demonstrated sufficient repeatability and recovery of Me phaeophorbide *a* and Me pyrophaeophorbide *a*. Thus it can be used in the preparative isolation of compounds for CSRA.

3.5. Radiocarbon analysis

3.5.1. Isotopic fractionation

Isotopic fractionation can be caused by subjecting compounds to liquid chromatography; compounds containing a ^{14}C isotope can elute in the latter portion of the peak compared to those containing ^{12}C and ^{13}C only (Baumann *et al.*, 1992). The Me pyrophaeophorbide *a* standard was used to investigate if isotopic fractionation was caused by preparative HPLC isolation. The fraction collector was used in timed collection mode to split the standard peak in two. The sharpness of the peak apex for Me pyrophaeophorbide *a* peak and narrow peak width made it difficult to collect two portions of the same magnitude. Hence, the first portion collected (83.9 µg) encompassed both the first half of the peak and the area corresponding to the 1st standard deviation (68%) of the second half of the peak (Figure 44). The second portion of the peak collected (19.6 µg) comprised the remaining 32% of the second half of the peak (Figure 44). If isotopic fractionation were to occur during HPLC, the first portion of the peak would be expected to be radiocarbon poor and the second portion radiocarbon rich (Figure 44). Both portions of the split standard peak were subjected to radiocarbon analysis, with the comparison of the measurements expected to reveal if fractionation had occurred (see Chapter 4).

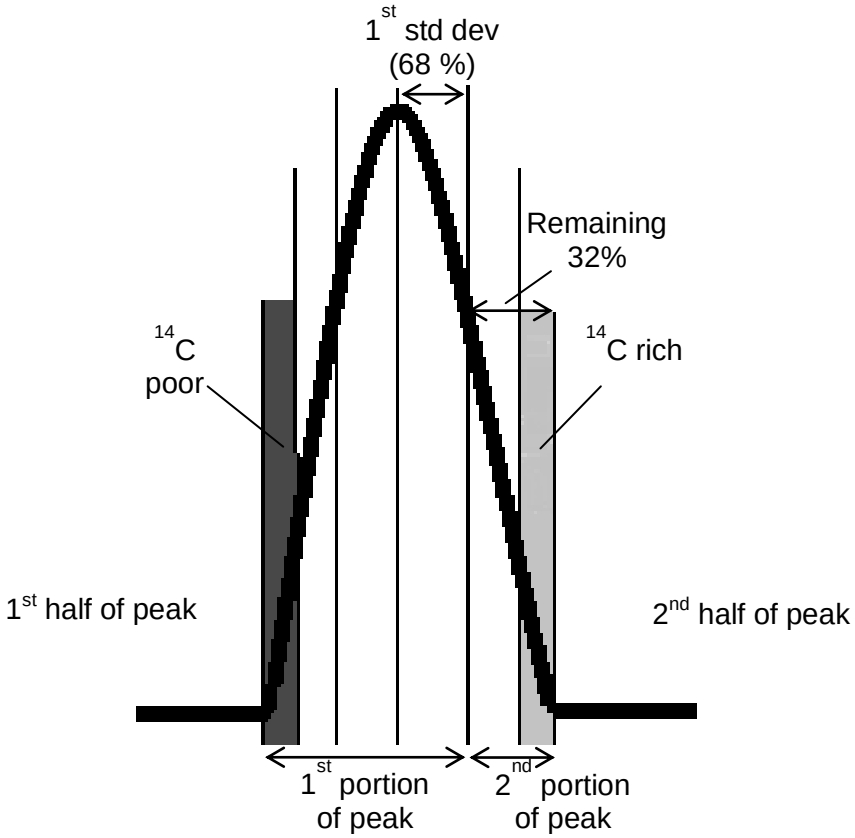

Figure 44. Model peak with potential isotopic fractionation biases and areas of peak comprising each portion collection.

3.5.2. Determination of the sediment mass required to achieve sufficient sample for CSRA

Me phaeophorbide *a* is theoretically 71.3% carbon, thus 60.7 µg of the Me phaeophorbide *a* isolated from the mixed Lake Chiprana methanolysis product by preparative HPLC was carbon. Based upon radiocarbon analysis requiring 20 µg of carbon, three replicates of Me phaeophorbide *a* could be analysed. Carbon accounts for 74.5% of Me pyrophaeophorbide *a*, thus 58.4 µg of the isolated Me pyrophaeophorbide *a* is carbon, which allows for two radiocarbon analysis replicates.

The sediment mass used for extraction was 13.33 g and the total extract was subjected to acid methanolysis. Following extraction and trans-esterification by acid methanolysis, the total mass of chl pigment, was estimated to be ca. 1.7 mg by UV/vis. A portion of the acid methanolysis product corresponding to 15.6% (0.26 mg) was subjected to repetitive preparative HPLC and 85.2 µg of Me

phaeophorbide *a* and 78.4 µg of Me pyrophaeophorbide *a* were isolated. The masses of Me phaeophorbide *a* and Me pyrophaeophorbide *a* isolated was sufficient for triplicate and duplicate CSRA, respectively. Thus, the use of ASE, acid methanolysis and preparative HPLC required 2.08 g of mixed Chiprana sediment to provide an adequate mass of two single compounds for CSRA. This determination can be used to estimate the amount of sediment required from other sites with similar pigment abundances/g of TOC to Lake Chiprana. Similar sediments could be collected either as a 5 cm diameter core, from which a ¼ of a 1 cm layer (ca. 2.5 g) could be used, or as a 1.25 cm diameter core, from which a whole 1 cm layer is used to yield sufficient pigments for CSRA.

3.6. Conclusions

A stock of sufficiently pure Me phaeophorbide *a* standard for radiocarbon analysis was created by subjecting a BCC crude preparation to acid methanolysis, followed by a acid numbering extraction and purification by preparative HPLC. Modification of the acid numbering extraction procedure from previous methods to a stepwise process using 8 and 11% (w/v) HCl was essential to minimise de-esterification of Me pyrophaeophorbide *a* to the free acid. Preparative HPLC purified Me pyrophaeophorbide *a* by removing low abundance pigment impurities. Splitting the Me pyrophaeophorbide *a* peak using the fraction collector during elution of a small batch of standard yielded material from which potential isotopic fractionation caused by the preparative HPLC system could be assessed.

The trans-esterified pigment extract of Lake Chiprana was used to determine the inter-batch repeatability and total recovery of compounds isolated from a pigment-rich sediment extract by preparative HPLC. Both compounds isolated had high recoveries; 91.9% by HPLC peak area and 79.5% by UV/vis for Me phaeophorbide *a* and 96.5% by peak area and 86.7% by UV/vis for Me pyrophaeophorbide *a*. Repeatability was determined by comparison of the mass determined by UV/vis and by HPLC peak area of each compound collected per batch. The relative standard deviation of the mass determined by peak area are similar for both compounds; ± 12.7% for Me phaeophorbide *a* and ± 14.4% for Me pyrophaeophorbide *a*. The relative standard deviations of the masses

determined by UV/vis for Me phaeophorbide *a* were ± 5.3% and ± 10.3% for Me pyrophaeophorbide *a*, which are comparable to each other. Similarities in the relative standard deviations determined for the eleven batches of Me phaeophorbide *a* and Me pyrophaeophorbide *a* provides confidence that the preparative HPLC system gives repeatable results. The HPLC analysis of Me phaeophorbide *a* from batch 2 revealed that it had been contaminated. Accordingly, the standard deviation in mass recovered was determined by UV/vis excluding that batch. The total amount of isolated Me phaeophorbide *a* (85.5 µg) and Me pyrophaeophorbide *a* (78.4 µg) provides 60.7 µg and 58.4 µg of carbon, respectively, which would be adequate for CSRA by AMS. Total recovery of each compound was excellent, maximum values being 92% for Me phaeophorbide *a* and 97% for Me pyrophaeophorbide *a*. Thus, the evaluation of the preparative HPLC system shows it to be suitable for sample preparation for CSRA, as low relative standard deviations between the isolated mass determinations indicate good inter-batch repeatability and excellent total recovery was determined. The calculated mass of sediment (ca. 2 g) required for CSRA is a realistic one and could provide cm layer resolution from 1.25 cm diameter sediment core that has similar pigment abundances to Lake Chiprana.

Chapter 4. Compound specific radiocarbon analysis

4.1. Introduction

Sediments from two lacustrine sites of geochemical interest were selected to test the experimental protocols devised for CSRA (Chapter 3). The target compounds for CSRA for this work were photosynthetic pigments derived from prokaryotes and eukaryotes that lived in the water columns of the study sites at the time the sediments were deposited. Sedimentary chlorophyll and bacteriochlorophyll pigments from both locations have previously been profiled (Squier *et al.*, 2002; Wilson *et al.*, 2005) and it is known that the sediments contain sufficient pigment mass (Vidondo *et al.*, 1993; Squier *et al.*, 2002) to be subjected to the experimental plan.

4.1.1. Kirisjes Pond, Larsemann Hills

The Larsemann Hills, a region spanning 50 km^2, is the second largest ice free oasis in Antarctica; it incorporates over 150 freshwater lakes within its boundaries (Squier *et al.*, 2002). The region (Figure 45) comprises two mainland peninsulas (Stornes and Broknes) and several offshore islands including Kolloy Island (Hodgson *et al.*, 2001). The bedrock of the Larsemann Hills comprises proterozoic gneiss, leucogneiss and migmatitic paragneiss (Kiernan *et al.*, 2009). The area is of palaeolimnological importance as it remained ice free during the last glacial maximum, hence, it could contain the oldest sedimentary record in eastern Antarctica (Hodgson *et al.*, 2001). Sediments from several Larsemann Hills lakes have been subjected to bulk radiocarbon analysis. For example, Lake Reid and Progress Lake on the Broknes peninsula gave basal dates greater than 39,700 and 44,000 $^{14}C\ yr_{BP}$, which both are near the limit of radiocarbon analysis (Hodgson *et al.*, 2001). On the Stornes transect the basal dates were all determined to be less than 6000 yr_{BP}, excluding Kirisjes Pond which had a basal date of > 43,200 $^{14}C\ yr_{BP}$, thus it can be concluded that Kirisjes Pond was ice free during the last glacial maximum (ca. 21,000 years ago) (Hodgson *et al.*, 2001). Due to the altitude of Kirisjes Pond (7 m above sea level (a.s.l), (Squier *et al.*, 2002)), its current location 225 m from the sea (Verleyen *et al.*, 2004) and its long sedimentary record established by bulk radiocarbon dates (Hodgson *et al.*, 2001), it is of great importance in constraining local sea level changes. Alterations in sea level can be linked to regional ice sheet cover (Squier *et al.*,

2002), and by subjecting sediments to CSRA which have been effected by sea level fluctuations could provide information on the presence or absence of ice sheets.

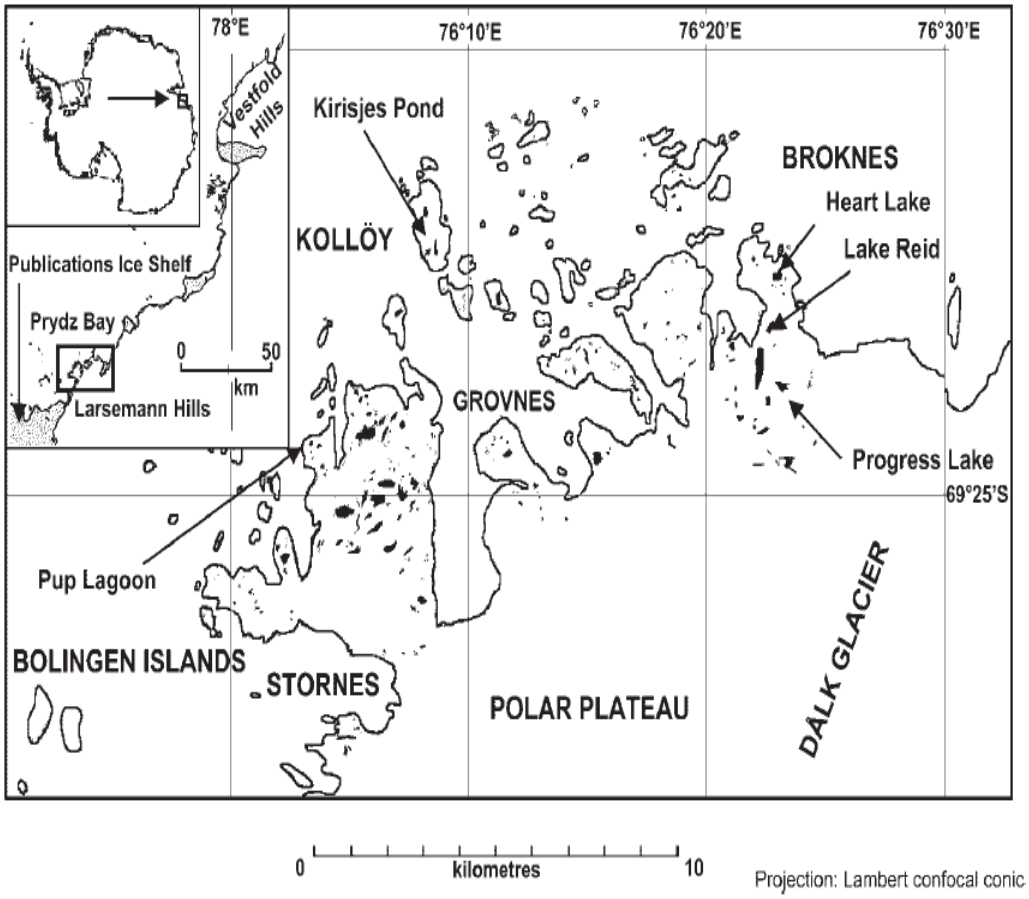

Figure 45. Map of the Larsemann Hills region showing the location of Kirisjes Pond (Verleyen *et al.*, 2004).

Sedimentary photosynthetic pigments in Kirisjes Pond have previously been profiled intensively, revealing the presence of derivatives from both oxygenic and anoxygenic photoautotrophs (Squier *et al.*, 2002; Wilson *et al.*, 2004; Wilson *et al.*, 2005). Three distinctly different depositional environments have been shown to have existed over the history of the pond. The oldest of which is a freshwater phase and has a pigment signature dominated by chl *a* and *b* derivatives including phaeophytins, phaeophorbides and SCEs, corresponding to 112–144 cm core depth. The radiocarbon ages for this zone were ca. 6525–11195 uncalibrated ^{14}C yrs $_{BP}$ (Squier *et al.*, 2002). The middle zone (94–110 cm depth, ca. 6285–6525 uncalibrated ^{14}C yrs $_{BP}$) was distinguished from the sediments below by a dramatic increase in pigment content. This is thought to be due to an

influx of sea water effectively fertilising the pond, causing a bloom in primary productivity which led to the formation of anoxygenic conditions and a bloom of bacterial primary production (Squier *et al.*, 2002). Thus bacteriochlorophyll *c* and *d* derivatives were the most dominant pigment components in this zone (Squier *et al.*, 2002) with the base layers of the section characterised by a high abundance of marine diatoms (Verleyen *et al.*, 2004). Bacterial pigments with greater degrees of alkylation at positions C8 (for example *n*-propyl or *i*–butyl instead of ethyl) and C12 (ethyl in place of methyl) (see Figure 46) were predominant in the upper layers of the section (Wilson *et al.*, 2004). The occurrence of increased alkylation in bchl *e* homologues has been reported by Borrego *et al*. (1997) as a marker for light restriction in meromictic lakes. High bacterial primary productivity may cause light restriction due to self shading, thus leading to the formation of derivatives with increased alkylation.

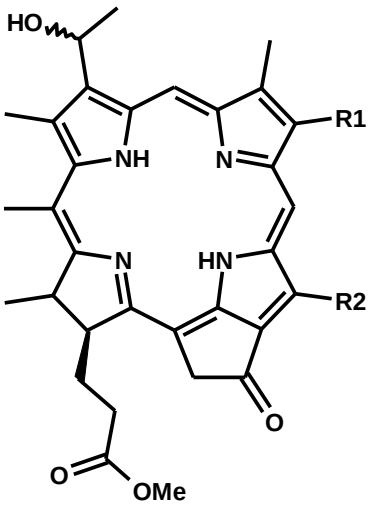

32

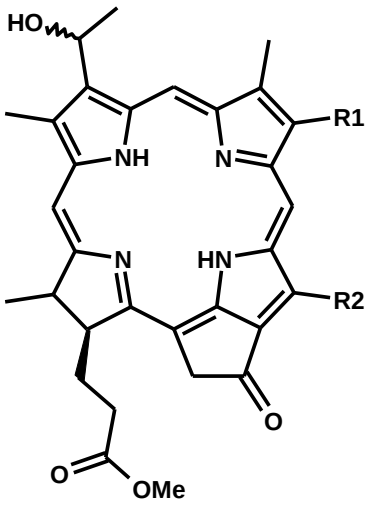

31

Figure 46. Structures of BPME *c* (**32**) and BPME *d* (**31**), R1 = Et, *n*-Pr, *i*-Bu and R2 = Me or Et.

The uppermost zone of the core (surface to 88 cm) yielded radiocarbon ages of modern to 6205 ^{14}C yrs $_{BP}$ (Hodgson *et al.*, 2001). The pigments reflect a return to freshwater conditions with phaeophytin *a* and pyrophaeophytin *a* dominating the distributions (Squier *et al.*, 2002). Phaeophorbide derivatives and SCEs were of much lower abundance than in the bottom zone (first fresh water phase) suggesting that zooplankton communities were not re-established in the water

column following transition from the anoxic conditions which resulted from the marine incursion (Squier *et al.*, 2002).

4.1.2. Rationale for CSRA of Kirisjes Pond pigments

Photosynthetic derivatives from sediments in the marine zone (94 – 110 cm) and from layers in the surrounding freshwater zones were targeted for CSRA as they could provide radiocarbon ages of their source organisms and thus estimates of the date of sediment formation. CSRA of algal and bacterial pigments would constrain the time when the marine incursion occurred and hence the timing of the local sea level rise. A further perceived benefit of CSRA of Kirisjes Pond pigments was the ability to compare and contrast the results with those from the bulk ^{14}C measurements.

4.1.3. Lake Chiprana

Lake Chiprana (known in Spanish as Salada de Chiprana) is a hypersaline lake located in the Ebro basin, surrounded by the Pyrenees, Iberian and Catalan mountain ranges (Valero-Garces *et al.*, 2000). The bedrock of catchment area of Lake Chiprana is predominately limestone (Morellon *et al.*, 2008). The lake, situated 130 m a.s.l comprises three basins with sandstone palaeochannels extending over a total area of 31 ha, and it has a maximum depth of 5.6 m (Vidondo *et al.*, 1993). The water is stratified during the greater part of the year (Vidondo *et al.*, 1993) with the halocline situated between 1.75 and 4.5 m depth (Vila *et al.*, 2002). Both the salinity and the depth of the water are greatly dependent on rainfall (Vila *et al.*, 2002). The salt content of the lake is dominated by magnesium sulfate and sodium chloride (salinity 30 to 73‰ during the hydrological cycle of 1989) (Vidondo *et al.*, 1993). Cyanobacterial mats overlie the sediments and relict features are dominant above 1.5 m (Vidondo *et al.*, 1993). The hypolimnion of Lake Chiprana is anoxic during periods of stratification. Primary production in this layer is dominated by green sulfur bacteria and specifically the species *Chlorobium vibrioforme* (Vila *et al.*, 2002). Sedimentary photosynthetic pigments of bacterial origin were profiled by Wilson *et al.* (2005) who subjected sediment extracts to acid methanolysis before analysis. Acid methanolysis allowed the identification of side chain modifications

at C8 and C12 of bacteriophaeophorbide methyl esters *c* and *d* (Wilson *et al.*, 2005). The identification of BPMEs *c* and *d* with increased alkylation at C8 and C12 (for example *n*-Pr, Et and *i*-Bu, Et) and the high abundance of BPME *c* [*n*-Pr, Et] (see Figure 46 for structures) suggests that light was restricted (Wilson *et al.*, 2005). Sediment was sampled from Lake Chiprana using a box core, comprising the surface sediment to 12 cm depth. A section of sediment from the centre of the core was removed and divided into 1 cm layers (12 in total).

4.1.4. Rationale for CSRA of Lake Chiprana pigments

The Sediment layers from Lake Chiprana contain both oxygenic and anoxygenic photosynthetic pigments (for example, pyrophaeophytin *a* and bacteriophaeophytin *d,* respectively). It is postulated that pigments synthesised by green sulfur bacteria in the anoxic hypolimnion will have older radiocarbon ages than contemporary oxygenic pigments synthesised by algae in the epilimnion. Algal pigment derivatives can be expected to have younger radiocarbon ages because the source organism would have assimilated CO_2 with an atmospheric carbon isotope signature. By contrast, the CO_2 available to bacteria in the hypolimnion would have been limited in its capacity for exchange with the atmosphere due to stratification and would incorporate more carbon from heterotrophy (which releases CO_2 from relict OM), leading to older radiocarbon ages than expected. This effect is likely to be exacerbated due to the limestone bedrock surrounding Lake Chiprana. Due to the potential age discrepancy of pigment derivatives located within the same sedimentary layer it may be possible to estimate the reservoir effect.

4.2. Results and discussion

4.2.1. Analysis of Lake Chiprana sediment

Each horizon was from Lake Chiprana was processed according to the experimental plan outlined in Chapter 3 (section 3.3.1). HPLC analysis with online PDA detection of two methanolysis products (3 and 11 cm depth) showed that they did not contain any photosynthetic pigments above the LOD. Analysis of the methanolysis product from 8 cm depth revealed the presence of Me

phaeophorbide *a* and Me pyrophaeophorbide *a,* although not in sufficient abundance to be considered for isolation by preparative HPLC. The most abundant component in the deepest pigment-containing layer (10 cm depth) was Me phaeophorbide *a*, identified by its retention time of 28.1 min and maximum absorbance of 407 and 663 nm (peak 3, Figure 47), followed by Me pyrophaeophorbide *a* which had a t_R = 39.6 min and maximum absorbance of 409 and 665 nm (peak 7, Figure 47). The distribution of algal derivatives were similar in all pigment-containing layers, see for example 0 cm depth (Figure 48) compared with 10 cm depth (Figure 47). To identify peak 1 (Figure 47), peak 2 (Figure 47 and Figure 48) and two additional component revealed by HPLC analysis in several layers between 0 and 10 cm (peaks 5 and 6, Figure 48), samples were subjected to $LCMS^n$. Peak 1 (Figure 47) had a $[M+H]^+$ at *m/z* 576, thus it was identified as BPME *d* [Et,Me] and it was only present in the deepest portion of the core. Peak 2 (Figure 47 and Figure 48) had a $[M+H]^+$ at *m/z* 581 and fragmentation pattern consistent with BPME *d* [Et,Et] as reported by Wilson *et al.* (2005). The abundance of BPME *d* [Et,Et] changed between 10 (Figure 47) and 0 cm depth (Figure 48) as it became more abundant in the upper section of the core. All of the components revealed in Figure 47 and Figure 48 are identified in Table 13.

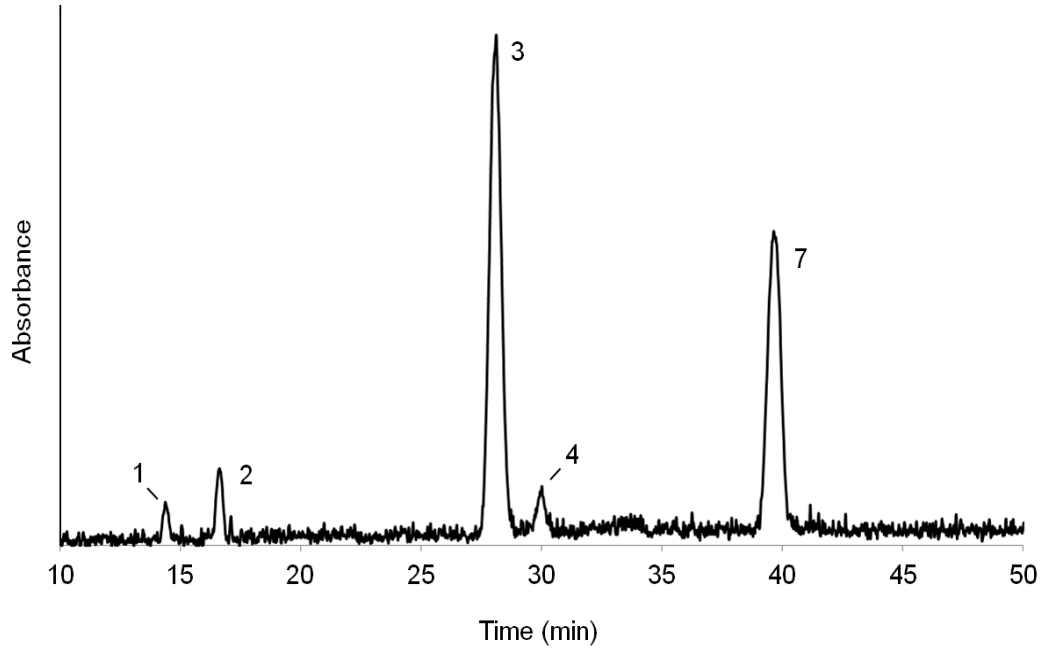

Figure 47. Partial RP-HPLC-UV/vis chromatogram (350-800 nm) of the acid methanolysis product from Lake Chiprana 10 cm depth.

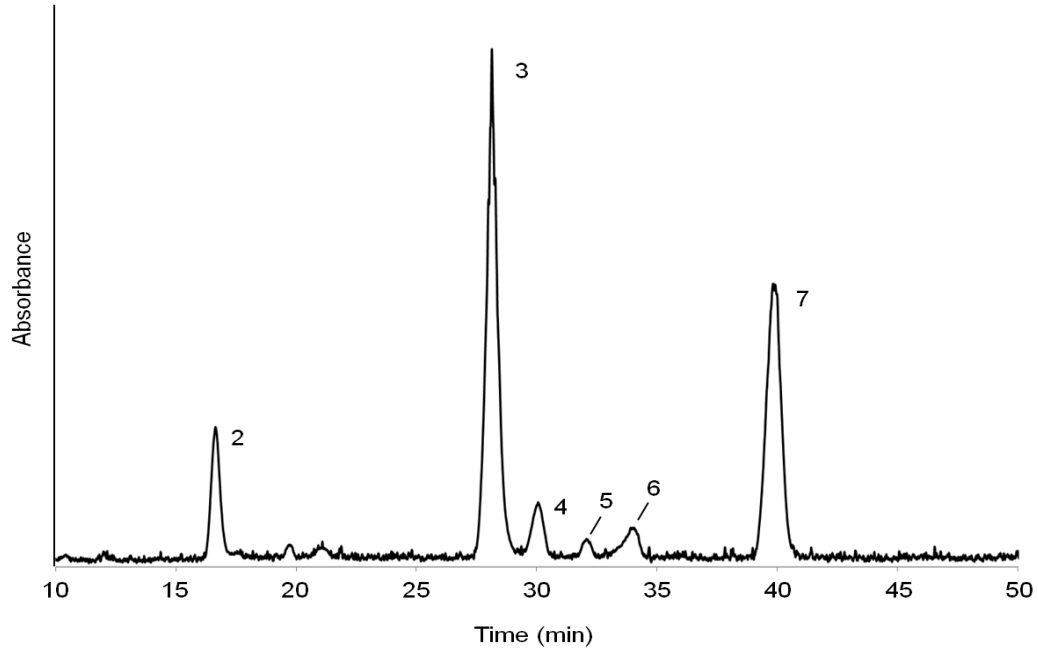

Figure 48. Partial RP-HPLC-UV/vis chromatogram (350-800 nm) of the acid methanolysis product from Lake Chiprana 0 cm depth.

Table 13. Identification of components revealed in Lake Chiprana.

Peak	Molecular ion (*m/z*)	Identification
1	576	BPME *d* [Et,Me]
2	581	BPME *d* [Et,Et]
3	607	Me Phaeophorbide *a*
4	607	Me Phaeophorbide *a* epimer
5	623	Unidentified
6	595	Unidentified
7	549	Me Pyrophaeophorbide *a*

The acid methanolysis products from the pigment-containing layers (nine in total) of Lake Chiprana were subjected to preparative HPLC using method M3 (Wilson *et al.*, 2003) and the most abundant components were isolated (Table 14). Me phaeophorbide *a*, Me pyrophaeophorbide *a* and BPME *d* were recovered from each layer, the mass of each compound isolated was determined by UV/vis spectrophotometry using the Beer-Lambert law and the specific extinction coefficient of Me pyrophaeophorbide *a* (see Chapter 6, Experimental). The contribution of carbon in each isolate was calculated according to its molecular formula: carbon represents 71.3% of Me phaeophorbide *a*, 74.5% of Me pyrophaeophorbide *a* and 72.4% of BPME *d* by mass (Table 14).

Table 14. Identity and masses of compounds isolated from Lake Chiprana acid methanolysis products.

Depth (cm)		Me phaeophorbide *a*	Me pyrophaeophorbide *a*	BPME *d* [Et,Et]
0	mass (µg)	20.5	0.8	5.5
	mass of carbon (µg)	14.6	0.6	4.0
1	mass (µg)	15.0	6.2	2.8
	mass of carbon (µg)	10.7	4.6	2.0
2	mass (µg)	26.0	2.0	3.3
	mass of carbon (µg)	18.5	1.5	2.4
4	mass (µg)	7.6	19.2	6.9
	mass of carbon (µg)	5.4	14.3	5.0
5	mass (µg)	29.3	3.6	5.8
	mass of carbon (µg)	20.9	2.7	4.2
6	mass (µg)	25.8	4.8	0.3
	mass of carbon (µg)	18.4	3.6	0.2
7	mass (µg)	3.1	7.9	0.3
	mass of carbon (µg)	2.2	5.9	0.2
9	mass (µg)	8.9	4.6	2.9
	mass of carbon (µg)	6.3	3.4	2.1
10	mass (µg)	15.4	11.9	1.1
	mass of carbon (µg)	11.0	8.9	0.8

4.2.2. Preparation of sedimentary pigments from Lake Chiprana for CSRA

Based on a requirement of 20 µg of carbon per AMS analysis, insufficient masses of single compounds were isolated to provide measurements at cm resolution, except in the case of Me phaeophorbide *a* from 5 cm depth. Thus, in order to maximise the information that could be gained from the isolated compounds and determine the relative age of sediment collected from Lake Chiprana, Me phaeophorbide *a* fractions were combined in a manner which provided the best stratigraphic resolution. Thus, Me phaeophorbide *a* isolates were grouped to provide five measurements with enough carbon for a single AMS analysis (see Table 15).

Table 15. Strategy for the analysis of Me phaeophorbide *a* isolated from Lake Chiprana sediments.

Layers combined	Mass	Mass of carbon	Replicates
0cm and 1 cm (x 0.5)	28.0	20.0	1
1 cm (x 0.5) and 2cm	33.5	23.9	1
5 cm	29.3	20.9	1
6 cm and 7 cm	28.9	20.6	1
9 cm and 10 cm	24.3	17.3	1

In an attempt to provide an estimate of the reservoir effect in Lake Chiprana, Me pyrophaeophorbide *a* isolated from each layer was combined to achieve a single sample of mass 61.2 µg (45.6 µg of carbon), sufficient for two replicate AMS analyses and BPME *d* isolated from all layers was combined to give a total mass of 28.9 µg (20.9 µg of carbon), sufficient for a single radiocarbon measurement.

Due to time constraints, photosynthetic pigments isolated from Lake Chiprana were not subjected to CSRA.

4.2.3. Analysis of Kirisjes Pond sediment

Sediments from Kirisjes Pond were subjected to the experimental plan developed in Chapter 3 (section 3.3.1). Methanolysis products were selected for isolation of single chlorin compounds and CSRA based on the abundances of pigments and their location within the core.

4.2.4. First freshwater zone (112 – 144 cm depth)

The first freshwater zone of Kirisjes pond is dominated by oxygenic photosynthetic pigments synthesised by algae (Squier *et al.*, 2002). One aim of this work was to constrain the timing of the sea water incursion, thus the deepest sample analysed was from 132 cm as the pond was purely freshwater at this point. TOC contents of 112 to 132 cm depth were determined in order to estimate the mass of pigments in each layer based on preliminary work by Squier *et al*. (2002). Prior to extraction by ASE, samples from adjacent depths were combined if they contained insufficient concentrations of pigments to be isolated for CSRA. Thus, ten depths were combined to create five samples; layers were

combined in pairs between 112 and 117, 120 and 121, and 131 and 132 cm depth (see Figure 52). Following acid methanolysis, Figure 49 shows a typical profile of the deepest layers, it contains only chl *a* (peak 4 Me phaeophorbide *a*, peak 5 its epimer and peak 7 Me pyrophaeophorbide *a*, Figure 49) and chl *b* derivatives (peak 3 Me phaeophorbide *b* and peak 6 Me pyrophaeophorbide *b;* Figure 49). These pigments were identified by their online UV/vis spectra and retention time.

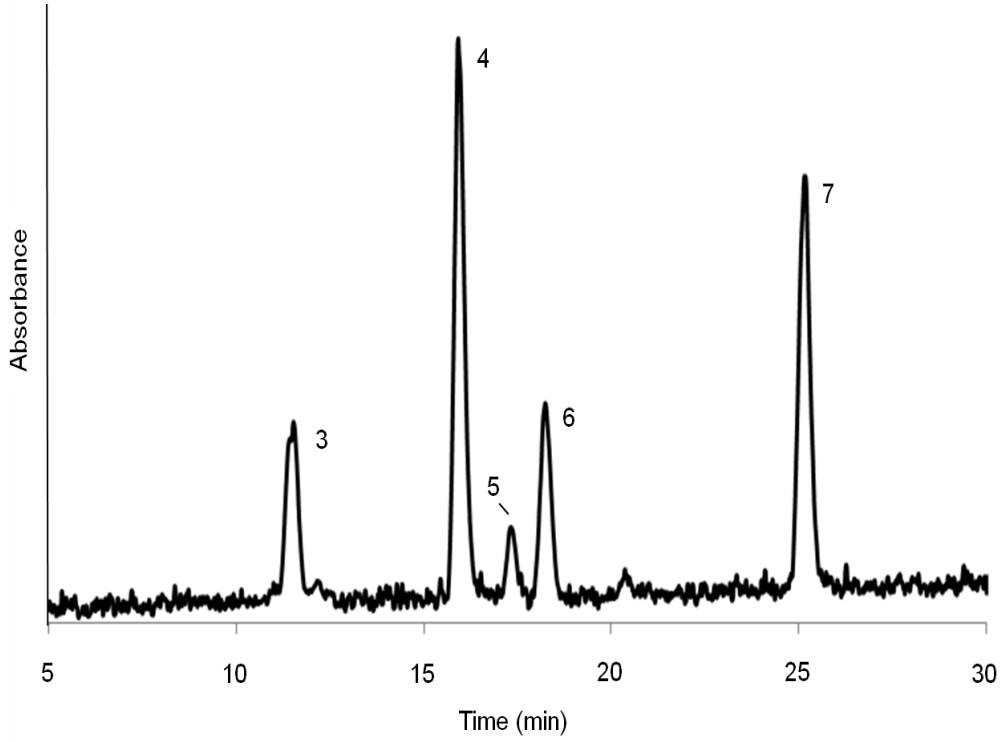

Figure 49. Partial RP-HPLC-UV/vis chromatogram (350-800 nm) of Kirisjes Pond first freshwater zone, 129 and 130 cm depth acid methanolysis product.

The sedimentary pigment profiles at the top of the zone exhibited very similar chl *a*- and *b*-derived pigment profiles as the bottom. Extra components in the upper portion of the zone were revealed by HPLC with UV/vis detection, for example peaks 1 and 2 at 118 cm depth (Figure 50). $LCMS^n$ was used to identify these peaks, peak 1 (Figure 50) had a protonated molecule at *m/z* 581 and a fragmentation pattern consistent with that reported by Wilson *et al.* (2005) for BPME *c* [Et, ME]. Peak 2 (Figure 50) had a $[M+H]^+$ at *m/z* 623 followed by losses of 18 Da and 44 Da which correspond to water and a CH_3CHO substituent, respectively in MS^2 (Figure 51). MS^3 and MS^4 had fragments at *m/z* 577 and

491, which were formed from losses of CO (28 Da) and 86 Da which could correspond to the methyl propionate ester at C17. The protonated molecule in the MS spectrum and subsequent fragmentation patterns identified peak 2 as a BPME *c* derivative. The MS^5 spectrum was used to identify the specific homologue as BPME *c* [*i*-Bu, Et] due to the losses corresponding to methyl, propyl and butyl (Figure 51) (Wilson *et al.*, 2005). The presence of bacterial photosynthetic pigment derivatives in the methanolysis product of 118 cm depth suggests that at the time this horizon was deposited, primary productivity in the pond had increased due to fertilisation of the water from the entry of sea water, which led to stratification of the water column. The occurrence of both algal and bacterial derivatives in one sample is significant as it could allow estimation of the reservoir effect, provided sufficient quantities of components from both sources could be isolated in high purity.

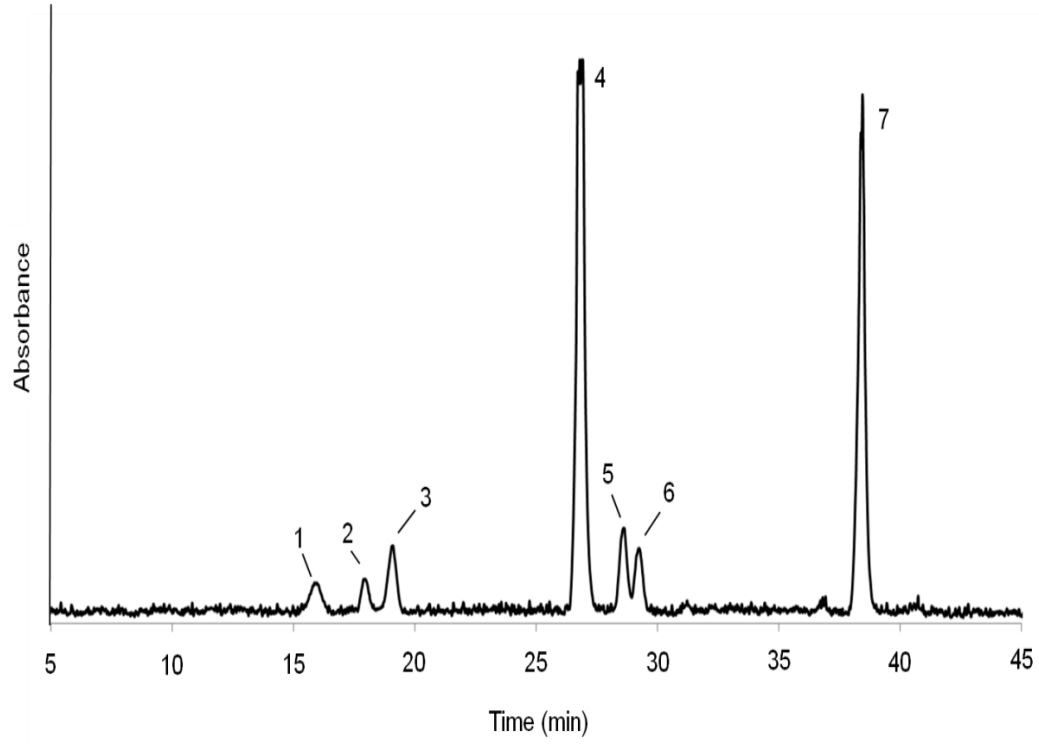

Figure 50. Partial RP-HPLC-UV/vis chromatogram (350-800 nm) of Kirisjes Pond first freshwater zone 118 cm depth acid methanolysis product.

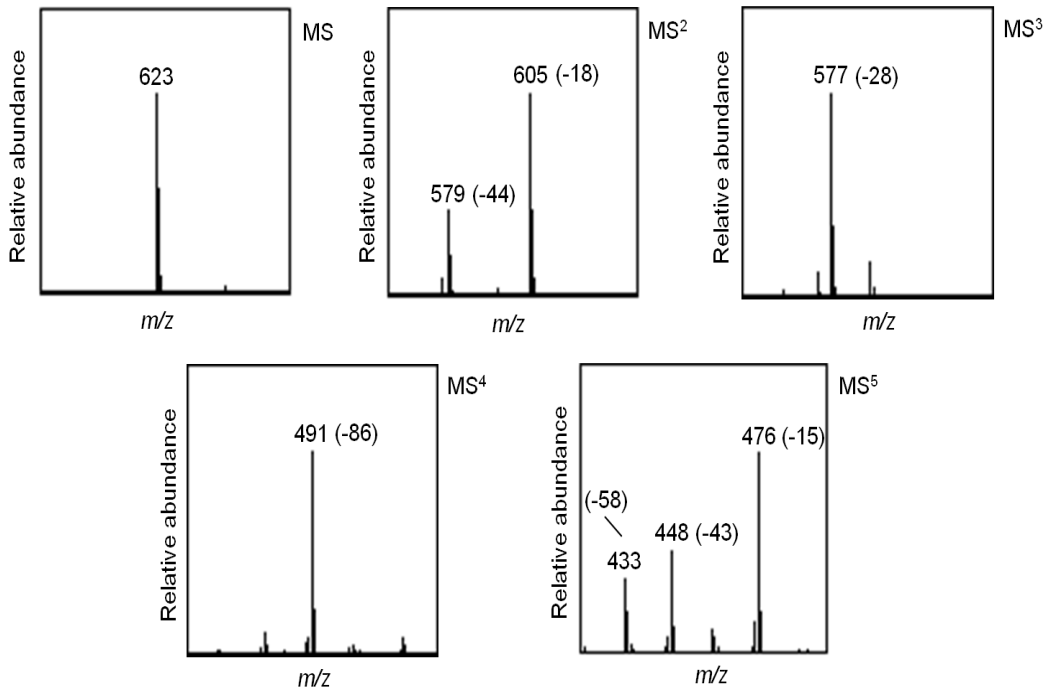

Figure 51. APCI MS fragmentation pattern of BPME *c* [*i*-Bu, Et].

The derivatives in each layer were normalised to TOC to allow the masses to be compared, the most abundant compounds from each layer are shown in Figure 52. The sample from 112 to 113 cm depth contained the greatest mass of pigment and included the bacterial derivative BPME *d* [Et, Et] in significant abundance. Normalisation of the mass of BPME *d* [Et, Et] revealed there was an insufficient amount for replicate AMS analysis. Thus, it was decided to combine 112 to 113 and 114 and 115 cm depth to create a sample with 458 µg/g of TOC of BPME *d* [Et, Et].

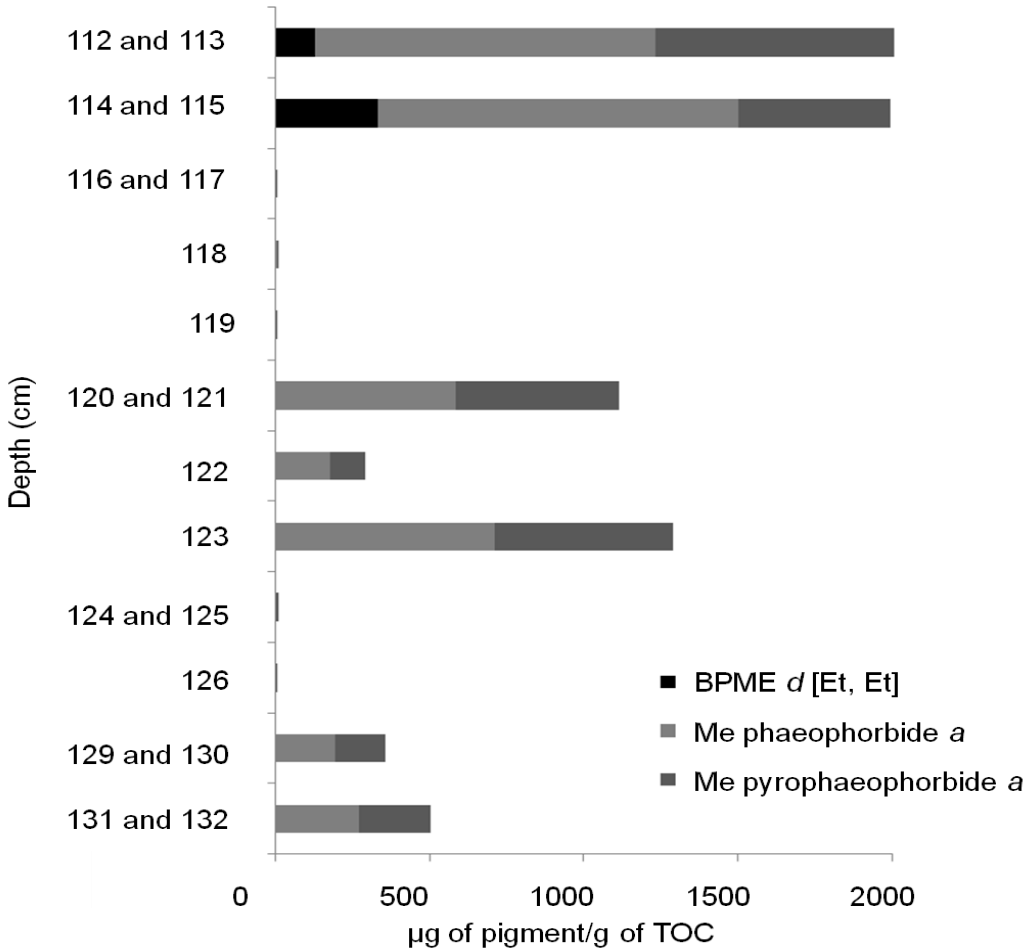

Figure 52. Pigment masses (normalised to TOC) from Kirisjes Pond first freshwater zone sediment.

The combined sample from 112 to115 cm depth was subjected to preparative HPLC using method M3 (Wilson *et al.*, 2003) and three components were isolated. Each fraction was analysed by UV/vis to identity the component and to determine its mass (Table 16). Thus Me phaeophorbide *a* and Me pyrophaeophorbide *a* and BPME *d* [Et, Et] were assigned from their UV/vis spectra and retention times by comparison with the results from LC-MS^n of the total methanolysis products. Sufficient mass was isolated for three replicate AMS analyses of Me phaeophorbide *a* and two of Me pyrophaeophorbide *a* (Table 16). Only ca. 13 µg of BPME *d* was isolated, representing only half of the target of 20 µg of carbon for AMS measurement. Samples of individual compounds as small as 2 µg carbon have been prepared using small reactors to form graphite targets for AMS (Santos *et al.*, 2007). Hence, given the significance of BPME *d* for estimating the reservoir effect it was retained for radiocarbon analysis.

Table 16. Components isolated from Kirisjes Pond first freshwater zone 112 to 115 cm depth acid methanolysis product.

Compound isolated	Mass (µg)	Mass of carbon (µg)	Replicates
BPME *d*	13.2	9.6	0
Me phaeophorbide *a*	98.0	69.9	3
Me pyrophaeophorbide *a*	70.4	52.4	2

4.2.5. Marine zone (88 – 110 cm depth)

The profile of sedimentary pigments in the marine zone of Kirisjes pond has been intensively investigated (Wilson *et al.*, 2004; Wilson *et al.*, 2005) and the published literature was used to guide the identification of the bacterial homologues. Similar distributions of BPMEs were identified by $LCMS^n$ throughout the zone, differing only in the relative abundances of individual components. The stereochemistry at $C3^1$ of the BPMEs was assigned from the elution order of the distereoisomers as it is known that the *R* form elutes before the *S* (Smith *et al.*, 1980; Smith *et al.*, 1982). The deepest portion of the zone was dominated by peaks 2 and 3 (Figure 53). Peak 2 had a protonated molecule at *m/z* 581 and a fragmentation pattern corresponding to BPME *d* [Et, Et] and peak 3 which had a protonated molecule at *m/z* 595 and a fragmentation pattern corresponding to BPME *c R* [Et, Et]. Only minor contributions from other BPME *c* homologues were identified in the deepest section of the zone. The prominence of BPMEs *c* and *d* indicates that photosynthetic primary production was dominated by green sulfur bacteria. The presence of both BPMEs *c* and *d* suggests a species of green sulfur bacteria was present which produced both bacteriochlorophyll *c* and *d*, or that two species of equal abundance were present, each producing a different bacteriochlorophyll (Wilson *et al.*, 2004). All components revealed in Figure 53 are identified in Table 17.

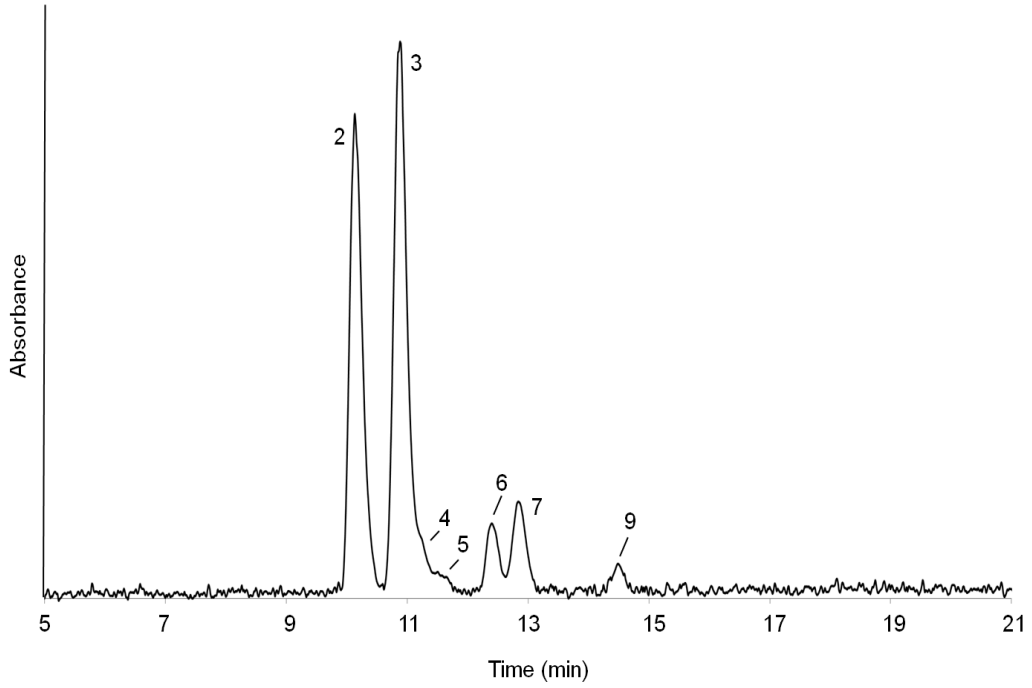

Figure 53. Partial RP-HPLC-UV/vis chromatogram (350-800 nm) of Kirisjes Pond marine zone 108 cm depth methanolysis product.

Table 17. Chlorophyll- and bacteriochlorophyll-derived components identified in Kirisjes Pond marine zone acid methanolysis products.

Peak	Molecular ion (*m/z*)	Identification
1	625	BPME *a*
2	581	BPME *d* [Et,Et]
3	595	BPME *c R* [Et,Et]
4	595	BPME *c S* [Et,Et]
5	595	BPME *d* [*n*-Pr,Et]
6	609	BPME *c R* [*n*-Pr,Et]
7	609	BPME *c S* [*n*-Pr,Et]
8	623	BPME *c R* [*i*-Bu, Et]
9	623	BPME *c S* [*i*-Bu, Et]
10	607	Me Phaeophorbide *a*

At the top of the marine zone BPME *c R* [Et, Et], BPME *c R* [*n*-Pr, Et] and BPME *c R* [*i*-Bu, Et] were the most abundant components (peaks 3, 6 and 9 Figure 54). The contribution to the sedimentary profile from BPME *d* [Et, Et] (peak 2, Figure 54) was significantly lower than at the base of the marine zone. An increase in the abundance of bchl *c* homologues relative to bchl *d* homologues in a laboratory culture study was interpreted to be a consequence of adaptation of a

bchl *d* producing species to produce bchl *c* (Bobe *et al.*, 1990). The change in bacteriochlorophyll production was suggested to be in response to light limitation as the maximum absorbance wavelength *in vivo* for bchl *d* [Et, Et] is 714 nm and it is 750 nm for bchl *c* [Et, Et] (Bobe *et al.*, 1990). A further outcome of the study by Bobe *et al.* (1990) was that the change in production between bchls *c* and *d* was accompanied by an increase in the extent of the alkylation of the substituent groups, which was also identified in Kirisjes Pond marine zone sediment. Increased abundances of BPMEs with greater extents of alkylation (for example [*n*-Pr, Et] and [*i*-Bu, Et]) were identified by LC-MS^n at 89 cm depth (Figure 54) which is an upper layer of the marine zone. Thus, the increased abundance of BPME *c* derivatives and greater alkylation of C8 and C12 substituent groups provides evidence of self-shading at the top of the zone. The sedimentary profile suggests that a limited number of primary producers dominated production during deposition of the upper section of the marine zone. Analysis of the horizon from 89 cm depth also revealed low abundance levels of Me phaeophorbide *a* (peak 10, Figure 54), an algal derivative. This suggests an increase in the algal production relative to bacterial production and implies that the extent of the anoxic conditions in the water column was changing. The alteration of the conditions in the pond could be a result either of increased mixing in the water column thus reducing the height of the chemocline, or of addition of freshwater into the system (Wilson, 2004).

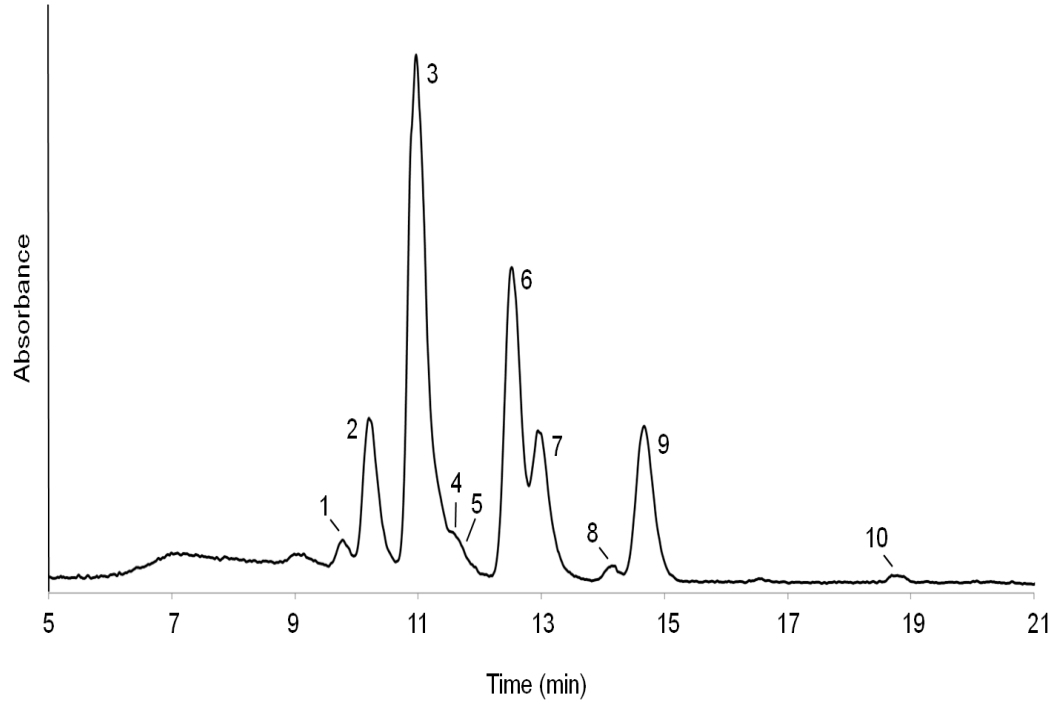

Figure 54. Partial RP-HPLC-UV/vis chromatogram (350-800 nm) of Kirisjes Pond marine zone 89 cm depth acid methanolysis product.

The derivatives in each layer from the marine zone were normalised to TOC to allow their masses to be compared, the most abundant components are shown in Figure 55. The layers with the greatest pigment mass, 103 and 96 cm depth, were subjected to preparative HPLC using method M3 (Wilson *et al.*, 2003) to isolate individual components.

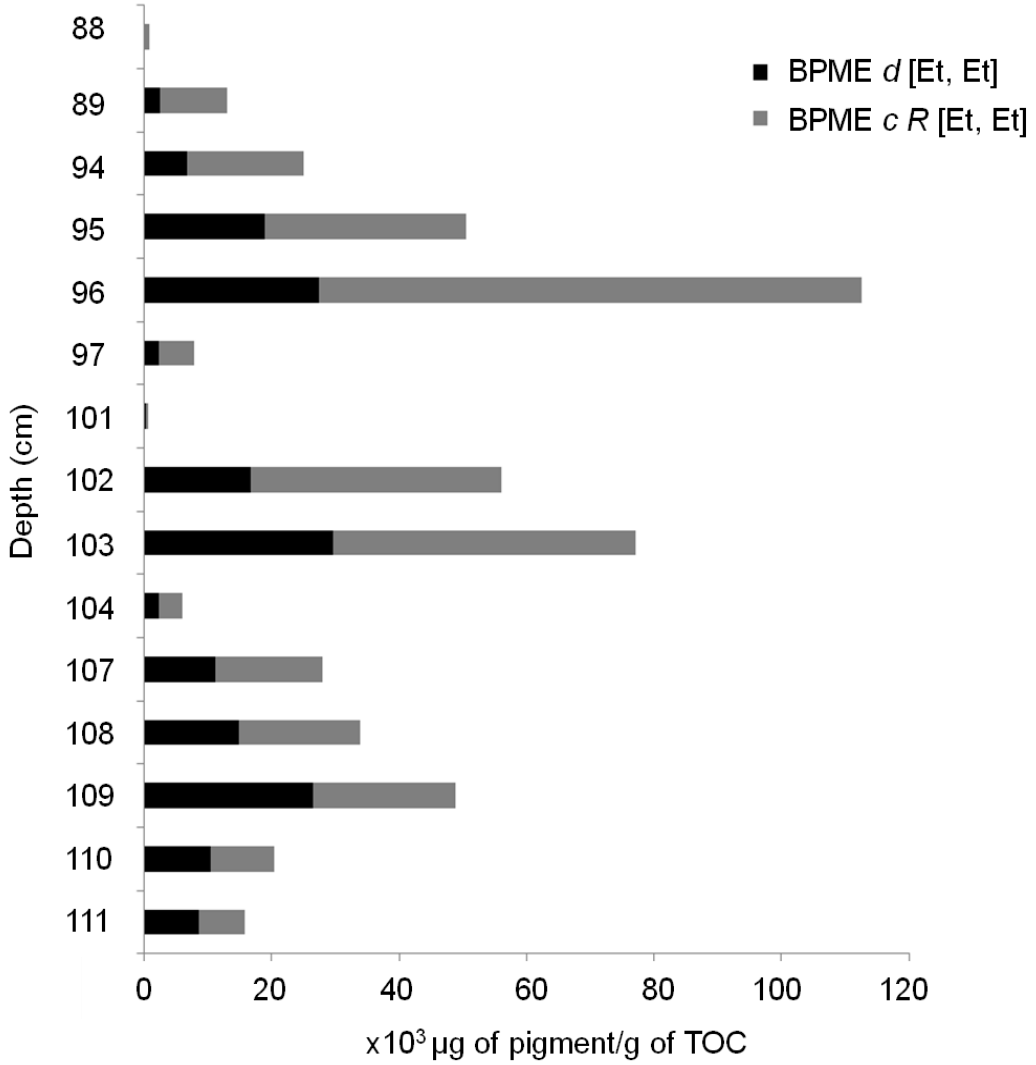

Figure 55. Pigment masses (normalised toTOC) from Kirisjes Pond marine zone.

BPME *d* [Et, Et] and BPME *c R* [Et, Et] were identified by LCMS^n. Both components were isolated from the methanolysis products of 96 and 103 cm depth (Table 18). The recoveries of both BPMEs were high, ca. 200 to 300 µg, respectively, providing sufficient material for between 7 and 12 replicate AMS analyses (Table 18). Bacteriochlorophyll *c* and *d* derivatives were both targeted for AMS measurement because the analysis has the potential to show if the biosynthesis of bacteriochlorophyll *c* with a methyl group at C20 is accompanied by a difference in isotopic signature by comparison with bacteriochlorophyll *d*, which does not contain the C20 substituent group.

Table 18. Bacteriophaeophorbide methyl esters isolated from Kirisjes Pond marine zone 96 and 103 cm depth.

Depth (cm)	Compound isolated	Mass (µg)	Mass of carbon (µg)	Replicates
96	BPME *d* [Et,Et]	210.9	152.7	7
96	BPME *c R* [Et,Et]	345.1	250.9	12
103	BPME *d* [Et,Et]	247.6	179.3	9
103	BPME *c R* [Et,Et]	269.2	195.7	9

4.2.6. Second freshwater zone (0 – 87 cm depth)

A previous study of the upper freshwater zone revealed pigments derived from oxygenic primary producers, but Squier *et al.* (2002) suggested that layers up to ca. 71 cm may contain bacterial pigments but these layers were not analysed by the study. The analysis of the methanolysis product from 85 to 87 cm depth (combined sample) revealed two peaks (peaks 1 and 2, Figure 58) of anoxygenic bacterial origin thus LC-MS^n was used to identify the components. Both peaks had a protonated molecule at *m/z* 595 (Figure 56) which corresponds to BPME *c* with alkylation patterns of [Et, Et] or [*n*-Pr, Me], or BPME *d* with alkylation patterns of [*n*-Pr, Et] or [*i*-Bu, Me] (Figure 56). As the MS^2 spectrum of both peaks had *m/z* 577 as the base peak they were identified as BPME *c* derivatives (Wilson *et al.*, 2005). The loss of 18 Da from the protonated molecule (*m/z* 595) in MS^2 corresponds to a water molecule and the loss of 44 Da to form the fragment of *m/z* 551 corresponds to the C3 substituent group (Figure 57). In MS^3 the formation of the fragment ion at *m/z* 549 is due to the loss of CO (28 Da) from $C13^1$ which corresponds to both BPME *c* [Et, Et] and [*n*-Pr, Me]. The loss of the C17 methyl propionate ester (86 Da) forms the MS^4 fragment at *m/z* 463 in both compounds. MS^5 is used to determine the identity of the component, losses of 29 Da (ethyl radical from C8 or C12) and 15 Da (methyl radical from a methyl or ethyl substituent) to form fragments at *m/z* 419 and 433 corresponds to BPME *c* [Et, Et] (peak 1, Figure 58). Peak 2 had an MS^5 spectrum comprising fragments at *m/z* 448, 434 and 420 corresponding to losses of methyl (15 Da), ethyl from C8 or C12 (29 Da) and a propyl radical from C8 (43 Da), respectively (see Figure 57). Thus, peak 2 (Figure 58) was identified as BPME *c* [*n*-Pr, Me] (peaks 1 and 2 are identified in Table 19).

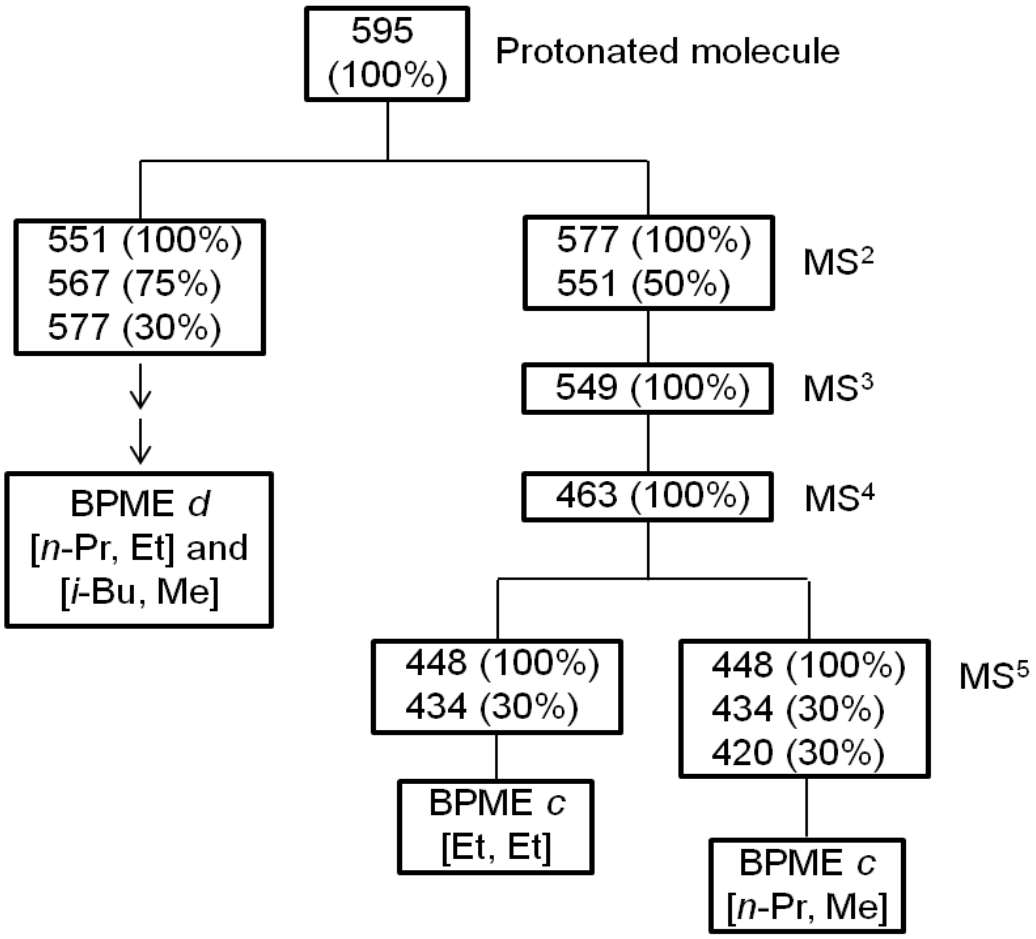

Figure 56. APCI MS fragmentation patterns possible for *m/z* 595, modified from Wilson *et al.* (2005).

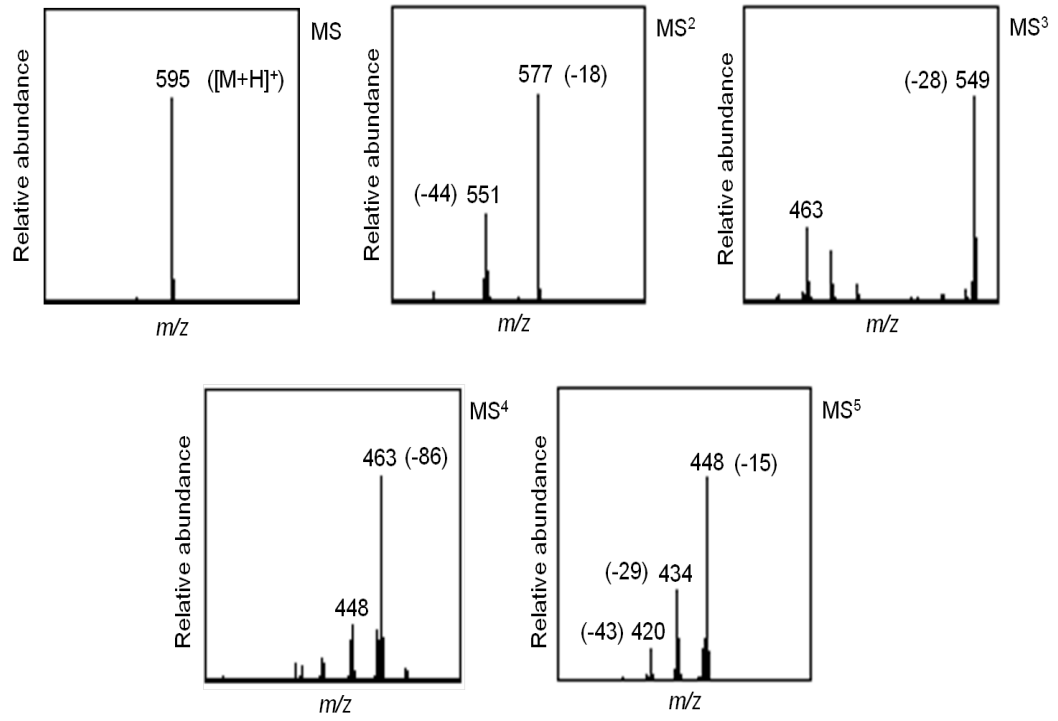

Figure 57. APCI MS fragmentation pattern of BPME *c* [*n*-Pr, Me].

The bacterial derivatives identified at 85 to 87 cm depth are of much lower abundance those in the marine zone. For example, the combined horizons from 85 to 87 cm depth contain ca. 320 µg of bacterial pigment/g TOC (Figure 59) versus ca. 1-120 x10^3 µg of bacterial pigment/g TOC (Figure 55) for single depths from the marine zone. Thus, the conditions within Kirisjes Pond were continuing to become more oxygenated, with 85 to 87 cm depth (Figure 58) the shallowest sample in which bacterial derivatives were identified.

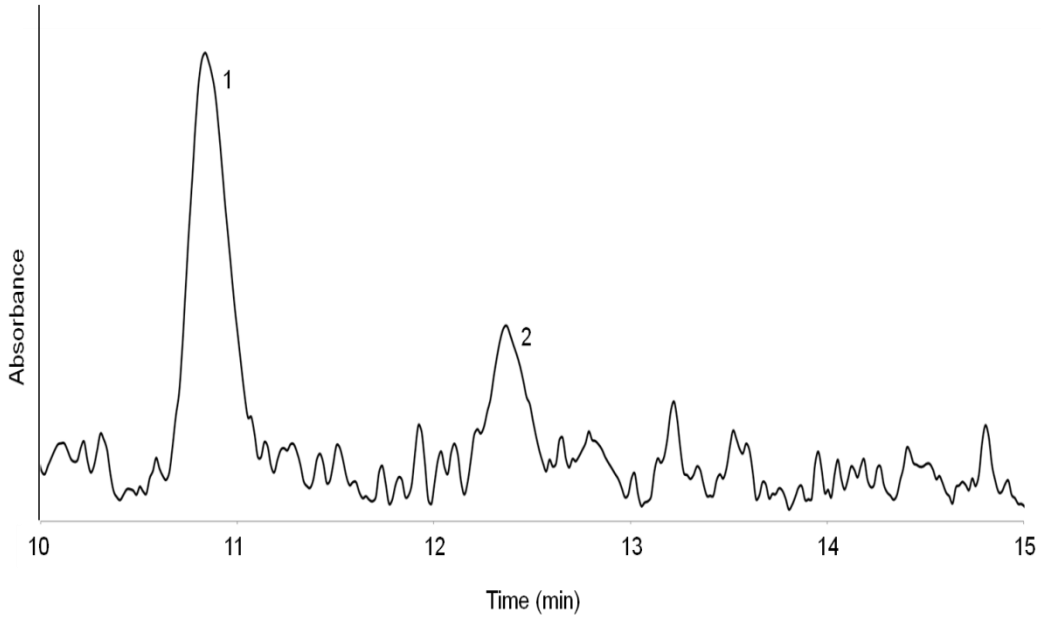

Figure 58. Partial RP-HPLC-UV/vis chromatogram (350-800 nm) of Kirisjes Pond second freshwater zone 85 to 87 cm depth acid methanolysis product.

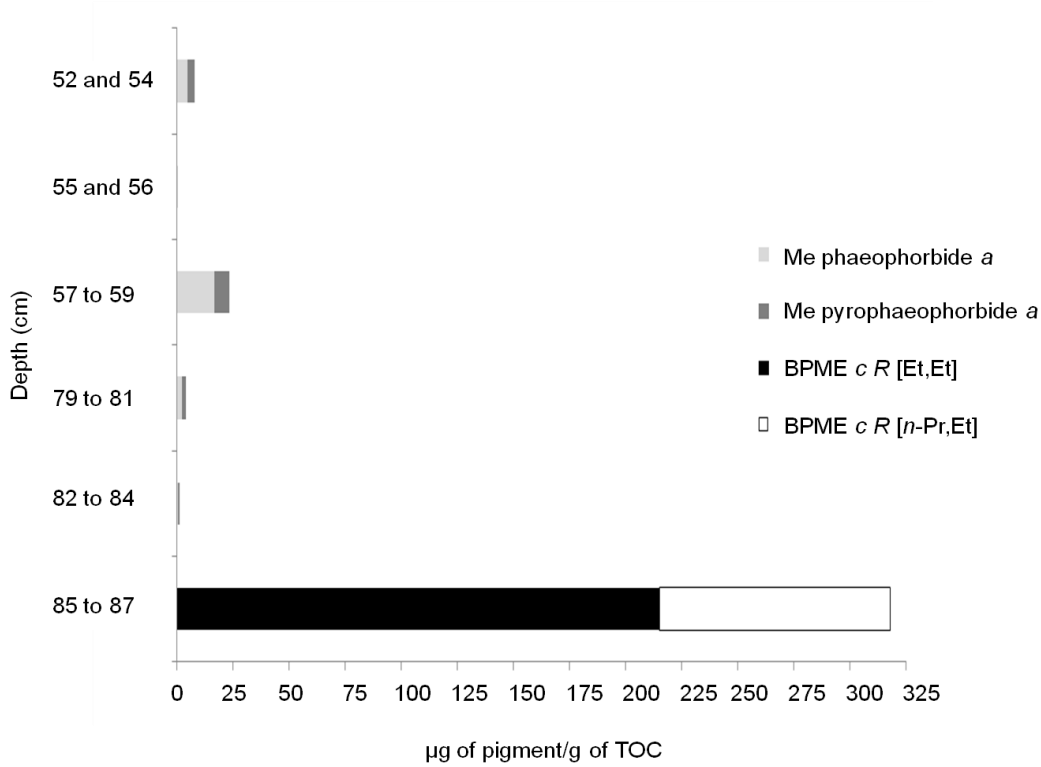

Figure 59. Masses of pigment (normalised by TOC) isolated from a section of Kirisjes Pond second freshwater zone (87 to 52 cm).

The remainder of the freshwater zone that was subjected to acid methanolysis (82 to 52 cm depth) contained only chl *a* derivatives, see for example 57 to 59 cm depth (Figure 60; peak identifications in Table 19). Depth 57 to 59 cm contained

ca. 25 µg of pigment/g of TOC (Figure 59) which was the highest content of chl pigments in the zone. Thus, the second freshwater zone contains a narrower distribution of pigments; only chl *a* derivatives were identified compared with both chl *a* and *b* derivatives in the first freshwater zone. The second freshwater zone also had lower abundance levels of pigments versus the first freshwater zone, for example the maximum abundance for the zone was 25 µg of pigment/g of TOC from a sample containing three layers compared with a maximum of 1600 µg of pigment/g of TOC from a sample containing two layers from the first freshwater zone. The differences between the freshwater zones indicate that the second freshwater zone was not as productive as the first and that it contained a different photosynthetic community. Thus following the marine incursion, primary production in Kirisjes Pond did not return to its original state. These findings are in agreement with the previous study by Squier *et al.* (2002), who also found that pigment abundances were lower in the second freshwater zone than in the first.

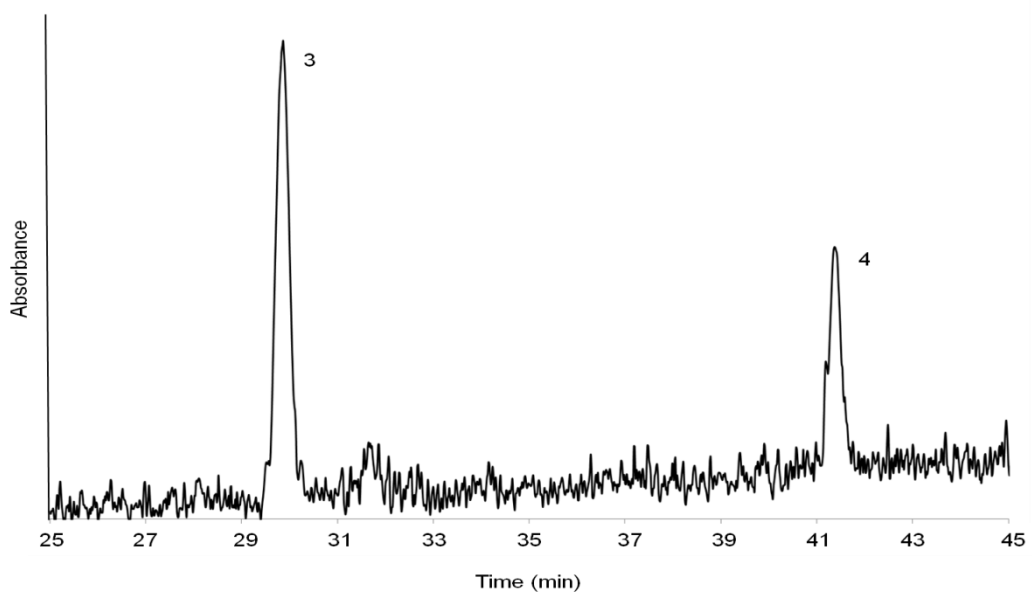

Figure 60. Partial RP-HPLC-UV/vis chromatogram (350-800 nm) of Kirisjes Pond 57 to 59 cm depth acid methanolysis product.

Table 19. Chlorophyll- and bacteriochlorophyll-derived components identified in Kirisjes Pond second freshwater zone acid methanolysis products.

Peak	Molecular ion (*m/z*)	Identification
1	595	BPME *c* [Et,Et]
2	609	BPME *c* [*n*-Pr,Et]
3	607	Me Phaeophorbide *a*
4	549	Me Pyrophaeophorbide *a*

The normalisation of pigment abundances to TOC showed that the samples from 52 to 84 cm depth contained insufficient pigment concentrations for CSRA based on compounds isolated from these samples (Figure 59). The sample from 85 to 87 cm depth contained the greatest mass of pigment and thus was selected for preparative isolation using method M3 (Wilson *et al.*, 2003). Two components were recovered (Table 20) and the identity of the most abundant component, BPME *c* [*n*-Pr, Et] was confirmed by $LCMS^n$. Sufficient BPME *c* [*n*-Pr, Et] was isolated (ca. 70 µg determined by UV/vis) for two AMS measurements (Table 20). The other component, BPME *c* [Et, Et] was identified by its HPLC retention time and online UV/vis spectra and as only ca. 11 µg was isolated by preparative HPLC (Table 20) it was not submitted for AMS measurement. The radiocarbon analysis of 85 to 87 cm depth would provide valuable information on the timing of the return to fresh-water conditions as it is the shallowest sample to contain bacteriochlorophyll derivatives.

Table 20. Bacteriophaeophorbide methyl esters isolated from Kirisjes Pond second freshwater zone 85 to 87 cm depth.

	Mass (µg)	Mass of carbon (µg)	Replicates
BPME *c* [Et,Et]	11.4	8.3	0
BPME *c* [*n*-Pr,Et]	69.9	51.0	2

4.2.7. Purity of compounds for CSRA

Samples intended for AMS analysis are combusted to produce CO_2 either for direct measurement or before graphitisation. Hence, ^{14}C measurement represents the combined signature of carbon from all organic components present in the sample analysed. It is, therefore, essential that compounds

isolated for CSRA are pure. Compounds were isolated from the methanolysis products of 85 to 87, 96 and 103 cm depth using the response from the online PDA detector to determine the start and completion of fraction collection. A threshold response was set to avoid collection of baseline noise (discussed in Section 3.4.7 Chapter 3), but as the samples evaporated during the hours spent in the auto-sampler they became more concentrated. Thus, minor components that did not trigger fraction collection were collected during some of the later preparative runs. The increased number of isolates for later injections compared with initial runs led to the contamination of later eluting isolates with minor components. Accordingly, the purity of the collected fractions was verified. EA of the standard (Section 3.4.5 Chapter 3) provided evidence that the experimental plan used to prepare single compound isolates produced pure compounds. Elemental analysis is a robust method of establishing purity, but it is a destructive technique that requires ca. mg quantities of sample. The size limitation renders elemental analysis unsuitable for assessing the purity of individual compounds isolated from sediments for radiocarbon analysis.

Therefore to assess the purity of the isolated components with respect to other pigments, small portions of each isolate were subjected to analytical scale HPLC using the binary method. It was postulated that bacterial pigment BPME *c* and *d* [Et, Et] isolates would not be affected by the collection of minor components as they eluted early in the chromatogram. The HPLC isolates of BPME *d* [Et, Et] from 96 and 103 cm depth had purities between ca. 98 and 99% (Table 21), see for example the HPLC chromatogram of BPME *d* [Et, Et] recovered from 103 cm (Figure 61). BPME *c* [Et, Et] recovered from both 96 and 103 cm depth had slightly lower purity by HPLC (ca. 95 to 96%, Table 21). The chromatogram of the isolate from 96 cm (Figure 62) shows a small co-eluting component eluting immediately prior to the recovered BPME *c* [Et, Et]. The minor component was identified by online PDA detection to be BPME *d* [Et, Et]. BPME *c* [*n*-Pr, Et] was isolated from 85 to 87 cm depth and its purity was determined to be ca. 88% by HPLC. Thus, its recovery was more affected by the collection of low abundance components as it was the latest eluting bacterial component isolated. Accordingly, early eluting components BPME *d* [Et, Et] and BPME *c* [Et, Et] were successfully recovered by preparative HPLC with excellent purity. The later eluting component BPME *c* [*n*-Pr, Et] was recovered with acceptable purity

assuming the radiocarbon signature contamination was not significantly different from the isolated component. Hence, the response-based method for isolation of target analytes was validated as it produced relatively pure isolates.

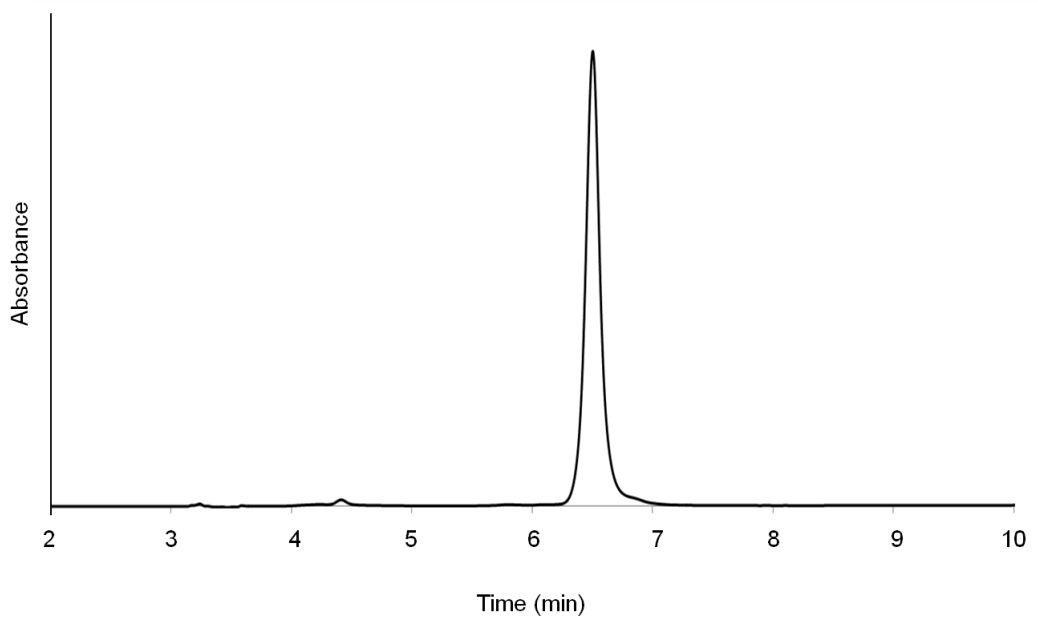

Figure 61. Partial RP-HPLC-UV/vis chromatogram (350-800 nm) of BPME *d* [Et, Et] isolated from 103 cm depth Kirisjes Pond.

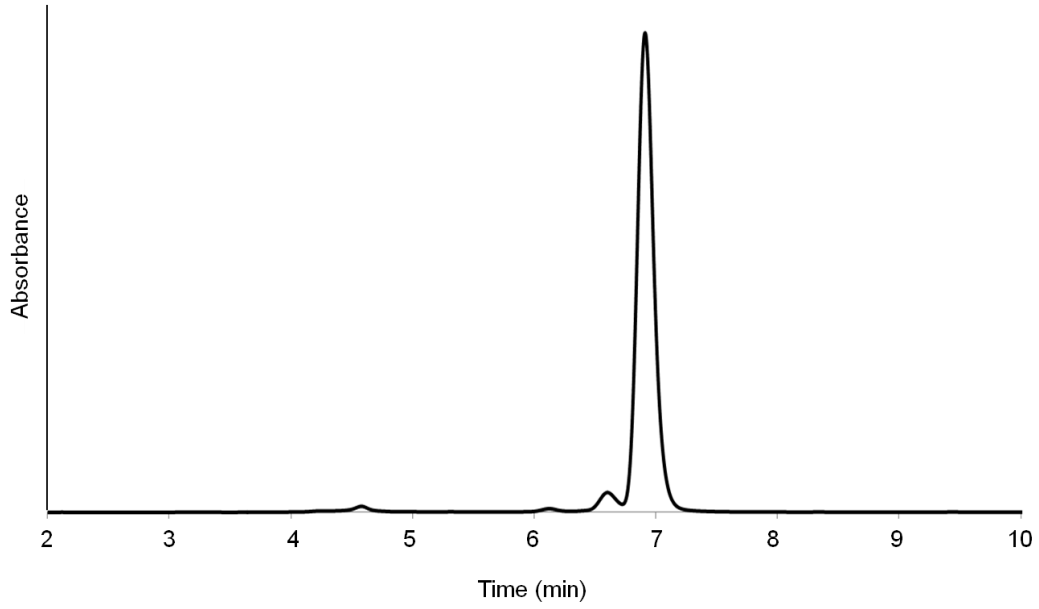

Figure 62. Partial RP-HPLC-UV/vis chromatogram (350-800 nm) of BPME *c* [Et, Et] isolated from 96 cm depth Kirisjes Pond.

Table 21. Purities of compounds isolated for CSRA.

Depth (cm)	Compound	Purity by HPLC (%)
85 to 87	BPME *c* [*n*-Pr,Et]	88.1
96	BPME *d* [Et,Et]	97.5
96	BPME *c R* [Et,Et]	95.6
103	BPME *d* [Et,Et]	98.7
103	BPME *c R* [Et,Et]	94.7

The most abundant pigments identified in the methanolysis product of the extract from 112 to 115 cm were algal derivatives, which elute much later than bacterial derivatives (t_R of ca. 27 and 38 min for Me phaeophorbide *a* and Me pyrophaeophorbide *a* versus t_R of ca. 10 and 11 min for BPME *d* [Et, Et] and BPME *c* [Et, Et)]. Due to the increased possibility of contamination, compounds from 112 to 115 cm depth were isolated using timed preparative HPLC. Timed collection was possible due to the high degree of separation between eluting compounds (for example see Figure 50) and the consistency in the retention times of the compounds. The sample comprising 112 to 115 cm depth was geologically significant as both algal and bacterial derivatives were isolated from it, therefore to preserve the maximum mass of pigments the isolates were not subjected to analytical scale HPLC.

4.2.8. Preparation of Me pyrophaeophorbide *a* standards for CSRA

Preparation of the Me pyrophaeophorbide *a* standard is discussed in Chapter 3. Me pyrophaeophorbide *a* has a similar molecular composition to all of the target chl derivatives, hence it can be isolated using the same chromatographic methods as those used for the samples isolated for CSRA. To enable AMS measurements to be corrected for any carbon added or lost during preparative HPLC, the standard was subjected to preparative HPLC immediately following the isolations of target analytes from individual depth horizons from Kirisjes Pond. This approach allows for the determination of absolute measurements from the CSRA results (Section 4.2.11, Chapter 4). Hence, the standard was isolated preparatively after the isolation of compounds from 96, 85 to 87 and 112 to 115 cm depth, the first, third and fourth samples subjected to preparative HPLC (controls 1, 2 and 3, Table 22). The preparative HPLC of the standard using the

same isolation conditions as the target sedimentary components will have exposed it to any residual contamination remaining on the column after isolation of the samples. An attempt was made to determine the added carbon by comparing the AMS measurements of the bulk standard of Me pyrophaeophorbide *a* with the same standard isolated by preparative HPLC (see Section 4.2.10 Chapter 4).

To enable high throughput of control samples high concentrations of Me pyrophaeophorbide *a* were injected on to the HPLC column (concentration overload), decreasing analysis time by requiring fewer preparative injections. Volume overload (large sample volumes) was not used to further increase throughput as this causes elution times to increase. This increase occurs because high volumes cause greater diffusion of the analytes on the column rather than them remaining in a tight band that elutes quickly as occurs during normal injections and concentration overload. Given that a total of 81 µg of Me pyrophaeophorbide *a* was required for 3 replicate AMS measurements, the bulk standard, which comprised ca. 0.5 mg, was dissolved in 1 mL to form double the optimum concentration of 0.25 mg/mL (Section 3.4.7 Chapter 3). Thus, 175 µL of the stock solution was required for preparative isolation to achieve 81 µg of Me pyrophaeophorbide *a*. To ensure that enough mass was recovered, 200 µL of the 0.5 mg/mL stock solution was subjected to preparative HPLC using five injections of 40 µL (ca. 19 µg of Me pyrophaeophorbide per injection). A chromatogram of an injection of control 1 (Figure 63) shows that it is possible to use concentration overload of the column and detector to achieve high throughput for all of the control samples as they contain only a single component. The only negative aspect of using this approach to increase throughput is that the online PDA detector is overloaded, causing the apex of the peak in the chromatogram and the UV/vis spectrum (not shown) to exhibit a high degree of noise (Figure 63). Due to the unstable nature of the response at the peak apex, time-based isolation was required. The fraction collector was activated 21 min after elution began and was set to collect the eluent from the column for 3.5 min. HPLC analyses of the concentrated Me pyrophaeophorbide *a* standard for controls 1, 2 and 3 showed that the standard was pure as no other components were detected (see for example Figure 63).

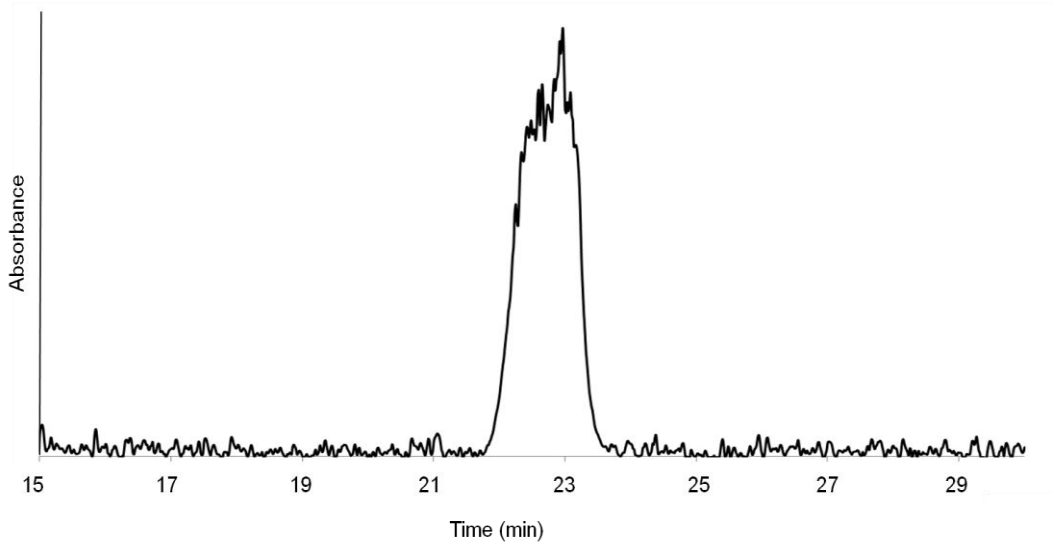

Figure 63. Partial RP-HPLC-UV/vis chromatogram (350-800 nm) of Me pyrophaeophorbide *a* Control 1.

The mass of Me pyrophaeophorbide *a* recovered from Control 1 was 93.4 µg (Table 22) from a possible 97.4 µg, corresponding to a loss of ca. 4%. Thus, the recovery of the standard was good. The recovered mass of Control 2, 66.7 µg, was much lower than for Control 1, it is most likely attributable to incorrect dilution of the bulk Me pyrophaeophorbide *a* standard which led to a concentration lower than 0.5 mg/mL. A mass of 84.2 µg was recovered from Control 3, which again was less than expected. The low recovery was due to solvent evaporating and precipitating standard material on the side of the injection vial. As more standard was subjected to preparative HPLC than was required for 3 replicate AMS analyses (97 µg versus 81 µg) it was decided not to recover the precipitated material. Sufficient material for 3 replicate AMS analyses was isolated from Controls 1 and 3 and for 2 analyses from Control 2 (Table 22). The mass of the bulk Me pyrophaeophorbide *a* standard remaining was 351 µg. This was reserved for validation of the AMS measurements, allowing up to 13 replicate AMS analyses (Table 22). Due to time restraints only one AMS analysis of each standard was carried out.

Table 22. Masses of Me pyrophaeophorbide *a* standard material available for AMS measurements and masses of standard material recovered from preparative HPLC.

	Mass (µg)	Mass of carbon (µg)	Replicates
Me pyrophaeophorbide *a*	351.1	261.6	13
Control 1	93.4	69.6	3
Control 2	66.7	49.7	2
Control 3	84.2	62.7	3

4.2.9. AMS measurement of Me pyrophaeophorbide *a* standards

Bulk, control and fractionation check (see Section 3.5.1 Chapter 3) standards were portioned into ca. 20 µg aliquots and sent to the ETH (*Eidgenössische Technische Hochschule*), Zurich for combustion to CO_2 and CSRA by AMS. Standards were oxidised with cupric oxide at 850°C for 5 h to form CO_2 and subsequently purified of water on a high vacuum line (modified from Pearson *et al.*, 1998). The CO_2 produced from the standards was determined manometrically, and hence the carbon content analysed was known (Table 23). The masses determined by manometric measurement are slightly larger than those determined by UV/vis except from Control 3 and Fraction check 2 which are lower (Table 23). Larger sample masses could be due to contamination added during the combustion process and a loss of mass could be due to incomplete combustion.

The combustion blank was determined to be 2.8 µg of carbon (Table 23) which corresponds to ca. 13% of the total standard mass by UV/vis. The extraneous carbon could be derived from contamination on the surface of the metal catalyst or on the combustion tubes.

Table 23. Masses of Me pyrophaeophorbide *a* standards subjected to CSRA determined by UV/vis and manometric analysis.

Standard	Mass of carbon by UV/vis (µg)	Mass of carbon manometrically (µg)	Added mass (µg)	
Me pyrophaeophorbide *a*	20.1	23.4	3.3	
Control 1	23.2	28.5	5.3	
Control 2	24.8	33.4	8.6	
Control 3	20.9	15.4	-5.5	
Fractionation check 1	20.8	18.0	-2.8	
Fractionation check 2	14.6	22.7	8.1	
			2.8	Average

The radiocarbon age determined for Fractionation check 1 (see section 3.5.1 Chapter 3) was - 481 ± 88 yr $_{BP}$ and for Fraction check 2 it was - 513 ± 84 yr $_{BP}$ (Table 24), the difference between the ages determined is 32 yr, which is within the reported error for both fraction checks. Thus, these radiocarbon ages suggest that fractionation of carbon isotopes did not occur during preparative HPLC, as the age determined from the front and latter portions of the peak are not significantly different. It can, therefore, be interpreted that the preparative HPLC system used in this study does not cause significant isotopic fractionation.

The radiocarbon age determined for the bulk Me pyrophaeophorbide *a* standard was 143 ± 79 yr $_{BP}$. The determination of an age greater than its real age (ca. 20 years) suggests that its isotopic composition has been influenced by radiocarbon dead contamination. Control 1 has a radiocarbon age of 222 ± 81 yr $_{BP}$ which is slightly older than the bulk standard radiocarbon age, although when their errors of ± 79 and ± 8 yr are considered the ages become indistinguishable. It is likely that the age of Control 1 has been more affected by radiocarbon dead contamination. The control was the second sample to be isolated on a new Jones Chromatography semi preparative column, and the additional carbon in the sample is likely to have been unbound stationary phase eluting from the column during the chromatographic run. The hypothesis of the elution of unbound stationary phase is further supported by the isolate of BPME *d* from 96 cm depth Kirisjes Pond (the first sample to be isolated on the new column) which contained incombustible material. The material was not identified but it is likely to be silica particles to which hydrocarbon chains of the stationary phase are bonded. Thus, the difference in radiocarbon age between Control 1 and the bulk standard is probably due to the stationary phase eluting from the column during the isolation of Me pyrophaeophorbide *a*. The subsequent controls became increasingly

modern: Controls 2 and 3 had radiocarbon ages of - 237 ± 87 yr $_{BP}$ and - 667 ± 88 yr $_{BP}$ suggesting that the elution of stationary phase lessened over time. The radiocarbon ages of Controls 2 and 3 are comparable to those determined for the isotopic fractionation checks (Table 24) implying that column bleed was minimal by the time of isolation of these standards and the corresponding samples between which they were interleaved. As the fractionation checks were conducted using an older Jones Chromatography semi preparative column their radiocarbon ages should not be affected by contamination eluting from the column. Thus the young radiocarbon ages determined for the Controls are likely to reflect the contamination derived from preparative isolation.

Table 24. CSRA measurements by the mini radiocarbon dating system (MICADAS) ETH, Zurich, measurements processed by Bats version 3.3 (9.5.2012) written by L. Wacker.

ETH number	ETH standard			^{14}C counts	^{12}C (µA)	^{14}C/^{12}C (10^{-12})	Error ± (%)	^{13}C/^{12}C (%)	Sigma (%)	$Fm_{\delta}{}^{13}{}_{C}$	Error ± (%)	Sigma (%)	Age (yr)	Error ± (y)	δ^{13}C (‰)	^{13}C(H) (nA)
41217.3.126	Oxa1 Gas (modern)			21,440	5.0	1.0654	0.68	1.0280	0.04	**1.0374**	**0.88**	0.62	**-295**	**70**	-17.1	0.30
41217.3.127	Oxa1 Gas (modern)			22,735	5.9	1.0714	0.66	1.0253	0.03	**1.0488**	**0.86**	0.71	**-382**	**69**	-19.7	0.35
41217.3.128	Oxa1 Gas (modern)			21,648	5.2	1.0611	0.68	1.0261	0.02	**1.0365**	**0.88**	0.78	**-288**	**70**	-19.0	0.40
41217.3.129	Oxa1 Gas (modern)			20,565	5.2	1.0567	0.70	1.0229	0.03	**1.0385**	**0.89**	0.62	**-303**	**71**	-22.0	0.41
41217.3.130	Oxa1 Gas (modern)			20,460	4.4	1.0606	0.70	1.0256	0.02	**1.0374**	**0.89**	0.69	**-295**	**72**	-19.4	0.28
41218.3.96	Blank CO_2 (radiocarbon dead)			176	5.8	0.0090	7.54	1.0068	0.02	**0.0069**	**12.34**	10.49	**40,022**	**991**	-37.4	0.34
41218.3.97	Blank CO_2 (radiocarbon dead)			155	5.9	0.0076	8.03	1.0061	0.02	**0.0051**	**16.19**	12.74	**42,423**	**1,300**	-38.0	0.39
41218.3.98	Blank CO_2 (radiocarbon dead)			175	6.1	0.0072	7.56	1.0073	0.03	**0.0051**	**14.09**	11.58	**42,468**	**1,132**	-36.9	0.34
43800.3.26	OXA2 Eglinton (modern)			12,264	5.6	1.3931	0.90	1.0240	0.02	**1.3677**	**1.06**	0.96	**-2,515**	**85**	-20.9	0.58
43800.3.27	OXA2 Eglinton (modern)			12,085	6.2	1.3492	0.91	1.0256	0.02	**1.3227**	**1.06**	0.92	**-2,247**	**85**	-19.4	0.28
43800.3.28	OXA2 Eglinton (modern)			35,369	7.5	1.3678	0.53	1.0291	0.04	**1.3323**	**0.76**	0.56	**-2,304**	**61**	-16.1	0.25
43800.3.29	OXA2 Eglinton (modern)			12,324	6.5	1.3572	0.90	1.0239	0.02	**1.3342**	**1.06**	0.91	**-2,316**	**85**	-21.0	0.41
43801.5.14	Blank Eglinton (radiocarbon dead)			398	6.1	0.0233	5.01	1.0201	0.02	**0.0157**	**9.43**	6.60	**33,348**	**758**	-24.7	0.31
43801.5.15	Blank Eglinton (radiocarbon dead)			470	6.0	0.0250	4.61	1.0210	0.02	**0.0175**	**8.37**	5.99	**32,504**	**673**	-23.8	0.29
	Sample code	**Depth (cm)**	**Compound**													
47517.1.1	Y8121-a	85 to 87	BPME c [n-Pr,Et]	12,447	6.1	0.5675	0.90	1.0200	0.02	**0.5579**	**1.07**	0.88	**4,688**	**86**	-24.7	0.32
47518.1.1	Y8122-a	96	BPME d [Et,Et]	7,371	5.7	0.4830	1.16	1.0153	0.02	**0.4781**	**1.31**	1.35	**5,927**	**106**	-29.2	0.29
47519.1.1	Y8123-a	96	BPME c [Et,Et]	10,841	7.1	0.5076	0.96	1.0173	0.02	**0.5013**	**1.13**	1.04	**5,547**	**90**	-27.4	0.30
47520.1.1	Y8124-a	103	BPME d [Et,Et] (10 µg sample)	4,440	6.9	0.4241	1.50	1.0139	0.01	**0.4203**	**1.63**	1.67	**6,963**	**131**	-30.6	0.32
47521.1.1	Y8125-a	103	BPME d [Et,Et]	10,134	7.3	0.4263	0.99	1.0170	0.03	**0.4203**	**1.16**	0.94	**6,964**	**93**	-27.6	0.29
47522.1.1	Y8126-a	103	BPME c [Et,Et]	10,885	7.4	0.4218	0.96	1.0176	0.03	**0.4148**	**1.14**	0.95	**7,069**	**91**	-27.1	0.37
47523.1.1	Y8127-a	112 to 115	BPME d [Et,Et]	5,386	7.5	0.1980	1.36	1.0205	0.04	**0.1899**	**1.58**	1.44	**13,343**	**127**	-24.3	0.33
47524.1.1	Y8128-a	112 to 115	Me phaeophorbide a	7,680	7.0	0.4327	1.14	1.0288	0.03	**0.4165**	**1.30**	1.09	**7,037**	**104**	-16.3	0.35
47525.1.1	Y8129-a	112 to 115	Me pyrophaeophorbide a	6,305	7.1	0.3950	1.26	1.0263	0.03	**0.3817**	**1.41**	1.08	**7,736**	**113**	-18.7	0.29
	Standard code		**Standard**													
47526.1.1	Y812 STD1		Me pyrophaeophorbide *a*	15,359	7.5	0.9956	0.81	1.0209	0.03	**0.9823**	**0.98**	0.78	**143**	**79**	-23.9	0.48
47527.1.1	Y812 STD2		Control 1	14,154	7.0	0.9807	0.84	1.0184	0.01	**0.9728**	**1.01**	0.96	**222**	**81**	-26.3	0.37
47528.1.1	Y812 STD3		Control 2	12,152	6.3	1.0285	0.91	1.0108	0.02	**1.0299**	**1.08**	0.69	**-237**	**87**	-33.6	1.26
47529.1.1	Y812 STD4		Control 3	11,100	6.3	1.0868	0.95	1.0151	0.02	**1.0866**	**1.10**	0.84	**-667**	**88**	-29.4	0.21
47530.1.1	Y812 STD5		Fractionation check 1	11,245	6.5	1.0614	0.94	1.0146	0.02	**1.0617**	**1.09**	0.67	**-481**	**88**	-29.9	0.27
47531.1.1	Y812 STD6		Fractionation check 2	12,825	6.5	1.0622	0.88	1.0129	0.01	**1.0660**	**1.04**	0.90	**-513**	**84**	-31.6	0.30

^{14}C counts = the measurement of radiocarbon, ^{12}C (µA) = ^{12}C current in micro amperes, ^{12}C/^{14}C = determined from count, current and time of collection, Error ± (%) = internal error based on counting statistics, ^{13}C/^{12}C = based on the count of the isotope, Sigma (%) = the error in ^{13}C/^{12}C measurement, **$fm_{\delta}{}^{13}{}_{C}$** = fraction modern corrected for δ^{13}C, **Error ± (%)** = error in fm, Sigma (%) = derived from internal error and allowing for errors on samples, **Age (yr)** = determined from fm and the atmospheric concentration of radiocarbon, **Error ± (%)** = determined from error in fm and atmospheric concentration of radiocarbon, δ^{13}C (‰) = measured concentration of δ^{13}C, ^{13}C(H) (nA) = ^{13}C current in nano amperes.

4.2.10. Procedural blank determination

The intention in the study was to estimate the magnitude of the procedural blank associated with the preparative HPLC system used in this study using the bulk Me pyrophaeophorbide *a* standard in conjunction with control Me pyrophaeophorbide *a* standards isolated between the Kirisjes Pond samples. As no blank HPLC column effluent was collected during the course of this study the absolute magnitude of extraneous carbon added to the standards during preparative HPLC and its fraction modern could not be determined. Thus the mass balance equation (1) could not be used to correct fraction modern measurements of samples. Determining the mass of standards before and after preparative isolation would be too inaccurate to determine the mass of the procedural blank as 100% recovery of injected compounds was not achieved by the preparative HPLC system used in this study.

$$fm_s = \frac{m_{mfm_m}}{m_s} - \frac{m_{pbfm_{pb}}}{m_s} \qquad (1)$$

fm_s = fraction modern of sample corrected for the procedural blank
m_m = measured mass of sample
fm_m = measured fraction modern of the sample
m_s = mass of sample minus contamination
m_{pb} = mass of procedural blank
fm_{pb} = fraction modern of procedural blank

4.2.11. CSRA of sedimentary pigments from Kirisjes Pond

Single compound samples derived from Kirisjes Pond were portioned into ca. 20 µg of carbon aliquots and combusted to form CO_2 using the same method used for the standards (outlined in Section 4.2.9 Chapter 4). The mass of carbon contained was derived from the manometric measurement of the CO_2 sample gas. The mass of each sample determined by UV/vis and manometrically are generally comparable to one another with two exceptions BPME *c* [Et, Et] from 103 cm depth and BPME *d* [Et, Et] from 112 to 115 cm depth (Table 25). These samples could have been affected by contamination added during combustion or from the presence of co-eluting non chlorophyll-derived components.

Table 25. Masses of pigments from Kirisjes Pond subjected to CSRA as determined by UV/vis and manometric analysis.

Depth (cm)	Compound	Mass of carbon by UV/vis (µg)	Mass of carbon manometrically (µg)	Difference in mass (µg)
85 to 87	BPME *c* [*n-P*r,Et]	25.5	33.6	8.1
96	BPME *d* [Et,Et]	21.8	24.9	3.1
96	BPME *c* [Et,Et]	20.9	25.5	4.6
103	BPME *d* [Et,Et] (small sample test)	10.0	13.6	3.6
103	BPME *d* [Et,Et]	19.9	26.7	6.8
103	BPME *c* [Et,Et]	21.7	44.1	22.4
112 to 115	BPME *d* [Et,Et]	9.6	32.5	22.9
112 to 115	Me phaeophorbide *a*	23.3	24.1	0.8
112 to 115	Me pyrophaeophorbide *a*	26.2	20.3	-5.9

Algal pigments Me phaeophorbide *a* and Me pyrophaeophorbide *a* isolated from 112 to 115 cm depth were subjected to CSRA and uncalibrated radiocarbon ages of 7037 ± 104 yr $_{BP}$ and 7736 ± 113 yr $_{BP}$ were determined (Table 24). Previous age determination by radiocarbon analysis of bulk organic material derived from 110 cm gave an age 7825 ± 70 uncal yr $_{BP}$ (Hodgson *et al.*, 2001). This age is comparable to that determined for Me pyrophaeophorbide *a* isolated from 112 to 115 cm depth. A bacterial pigment, BPME *d* [Et, Et] was also isolated from 112 to 115 cm depth and a sample of 9.6 µg of carbon (determined by UV/vis) provided a radiocarbon age of 13343 ± 127 uncal yr $_{BP}$ (Table 24).

The comparison of the radiocarbon age of BPME *d* [Et, Et] with those determined for the algal pigments revealed a significant difference in age, which may correspond to the reservoir effect (R). If so, R at 112 to 115 cm depth was determined to be ca. 5607 to 6306 yr. Reservoir effects of between 3500 to ca. 10,000 years were determined for discrete regions in Lake Myvatn, Iceland (Ascough *et al.*, 2011). The R of ca. 10,000 years determined from mollusc and algae grown on rocks was considered by Ascough *et al.* (2011) to be extremely high. Much lower reservoir effects were determined for Tonsberg Lake T1 and Barff Peninsula Lake, South Georgia. Surface sediments of these lakes were older than particulate organic matter by 850 to 1100 ^{14}C yr (Moreton *et al.*, 2004). Thus, by comparison to studies of other freshwater lakes a relatively large reservoir effect was determined for Kirisjes pond. The large magnitude of R could correspond to a system in which the chemocline was situated low in the water column (Figure 64). This may imply that the bacterial primary producer

community was restricted to a small region near the water-sediment boundary. Radiocarbon-depleted CO_2 can be released by microbial degradation of sedimentary refractory organic matter (for example derived from aquatic mosses and plants). Hence, the isotopic signature of compounds derived from organisms growing near the water-sediment boundary is more influenced by ^{14}C-depleted carbon dioxide than those growing higher in the water column.

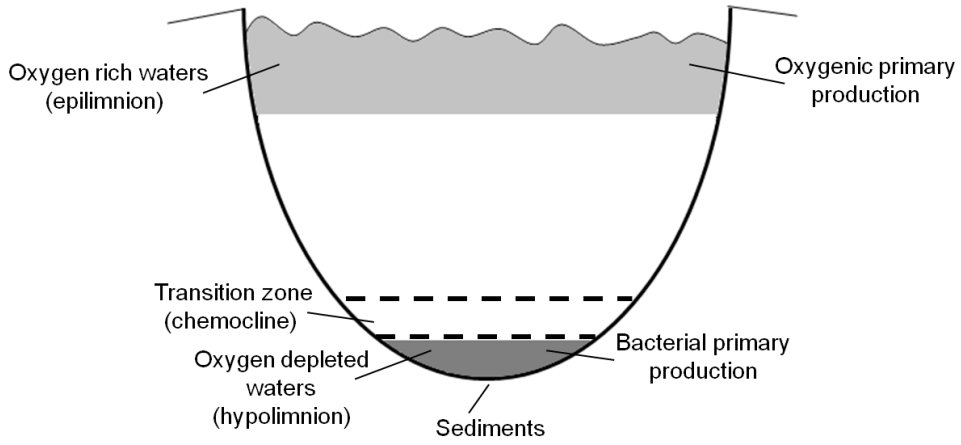

Figure 64. Schematic diagram of the proposed conditions within Kirisjes Pond corresponding to the period 112 to 115 cm depth sediments were formed.

Two bacterial derivatives, BPME *c* [Et, Et] and BPME *d* [Et, Et] were isolated from 103 cm depth in the marine zone and subjected to CSRA to determine uncalibrated radiocarbon ages. BPME *c* [Et, Et] was determined to have a radiocarbon age of 7069 ± 91 yr $_{BP}$ and BPME *d* [Et, Et] an age of 6964 ± 93 yr $_{BP}$ (Table 24). The ages derived from the bacterial derivatives isolated individually during preparative HPLC are extremely similar, validating the approach chosen. A small aliquot of BPME *d* [Et, Et] comprising 10 µg of carbon (by UV/vis) was subjected to CSRA to establish the feasibility of the use of small samples. The radiocarbon age determined was 6963 ± 131 yr $_{BP}$ (Table 24) which is statistically the same age as determined for 20 µg of BPME *d* [Et, Et], thus providing confidence in the measurement of small samples. Hence, the small sample of BPME *d* [Et, Et] isolated from 112 to 115 cm depth was subjected to CSRA. The same bacterial derivatives, BPME *c* [Et, Et] and BPME *d* [Et, Et], were isolated from a second layer in the marine zone (96 cm depth) of Kirisjes Pond and they provided radiocarbon ages of 5547 ± 90 yr $_{BP}$ and 5927 ± 106 yr $_{BP}$, respectively. Although the ages determined for BPME *c* [Et, Et] and BPME *d* [Et, Et] do not

agree as closely as those determined for the same derivatives at 103 cm depth, they are reasonably similar. Notably, because the two compounds could have been derived from separate members of the green sulfur bacteria which can inhabit different levels within a stratified water column, the differences in age could be attributable to differences in the reservoir effect.

Radiocarbon ages determined for the algal pigments isolated from the first freshwater transition zone and from the bacterial pigments recovered from two layers in the marine zone show a trend in progressively younger ages (Figure 65). The younger CSRA results determined for the pigment isolates from 112 to 115 and 96 cm depth appear to be more credible than bulk ages and older CSRA measurements from the same layer owing to the age sequence determined within the section examined (Figure 65).

The almost linear change in age versus depth between 112 to 115 cm depth and 96 cm depth (Figure 65) suggests that the environmental conditions have changed within the lake causing the reservoir effect on the isotopic composition of bacterial pigments to become less pronounced. Thus, it is likely that bacterial primary production occurred high in the water column under the influence of a largely atmospheric isotopic composition of CO_2 during the biosynthesis of bacteriochlorophyll *c* and *d* derivatives isolated from 103 and 96 cm depth. Figure 66 shows a schematic representation of the likely conditions within Kirisjes pond corresponding to the formation of the marine zone sediments.

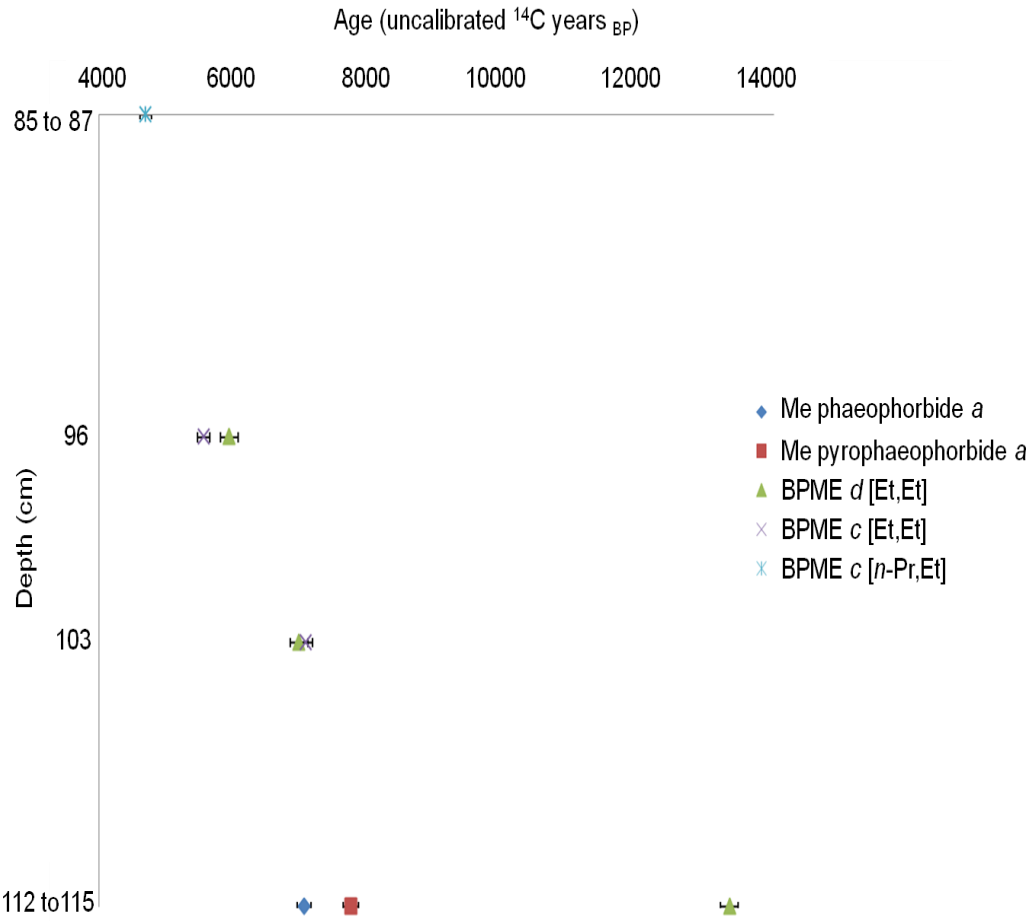

Figure 65. Radiocarbon ages determined for single pigment isolates from Kirisjes Pond.

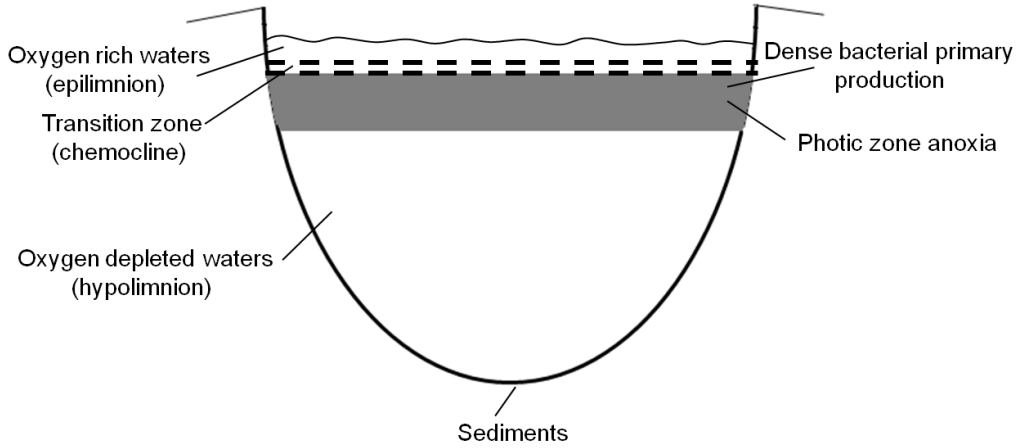

Figure 66. Schematic diagram of the proposed conditions within Kirisjes Pond corresponding to the period 96 and 103 cm depth sediments were formed.

BPME *c* [*n*-Pr, Et] was recovered from the shallowest of the horizons within Kirisjes Pond that contain bacterial photosynthetic pigments. It provided a radiocarbon age of 4688 ± 90 yr $_{BP}$ (Table 24). A bulk radiocarbon age of 6205 ± 50 yr $_{BP}$ previously measured (Hodgson *et al.*, 2001) is significantly older than that determined for BPME *c* [*n*-Pr, Et] by ca. 1500 yr. It is likely that the bulk measurement was effected by ^{14}C depleted refractory organic matter within the sediment which caused artificially old age to be determined. The radiocarbon age determined for the single compound isolated from 112 to 115 cm depth continues the generally linear change in age observed for the algal isolates from 112 to 115 cm depth and the bacterial pigments from 103 and 96 cm depth (Figure 65). The linearity of the radiocarbon ages suggests that the sedimentation rate within the pond was constant during the section analysed. The continued linearity also suggests that the green sulfur bacteria from which BPME *c* [*n*-Pr, Et] was derived was not significantly influenced by the reservoir effect and that, at this time, Kirisjes Pond contained a bacterial primary producer community relatively high in the water column (Figure 67). Thus, the return to completely freshwater conditions occurred more recently than previously thought.

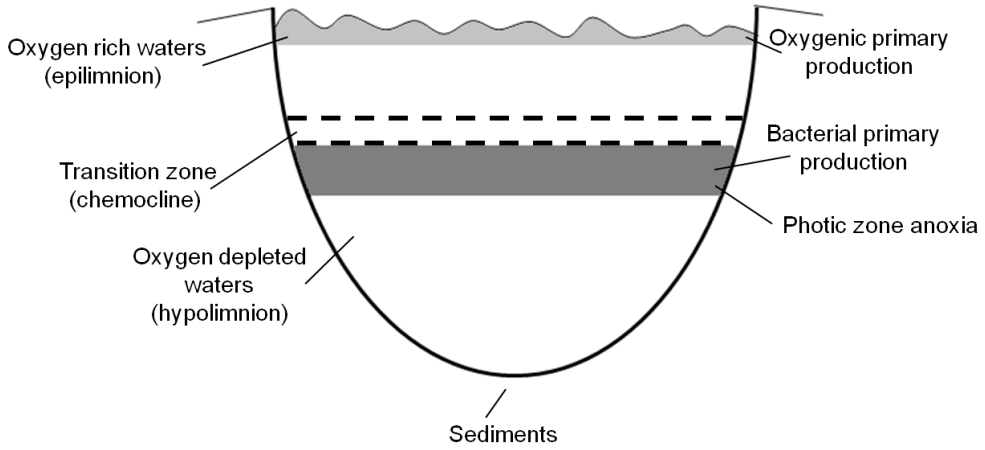

Figure 67. Schematic diagram of the proposed conditions within Kirisjes Pond corresponding to the period 85 to 87 cm sediments were formed.

4.3. Significance of radiocarbon measurements

Calibration curves are constructed from several different dating methods that are used to determine age, for example, dendrochronology, uranium series dating ($^{230}Th/^{234}U/^{238}U$), varved sediments and radiocarbon dating to correct for

fluctuations in radiocarbon production (see, Fairbanks *et al.*, 2005; Reimer *et al.*, 2009). The radiocarbon ages presented in this chapter have not been calibrated; therefore they cannot be compared to other calibrated ages. The ages, however can be compared to other uncalibrated ages to provide valuable insight into the radiocarbon reservoir affecting the primary producers of the pond (see section 4.2.11) and can be used to estimate the timing of the sea level rise that affected Kolloy Island and mainland Antarctica. Sea level rises caused the retreat of the ice sheet covering the Broknes and Stornes peninsulas on the mainland. The radiocarbon dates determined from the marine zone (caused by the incursion of sea water) of Kirisjes pond (ca. 5550 to 7100 yr $_{BP}$) agree with the estimated radiocarbon age (ca. 6000 yr $_{BP}$) of the ice sheet retreat from the edge Stornes peninsula (Hodgson *et al.*, 2001). Thus, the methods chosen to isolate photosynthetic pigments for radiocarbon dating are further validated.

4.4. Conclusions

A 12 cm sediment core collected from Lake Chiprana was sectioned into 1 cm layers and photosynthetic pigments were identified by HPLC with PDA detection in nine layers. Me phaeophorbide *a*, Me pyrophaeophorbide *a* and BPME *d* [Et, Et] were isolated from all pigment containing layers. Sufficient masses of Me phaeophorbide *a* were isolated to provide between 1 to 2 cm resolution in radiocarbon ages. Insufficient masses of Me pyrophaeophorbide *a* and BPME *d* [Et, Et] were isolated from each layer of sediment to provide acceptable resolution in radiocarbon measurements. Thus these pigments were designated for use in determining an approximate value of the reservoir effect in Lake Chiprana. Due to time restraints the pigments isolated from Lake Chiprana were not subjected to CSRA before the submission deadline of this thesis.

The analysis of Kirisjes Pond sedimentary extracts revealed a wide distribution of photosynthetic pigments which agreed with previous studies. BPME *c* [Et, Et] and BPME *c* [*n*-Pr, Et] were identified by LC-MS^n for the first time at 85 to 87 cm depth, a region thought to correspond to freshwater conditions. Photosynthetic pigments were isolated for CSRA by preparative HPLC (purities ranging between 88 and 99% by HPLC) from the marine zone and the freshwater zones surrounding it. Algal and bacterial pigments were isolated from 112 to 115 cm

depth (first freshwater transition zone), the algal pigments provided radiocarbon ages of 7037 ± 104 yr $_{BP}$ for Me phaeophorbide *a* and 7736 ± 113 yr $_{BP}$ for Me pyrophaeophorbide *a* which was comparable to a previously determined bulk age. A radiocarbon age of 13343 ± 127 yr $_{BP}$ was determined for the bacterial pigment BPME *d* [Et, Et] from 112 to 115 cm depth which revealed a large reservoir effect of up to 6000 yr, this suggests the pond was stratified with bacterial production restricted to the sediment-water interface. Bacterial derivatives BPME *c* [Et, Et] and *d* [Et, Et] isolated from marine zone layers 103 and 96 cm depth had radiocarbon ages of between 7037 to 7736 ± 113 yr $_{BP}$ and 6964 to 7069 ± 93 yr $_{BP}$ which are relatively linear with depth and the algal ages determined for the transition zone below. Linearity of ages from algal and bacterial derivatives suggests that bacterial communities were growing high in the water column. The ages determined for both bacterial derivatives isolated from 96 cm depth agree extremely well and thus provide confidence in the experimental plan used. The uppermost sample subjected to CSRA was BPME *c* [*n*-Pr, Et] isolated from 85 to 87 cm depth and its radiocarbon age of 4688 ± 86 yr $_{BP}$ continues the linear trend of dates. Bacterial primary production was therefore still occuring relatively high in the water column. The age determined for BPME *c* [*n*-Pr, Et] was ca. 1500 yr younger than a previously measured bulk age which indicates the return to freshwater conditions may have occurred more recently than previously expected.

CSRA of a batch of Me pyrophaeophorbide *a* standard split into two portions by the fraction collector gave radiocarbon ages of - 481 ± 88 yr $_{BP}$ for the first portion of the peak and - 513 ± 84 yr $_{BP}$ for the second. The ages are extremely similar which indicates that isotopic fractionation did not occur during preparative isolation. Radiocarbon analysis of Control 1 showed that ^{14}C depleted contamination elutes from new HPLC columns and this should be removed before its use. From the bulk standard, Controls and Fractionation checks a relatively large combustion blank of 2.8 µg of carbon was determined which corresponds to ca. 13% of the mass of standards subjected to CSRA.

Chapter 5. Conclusions and future work

5.1. Conclusions

The fundamental aim for this work was to use photosynthetic pigments as a means to investigate the past. This aim encompassed two main areas of study, firstly to identify archaeological water features by profiling pigments preserved in their sediments, and secondly to subject pigments to radiocarbon analysis as a means to date sediments and particular environmental events.

Sediments were collected from three archaeological sites: Beningbrough Hall, Cawood Castle and Hall Garth (and from 7 sampling points in total), all purported to contain structures that were formerly water features. A variety of analytical methods commonly used in organic geochemistry, for example HPLC with online PDA detection and GC-FID, were applied to study the extracts from the archaeological sediments and to characterise the organic matter present. Chlorophyll pigment derivatives including phaeophytin *a* and pyrophaeophytin *a* were identified from their online UV/vis spectra at two sampling points within a purported canal at Beningbrough Hall, providing evidence of algal primary production and an oxygenated water column. LC-MS^n analysis of extracts from these sampling points also revealed chlorophyll derivatives diagnostic of heterotrophic communities. The sediments collected from both sites corresponded to a period of aquatic primary production with associated communities of zooplankton, thus it is confirmed that the sediments indeed represent a former water feature. Both chlorophyll and bacterial pigment derivatives were identified at locations thought to represent two former fish ponds (Hall Garth and Cawood Castle) and a suspected canal (Cawood Castle). The identification of bacterial pigments not only provides further evidence of the presence of archaeological water features but also gives information on the environmental conditions in the water column, for example eutrophication and photic zone anoxia. GC-FID analysis was used to investigate anomalous elevated TOC contents of some of the sediments from the fish pond at Cawood Castle. Lipid profiles of fatty acids and *n*-alkanols from the anomalous region and surrounding layers revealed that terrestrial organic matter (likely to be leaf litter) had entered the pond. Thus, geochemical analysis can confirm the presence of water features and provide additional information on: periods of stratification with photic zone anoxia, the productivity of the system, the presence of heterotrophic

communities and inputs of terrestrial organic matter. Hence, the approach could be applied to other archaeological sites as a robust method of confirming or disputing the presence of archaeological structures purported to be water features.

To achieve the aim of subjecting photosynthetic pigments to CSRA, an experimental plan was developed to extract, isolate and purify pigments from bulk sediments. Two key requirements of the pre-treatment methods used to prepare pigments were that they had to be high yielding and introduce an aspect of orthogonality into the separation of pigments from other bulk components. Pre-treatment and analytical methods that were included in the experimental plan are identified in Figure 68. Both acid methanolysis and preparative HPLC added aspects of orthogonality to the experimental plan. Acid methanolysis formed pigment derivatives that are not found in natural environments and the phase transfer of pigments between aqueous and organic solvents during the work-up steps removes both polar and non polar contaminants. Preparative HPLC allowed compounds to be purified from contaminant components on the basis of their chromatographic retention times and using UV/vis detector response at a specific wavelength to trigger collection. Owing to the simplicity of the methods used to prepare samples for CSRA they can easily be used for the routine preparation of sedimentary pigments for radiocarbon dating.

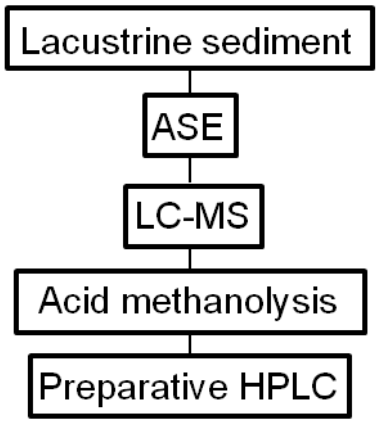

Figure 68. Methods used to achieve the isolation of single photosynthetic pigments from bulk sediments.

The preparative HPLC system available for use in this study was validated by determining its repeatability and recovery using a sediment extract containing high abundances of chl derivatives. Me phaeophorbide *a* and Me pyrophaeophorbide *a* were isolated by the preparative system with recoveries of between ca. 80 and 97% (determined by HPLC peak area and UV/vis analysis) from the bulk sample. The standard deviation in the repeatability of the collection of both derivatives was between ca. ± 5 and 14% which was determined by HPLC peak area and UV/vis analysis. Thus, the system was determined to be acceptable for use in the purification of pigments from environmental samples. It was attempted to determine the contamination added to samples by the HPLC system by subjecting a standard (comprising modern carbon and of similar chemical composition to the target analytes) to the isolation procedure. AMS analysis showed that preparative isolation using a new HPLC column added radiocarbon-dead contamination to the standard. To determine the contribution of carbon from preparative HPLC adequately, blank effluent should also be collected. This alternative approach of standards and blanks would provide a robust method as the initial blank and any subsequent changes in its magnitude during the analysis of samples could be determined. CSRA of Me pyrophaeophorbide *a* standards revealed that isotopic fractionation was not caused by the incomplete collection of a peak, thus providing greater confidence in the radiocarbon ages determined.

The sedimentary photosynthetic pigments of Kirisjes Pond were profiled and single compound derivatives from both oxygenic and anoxic primary production were isolated from the sediments. The purities of recovered chlorophyll and bacteriochlorophylls derivatives were high, thus the isolates were subjected to CSRA to constrain the timing of a past marine incursion. The radiocarbon ages of BPME *c* and *d* pigment derivatives isolated from contemporaneous sediments were generally in close agreement, providing confidence in the approach chosen to achieve compound specific radiocarbon ages. An age of 7736 ± 113 yr $_{BP}$ determined for the algal derivative Me pyrophaeophorbide *a* is in close agreement with a previously measured bulk radiocarbon date of 7825 ± 70 yr $_{BP}$ (Hodgson *et al.*, 2001) for the onset on the marine incursion. The younger CSRA results from each layer are more credible than bulk measurements owing to the age sequence determined within the section of sediments examined. CSRA of a

bacterial pigment from the upper transition zone, representing change from marine to freshwater conditions, revealed a much younger age than previous bulk measurements, 4688 ± 86 yr $_{BP}$ versus 6205 ± 50 yr $_{BP}$. Thus, the pond returned to freshwater conditions more recently than previously thought. Comparisons of CSRA ages determined in this study with those determined from bulk carbon measurement highlights the variability in the results from bulk samples which can either reveal the true age of sediments or be unknowingly affected by refractory organic matter. Radiocarbon ages of contemporaneous algal and bacterial derived pigments revealed the reservoir effect of Kirisjes Pond to be ca. 6000 years at the first freshwater/marine transition zone. From the large magnitude of the reservoir effect the environmental conditions within the pond could be postulated, for example the position of the hypolimnion in the water column and hence the location of bacterial communities. The linearity in the ages determined from algal derivatives within the freshwater/marine transition zone and bacterial derivatives isolated from the marine zone and second marine/freshwater transition zone can be used to reconstruct the movement of the chemocline and the likely changes to the environmental conditions within Kirisjes Pond.

Thus, this study has shown that CSRA of photosynthetic pigments can be used successfully to radiocarbon date sediments. Furthermore, the results have revealed the environmental conditions within a lacustrine environment. Accordingly, providing sufficient pigment is present in their sediments, the methods developed within the study could be applied to other locations that cannot be dated by other means.

5.2. Future work

5.2.1. Arising from sedimentary analysis of archaeological structures

The identification of water features by chemical analysis could be applied to many archaeological sites that feature structures thought to represent water features. To assist in the routine analysis of archaeological sediments two reference databases could be constructed. Firstly, a database of blank control sediments to establish background levels of lipids naturally found within soils and those linked to leaf litter. The second database would comprise TOC

measurements from ponds and canals with differing trophic statuses, for example eutrophic, mesotrophic and oligotrophic, in order to permit more accurate conclusions to be drawn from the TOC contents in the sediments from archaeological structures. A study involving the identification of an archaeological water feature from its sedimentary pigment profile followed by CSRA using the methods developed by this work would be an excellent prospect for expanding the archaeological knowledge of a given site.

5.2.2. Arising from standard preparation and instrument validation

The role of standards within instrument validation could be expanded by subjecting a radiocarbon-dead standard to the experimental plan as well as the modern Me pyrophaeophorbide *a* standard. A radiocarbon-dead standard could be used to determine if any modern carbon had been added during sample pre-treatment. The most efficient method to track changes in isotopic composition would be to add an internal standard of known isotopic composition to sediments before they are subjected to the experimental plan.

5.2.3. Arising from CSRA

The use of a UV/vis wavelength activated preparative HPLC system can result in contamination of isolates with closely eluting components that have similar UV/vis spectra. The possibility of this type of contamination could be minimised by using mass directed fraction collection to isolate single compounds. Further CSRA of the replicate samples isolated from Kirisjes Pond sediments in this study will provide greater degree of certainty in the radiocarbon ages through the determination of measurement errors. The resolution of Lake Chiprana measurements could be improved by subjecting a further quantity of the available sediment to the experimental plan developed by this work followed by radiocarbon analysis. CSRA of photosynthetic pigments could be used to radiocarbon date other lakes with marine incursions on the Antarctic coast (Heart Lake and Pup Lagoon) to provide a robust timescale for the local changes in relative sea level. By constraining basal radiocarbon dates of other lakes in the region CSRA of photosynthetic pigments has the potential to reveal the onset of

sedimentation and the retreat of the ice sheet covering the Stornes and Broknes peninsula during the last glacial maximum.

Chapter 6. Experimental

6.1. General procedures

6.1.1. Solvents and reagents

Solvents used for experimental work were analytical (AR) or HPLC grade, with laboratory grade solvents used for washing glassware (Fisher, Loughborough, UK). The crude chlorophyll preparation used in experiments outlined in Chapter 3 was obtained from the British Chlorophyll Company (BCC; Lincoln, UK) and was stored at 4°C. All other reagents were obtained from Sigma Aldrich (Gillingham, UK).

6.1.2. Preparation of glassware

Glassware was cleaned by rinsing with acetone and deionised water followed by soaking in dilute Decon90 solution (1%) for 12 h. Subsequently, glassware was rinsed sequentially with tap water, deionised water, acetone and AR acetone. Heating of glassware to 450°C for 4 hours in a Barnstead Thermolyne Pyroclean Trace oven (Thermo Fisher, UK) was often employed as an alternative cleaning method.

6.1.3. Sediment collection and storage

Sediments were collected from three archaeological sites and 7 sampling locations: Beningbrough Hall (fish pond and canal (two samples)), Cawood Castle (fish pond and moat) and Hall Garth (fish pond and moat) using cylindrical plastic sediment cores or an auger. The sediment cores were sectioned into 1 cm horizons and transferred into Whirlpak bags soon after collection. Each batch of sediment collected by the auger was transferred into separate Whirlpak bags. The stratigraphy of sediment removed by the auger is not adequately preserved, only 5-10 cm resolution was obtained. All sediment samples were stored in the dark at -20°C until analysis.

6.2. Sample preparation

6.2.1. Lyophilisation

Kirisjes Pond sediment and archaeological samples for lipid analysis by GC-FID and elemental analysis were lyophilised using a Thermo Scientific (UK) Heto PowerDry PL3000 freezer dryer with Lypro controller v0.4. Freeze dried samples were homogenised using a mortar and pestle and sieved through 1 mm, 400 µm and 200 µm mesh sieves. The < 200 µm fraction was used for EA and lipid extractions.

6.2.2. ASE sample extraction

Bulk sediment samples (3 to 5 g) were thawed and extracted with acetone (for pigment analysis) or with 9:1 DCM:methanol (for lipid analysis) using a Dionex (Camberley, Surrey, UK) ASE 350 accelerated solvent extractor (3 x 5 min cycles at 75°C for pigments and at 125°C for lipids). Extracts were reduced to dryness using a rotary vacuum concentrator (Christ (Osterode am Harz, Germany) RVC 2-25 CD plus and CT 02-50 SR cold trap) and stored protected from light at 4 or -20°C until analysis. Pigment extracts were reconstituted in analytical grade acetone and filtered through dichloromethane (DCM) defatted cotton wool to remove particulates prior to analysis by HPLC and LC-MS. The lipid extracts were reconstituted in DCM for analysis by GC-FID.

6.3. Standard preparation

6.3.1. Acid methanolysis

The BCC crude chlorophyll preparation (ca. 3 g) was dissolved in 200 mL of 5% (v/v) methanolic H_2SO_4 and magnetically stirred in the dark for 24 h (Wilson *et al.*, 2004). After stirring, diethyl ether (200 mL) and 60% (v/v) methanolic H_2SO_4 (50 mL) was added and the solution gently shaken. Unwanted components (for example carotenoids) were transferred into the ether phase, which was discarded. The aqueous phase was washed with ether until the organic phase appeared colourless. Esterified pigments were partitioned back into the organic

phase by slowly diluting the acid with water until the phase transfer occurred. The ether phase was neutralised by washing with water.

6.3.2. Acid numbers

The acid methanolysis product was dissolved in 250 mL of diethyl ether and an equal volume of 8% (w/v) HCl was added. The solution was shaken for ca. 5 min or until pigments transferred into the acidic phase. The extraction of the ether layer was repeated with a further 250 mL of 8% (w/v) HCl. The isolated Me pyrophaeophorbide *a* was transferred to the organic phase and washed as described for acid methanolysis (Section 6.3.1 Chapter 6). Acid numbering was carried out for a second time in analogous fashion using 11% (w/v) HCl as opposed to 8% (w/v) HCl. The combined extracts were concentrated to dryness using a rotary evaporator before reconstitution in acetone for HPLC analysis and preparative HPLC. The acid numbers procedure was modified from Naylor (1997) and Smith (1975).

6.4. Analytical Procedures

6.4.1. Total organic carbon and CHN measurement

The < 200 µm fraction of sieved sediments was prepared for total organic carbon (TOC) content measurement by removal of carbonate, using a method adapted from Columbo and Baccanti (1990), in which the sediment was heated to 80°C in aqueous HCl (18.5% w/v). CHN measurements were determined directly on the < 200 µm fraction. The TOC and CHN content of samples was determined using a Thermo Scientific (UK) Flash 2000 organic elemental analyser equipped with an autosampler and a thermal conductivity detector.

6.4.2. GC-FID analysis

GC analysis of lipid samples was carried out using a Thermo Scientific (UK) Trace GC Ultra with a DB5 60 m column (0.25 µm film thickness and 0.32 mm ID). The injector temperature was 230°C, the split ratio was 10:1 and a 1 µL sample injection volume was used throughout. Helium was employed as carrier

gas at a flow rate of 2.0 L min^{-1} and the FID detector temperature was 330°C. The oven temperature program was as follows: 70°C (initial temperature) followed by a ramp of 20°C/min to 130°C, a second ramp of 4°C/min to 320°C, and a final isothermal period of 40 min.

6.4.3. HPLC analysis

Reversed phase HPLC was carried out using a Waters system (Milford, Ma, USA) comprising a 717 autosampler, 600MS system controller and a 996 photodiode array detector scanning over the range 350-800 nm. Data processing and analysis was achieved using Waters Millennium 2010 software. MaxPlot chromatograms were generated by plotting each component at its wavelength of maximum absorbance. Two reversed phase Waters ODS 2 columns (150 mm x 4.6 mm I.D; 3 µm particle size), fitted with a pre-column guard cartridge with the same stationary phase (10 mm x 5 mm ID), were used in series for the separations. The columns were eluted with a flow rate of 0.7 mL min^{-1} using method A (Airs *et al.*, 2001) for archaeological samples, method B (Airs *et al.*, 2001) for analyses of Me pyrophaeophorbide *a* standard and Lake Chiprana extracts and method M3 (Wilson *et al.*, 2003) for Kirisjes Pond extracts (Table 26). Samples were prepared in acetone for injection.

Table 26. HPLC solvent gradient programs of methods A and B(Airs *et al.*, 2001) and method M3 (Wilson *et al.*, 2003).

Method	Time (min)	Ammonium acetate (0.01M)	Methanol	Acetonitrile	Ethyl acetate
A	0	5	80	15	0
	5	5	80	15	0
	100	0	20	15	65
	105	0	1	1	98
	110	0	1	1	98
	115	5	80	15	0
B	0	5	80	15	0
	5	5	80	15	0
	81	1	32	15	52
	85	5	80	15	0
M3	0	5	80	15	0
	10	5	80	15	0
	55	4	68	15	13
	60	0	1	1	98
	65	0	1	1	98
	70	5	80	15	0

6.4.4. LC-MS and direct injection MS analysis

LC-MS analyses were carried out using a Dionex Ultimate 3000 RSLC system (Camberley, Surrey, UK) or with a DAD detector controlled by Chromeleon software or a Dionex 3000 system controlled by Chromeleon Xpress software (software interface with MS was Hystar 3.2). The HPLC conditions were as described above. MS was performed using a Bruker HCTultra ETD II ion trap with an APCI source operated in positive ion mode. Instrument settings were as follows: capillary current 1 µA, capillary vaporiser temperature 450°C, corona discharge current 4000 µA, nebuliser gas 10 psi and drying gas 10 L min^{-1}. Scan range of *m/z* 50-1200 was used. LC-MS^n was carried out using an Auto MS^n feature of the spectrometer in which the base peak ion in each scan is selected for CID, multistage tandem mass spectra generated up to MS^5. Auto MS^n settings were as follows: activation voltage 1.0 V, isolation width 1.5 *m/z* and a maximum accumulation time of 1 min. Data analysis was performed using Bruker DataAnalysis software.

Direct injection MS was achieved using the autosampler of a Dionex Ultimate 3000 RSLC system coupled directed to a Bruker HCTultra ETD II ion trap with an APCI source operated in positive ion mode. The delivery solvent was 80% methanol, 15% acetonitrile and 5% 0.01 M ammonium acetate (starting composition of method A (Airs *et al.*, 2001)) at a flow rate of 0.7 mL min^{-1}. The MS conditions were the same as those used for LC-MS. Samples for both LC-MS and directed injection analysis were prepared in acetone.

6.4.5. Preparative HPLC

Preparative HPLC was carried out using the same instrumental setup to that was detailed in Section 6.4.3 (Chapter 6), with the exception that a Gilson 201 fraction collector was incorporated to collect fractions of the eluent. A Jones Chromatography Apex ODS2 semi preparative column (250 mm x 10 mm i.d and a 5 µm particle size) and a 1 mL min^{-1} flow rate were used for preparative isolations. A short binary elution program was developed in Chapter 3 (Section 3.4.4) for preparative HPLC of samples containing a limited number of components (Table 27). Lake Chiprana and Kirisjes Pond samples were subjected to preparative HPLC using method M3 (Wilson *et al.*, 2003). Samples were prepared in acetone for injection.

Table 27. HPLC solvent gradient program of the binary method.

Time (min)	Methanol (%)	Ethyl acetate (%)
0	95	5
20	40	60
21	95	5
25	95	5

6.4.6. UV/vis spectroscopy

Samples were dissolved in acetone and UV/vis spectroscopy was carried out using a Shimadzu UV-1800 with a scan range of 350 – 800 nm and speed of 3000 nm min^{-1}. The cell path length was 1 cm. UV Probe software was used to control the spectrometer. The concentrations of sample solutions were

determined using the Beer-Lambert law: A = εcl with A = absorbance (AU), ε = specific extinction co-efficient (Soret band ε of Me pyrophaeophorbide *a*, 194.6 g L^{-1} cm^{-1}), and l = path length (1 cm). Masses of dissolved components were subsequently determined by multiplying the concentration of the solution by its dissolution volume. The specific extinction co-efficient of Me pyrophaeophorbide *a* was used to determine the concentration and hence the mass of all compounds as it is largely dependent on the chromophore of the tetrapyrrole macrocycle, which was common to the other tetrapyrrole pigments investigated (only differ in the nature of peripheral functional groups). Algal pigments in sediment samples were quantified by reference to a calibration curve constructed following HPLC analysis of a series of Me pyrophaeophorbide *a* solutions of known concentrations (as determined by UV/vis spectroscopy). To quantify bacteriophaeophytin *a* a correction factor of 0.298 (specific extinction co-efficient of bacteriophaeophytin *a*/specific extinction co-efficient for Me pyrophaeophorbide *a*) was applied to the calibration curve.

6.5. Radiocarbon analysis

6.5.1. Preparation of CO_2

Samples comprising ca. 20 µg of carbon were combusted to CO_2 for AMS analysis using a method modified from Pearson *et al.* (1998) at the ETH (Zurich, Switzerland). Briefly, samples were transferred into pre-combusted quartz tubes and the solvent evaporated. The tubes were then charged with cupric oxide (ca. 100 to 200 µg of 0.5 mm wire), evacuated, flame sealed and heated for 5 h at 850°C. The resultant CO_2 was purified on a vacuum line, with water removed over a cryogenic trap. The purified CO_2 was quantified manometrically and transferred into a pyrex tube for AMS analysis.

6.5.2. AMS analysis

Samples were analysed on a mini radiocarbon dating system (MICADAS), at the ETH Honggerberg (Zurich, Switzerland) using a gas ion source. The system represents a low energy AMS, first reported by Synal *et al.* (2004), with a terminal voltage of 200 kV. Sample measurements were processed using Bats version

3.3 (9.05.2012) written by L. Wacker. Fm values were corrected for $\delta^{13}C$ fractionation (-25‰) and converted into radiocarbon ages using established conventions (Stuiver and Polach, 1977). Single AMS analyses were carried out on standards and samples.

Structure Appendix

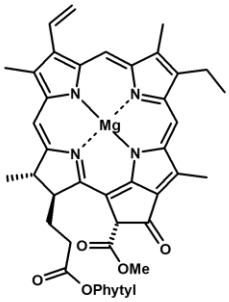

Chlorophyll *a*
1

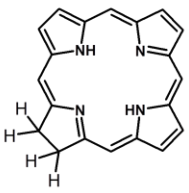

Chlorin
2

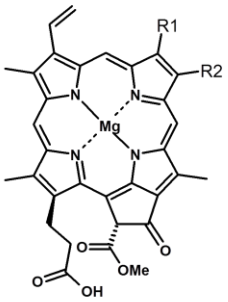

Chlorophyll *c*
c_1 R1 = Et, R2 = Me
c_2 R1 = vinyl, R2 = Me
c_3 R1 = vinyl, R2 = CO_2Me
3

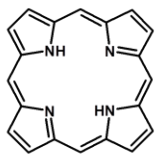

Porphyrin
4

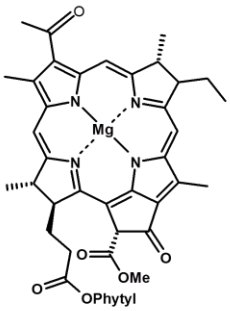

Bacteriochlorophyll *a*
5

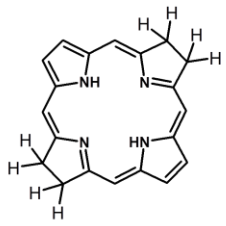

Bacteriochlorin
6

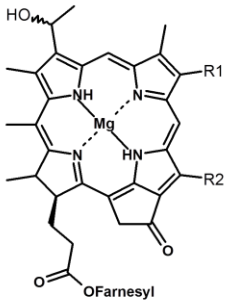

Bacteriochlorophyll *c*
R1 = Me, Et, *n*-Pr, *i*-Bu
R2 = Me, Et
7

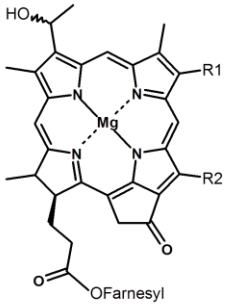

Bacteriochlorophyll *d*
R1 = Me, Et, *n*-Pr, *i*-Bu, *neo*-Pent
R2 = Me, Et
8

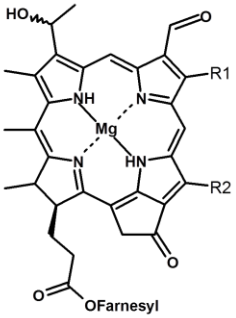

Bacteriochlorophyll *e*
R1 = Me, Et, *n*-Pr, *i*-Bu
R2 = Me, Et
9

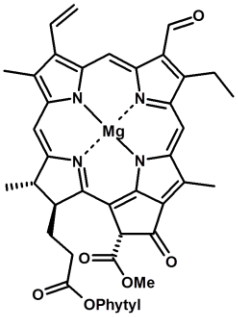

Chlorophyll *b*
10

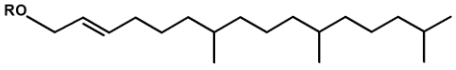

Phytyl
11

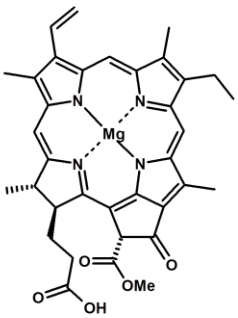

Chlorophyllide *a*
12

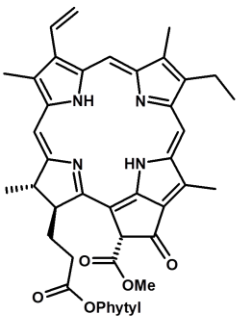

Phaeophytin *a*
13

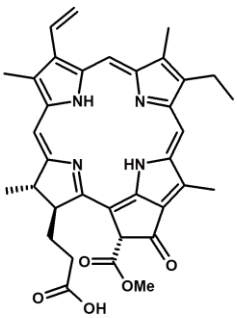

Phaeophorbide *a*
14

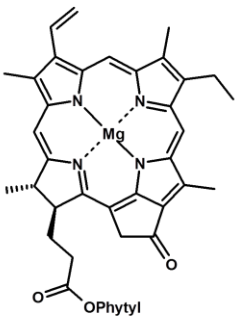

Pyrochlorophyll *a*
15

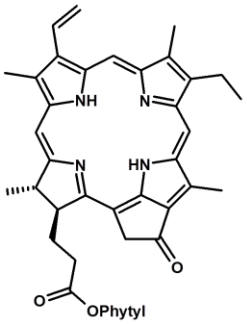

Pyrophaeophytin *a*
16

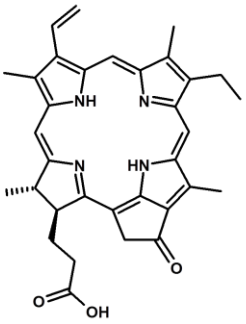

Pyrophaeophorbide *a*
17

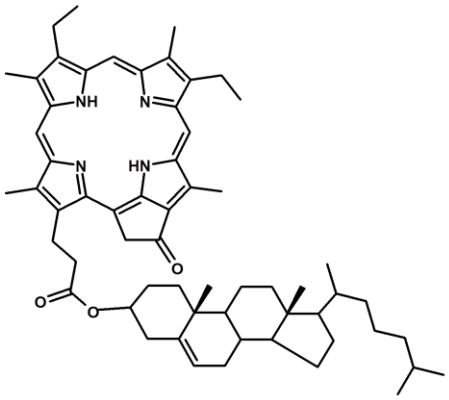

Steryl chlorin ester (SCE)
18

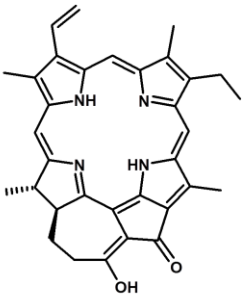

13^2 17^3 cyclophaeophorbide-*a*-enol
19

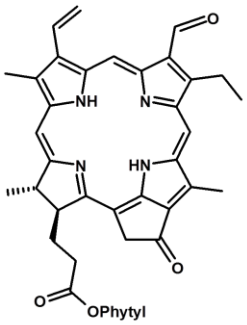

Pyrophaeophytin *b*
20

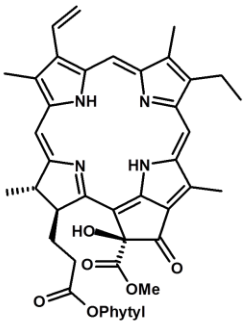

Hydroxyphaeophytin *a*
21

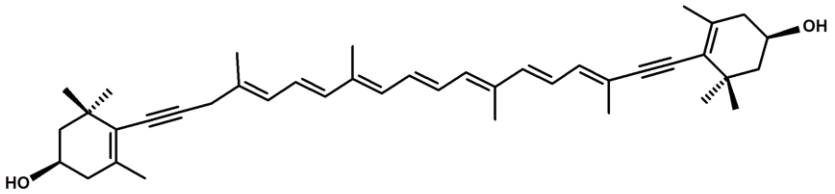

Alloxanthin
22

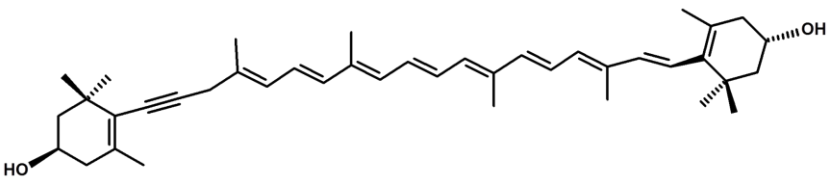

Monadoxanthin
23

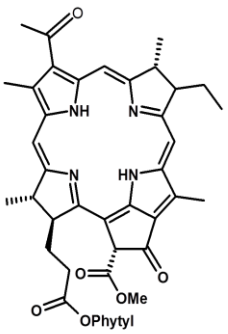

Bacteriophaeophytin *a*
24

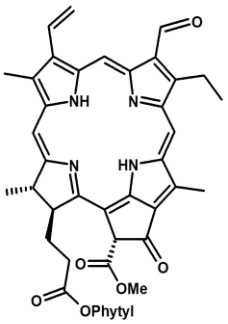

Phaeophytin *b*
25

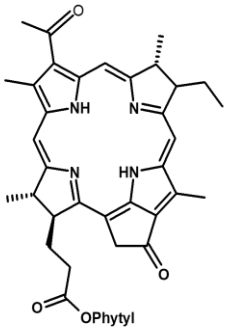

Pyrobacteriophaeophytin *a*
26

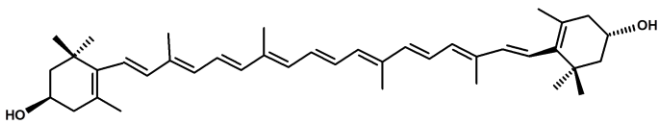

Lutein
27

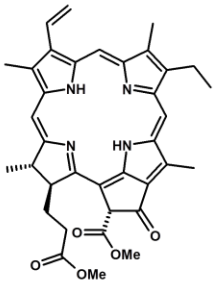

Me phaeophorbide a
28

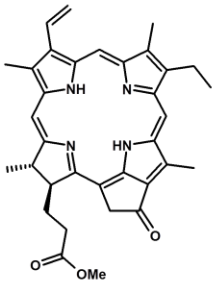

Me pyrophaeophorbide a
29

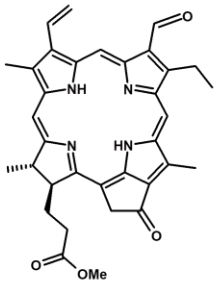

Me pyrophaeophorbide *b*
30

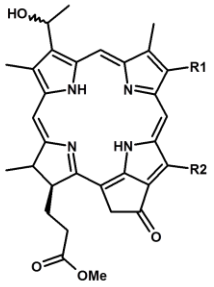

Me bacteriophaeophorbide *d*
R1 = Me, Et, *n*-Pr, *i*-Bu, *neo*-Pent
R2 = Me, Et
31

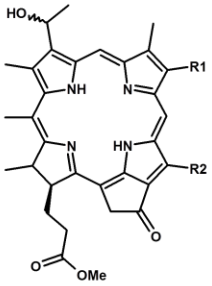

Me bacteriophaeophorbide *c*
R1 = Me, Et, *n*-Pr, *i*-Bu
R2 = Me, Et
32

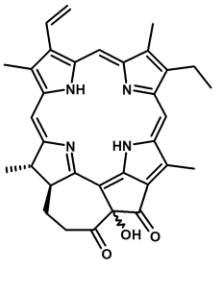

Chlorophyllone
33

References

Airs, R. L., J. E. Atkinson and B. J. Keely, (2001). Development and application of a high resolution liquid chromatographic method for the analysis of complex pigment distributions. Journal of Chromatography A 917, 167-177.
Airs, R. L. and B. J. Keely, (2003). A high resolution study of the chlorophyll and bacteriochlorophyll pigment distributions in a calcite/gypsum microbial mat. Organic Geochemistry 34, 539-551.
Ascough, P., G. Cook and A. Dugmore, (2005). Methodological approaches to determining the marine radiocarbon reservoir effect. Progress in Physical Geography 29, 532-547.
Ascough, P. L., G. T. Cook, H. Hastie, E. Dunbar, M. J. Church, A. Einarsson, T. H. McGovern and A. J. Dugmore, (2011). An Icelandic freshwater radiocarbon reservoir effect: Implications for lacustrine C-14 chronologies. Holocene 21, 1073-1080.
Baird, C. (1995). Environmental Chemistry. New York, W. H. Freeman and Company.
Barker, J. and R. C. Garner, (1999). Biomedical applications of accelerator mass spectrometry isotope measurements at the level of the atom. Rapid Communications in Mass Spectrometry 13, 285-293.
Baumann, P. Q., D. B. Ebenstein, B. D. O'Rourke and K. S. Nair, (1992). High-performance liquid-chromatographic technique for non-derivatized leucine purification - evidence for carbon isotopic fractionation. Journal of Chromatography-Biomedical Applications 573, 11-16.
Bennett, C. L., R. P. Beukens, M. R. Clover, H. E. Gove, R. B. Liebert, A. E. Litherland, K. H. Purser and W. E. Sondheim, (1977). Radiocarbon dating using electrostatic accelerators - negative-ions provide key. Science 198, 508-510.
Bobe, F. W., N. Pfennig, K. L. Swanson and K. M. Smith, (1990). Red shift of absorption maxima in chlorobiineae through enzymatic methylation of their antenna bacteriochlorophylls. Biochemistry 29, 4340-4348.
Borrego, C. M., L. J. Garcia-Gil, X. Vila, X. P. Cristina, J. B. Figueras and C. A. Abella, (1997). Distribution of bacteriochlorophyll homologs in natural populations of brown-colored phototrophic sulfur bacteria. Fems Microbiology Ecology 24, 301-309.
Bronk, C. R. and R. E. M. Hedges, (1987). A gas ion-source for radiocarbon dating. Nuclear Instruments & Methods in Physics Research Section B-Beam Interactions with Materials and Atoms 29, 45-49.
Bronk, C. R. and R. E. M. Hedges, (1989). Use of the CO2 source in radiocarbon dating by AMS. Radiocarbon 31, 298-304.
Brothwell, D., B. J. Keely and M. R. Usai, (2001). InterArChive: "Interred with their bones" - Linking soil micromorphology and chemistry to unlock the hidden archive of archaeological human burials. ERC Mid-term report ERC-2008-AdG 230193.
Bull, I. D., I. A. Simpson, S. J. Dockrill and R. P. Evershed, (1999). Organic geochemical evidence for the origin of ancient anthropogenic soil deposits at Tofts Ness, Sanday, Orkney. Organic Geochemistry 30, 535-556.
Bull, I. D., P. F. Van Bergen, P. R. Poulton and R. P. Evershed, (1998). Organic geochemical studies of soils from the Rothamsted Classical Experiments - II, Soils from the Hoosfield Spring Barley Experiment treated with different quantities of manure. Organic Geochemistry 28, 11-26.
Calcagnile, L., G. Quarta, M. D'Elia, A. Rizzo, A. Gottdang, M. Klein and D. J. W. Mous, (2004). A new accelerator mass spectrometry facility in Lecce,

Italy. Nuclear Instruments & Methods in Physics Research Section B-Beam Interactions with Materials and Atoms 223, 16-20.
Carpenter, S. R., M. M. Elser and J. J. Elser, (1986). Chlorophyll production, degradation, and sedimentation - Implications for paleolimnology. Limnology and Oceanography 31, 112-124.
Cavallo, L. M. and W. B. Mann, (1980). New National-Bureau-of-Standards contemporary C-14 standards. Radiocarbon 22, 962-963.
Columbo, B. and M. Baccanti (1990). Process and equipment for the determination of organic carbon content in complex matrixes, Erba Strumentazione, Italy.
Currie, C. K., (1990). Fish ponds as garden features. Garden History 18, 22 - 46.
Currie, L. A., (2004). The remarkable metrological history of radiocarbon dating II. Journal of Research of the National Institute of Standards and Technology 109, 185-217.
Damon, P. E., D. J. Donahue, B. H. Gore, A. L. Hatheway, A. J. T. Jull, T. W. Linick, P. J. Sercel, L. J. Toolin, C. R. Bronk, E. T. Hall, R. E. M. Hedges, R. Housley, I. A. Law, C. Perry, G. Bonani, S. Trumbore, W. Woelfli, J. C. Ambers, S. G. E. Bowman, M. N. Leese and M. S. Tite, (1989). Radiocarbon dating of the shroud of Turin. Nature 337, 611-615.
de Hoffmann, E. and V. Stroobant (2007). Mass Spectrometry: Principles and Applications. Chichester, Wiley.
Dobeli, M., C. Kottler, M. Stocker, S. Weinmann, H. A. Synal, M. Grajcar and M. Suter, (2004). Gas ionization chambers with silicon nitride windows for the detection and identification of low energy ions. Nuclear Instruments & Methods in Physics Research Section B-Beam Interactions with Materials and Atoms 219, 415-419.
Eglinton, G. and R. J. Hamilton, (1967). Leaf epicuticular waxes. Science 156, 1322-&.
Eglinton, T. I., L. I. Aluwihare, J. E. Bauer, E. R. M. Druffel and A. P. McNichol, (1996). Gas chromatographic isolation of individual compounds from complex matrices for radiocarbon dating. Analytical Chemistry 68, 904-912.
Eiriksson, J., K. L. Knudsen, H. Haflidason and J. Heinemeier, (2000). Chronology of late Holocene climatic events in the northern North Atlantic based on AMS C-14 dates and tephra markers from the volcano Hekla, Iceland. Journal of Quaternary Science 15, 573-580.
Elmore, D. and F. M. Phillips, (1987). Accelerator mass-spectrometry for measurement of long-lived radioisotopes. Science 236, 543-550.
Evershed, R. P., (1993). Biomarker archaeology and lipids. World Archaeology 25, 74-93.
Evershed, R. P., (2008). Organic residue analysis in archaeology: The archaeological biomarker revolution. Archaeometry 50, 895-924.
Fairbanks, R. G., R. A. Mortlock, T. C. Chiu, L. Cao, A. Kaplan, T. P. Guilderson, T. W. Fairbanks, A. L. Bloom, P. M. Grootes and M. J. Nadeau, (2005). Radiocarbon calibration curve spanning 0 to 50,000 years BP based on paired Th-230/U-234/U-238 and C-14 dates on pristine corals. Quaternary Science Reviews 24, 1781-1796.
Falkowski, P. G. and J. A. Raven (1997). Aquatic Photosynthesis, Blackwell Science.
Felus, K., (2006). Boats and boating in the designed landscape 1720 - 1820. Garden History 34, 22 - 46.
Fifield, L. K., (1999). Accelerator mass spectrometry and its applications. Reports on Progress in Physics 62, 1223-1274.

Foyer, C. H. (1984). Photosynthesis, Wiley Interscience.
Godwin, H., (1962). Half-life of radiocarbon. Nature 195, 984-&.
Gottdang, A., D. J. W. Mous and R. G. Haitsma, (2002). The novel HVEE 5 MV Tandetron (TM). Nuclear Instruments & Methods in Physics Research Section B-Beam Interactions with Materials and Atoms 190, 177-182.
Hall, D. O. and K. K. Rao (1999). Photosynthesis. Cambridge, Cambridge University Press.
Harradine, P. J., P. G. Harris, R. N. Head, R. P. Harris and J. R. Maxwell, (1996). Steryl chlorin esters are formed by zooplankton herbivory. Geochimica Et Cosmochimica Acta 60, 2265-2270.
Hellborg, R. and G. Skog, (2008). Accelerator mass spectrometry. Mass Spectrometry Reviews 27, 398-427.
Hendry, G. A. F., J. D. Houghton and S. B. Brown, (1987). Tansley review No-11 - The degradation of cholorphyll - A biological enigma. New Phytologist 107, 255-302.
Hodgins, G. W. L., T. D. Butters, C. B. Ramsey and R. E. M. Hedges, (2001). The chemical and enzymatic hydrolysis of archaeological wood cellulose and monosaccharide purification by high pH anion exchange chromatography for compound-specific radiocarbon dating. Radiocarbon 43, 209-215.
Hodgson, D. A., P. E. Noon, W. Vyverman, C. L. Bryant, D. B. Gore, P. Appleby, M. Gilmour, E. Verleyen, K. Sabbe, V. J. Jones, J. C. Ellis-Evans and P. B. Wood, (2001). Were the Larsemann Hills ice-free through the Last Glacial Maximum? Antarctic Science 13, 440-454.
Hodgson, D. A., E. Verleyen, A. H. Squier, K. Sabbe, B. J. Keely, K. M. Saunders and W. Vyverman, (2006). Interglacial environments of coastal east Antarctica: comparison of MIS 1 (Holocene) and MIS 5e (Last Interglacial) lake-sediment records. Quaternary Science Reviews 25, 179-197.
Holden, J., A. Howard, A. Lockwood and D. Stanley (2002). Restoration of water features at Bramham Park: A Hydrological Feasibility study Part I, Geocat, University of Leeds**:** 1-41.
Hurley, J. P. and D. E. Armstrong, (1990). Fluxes and transformations of aquatic pigments in lake Mendota, Wisconsin. Limnology and Oceanography 35, 384-398.
Ingalls, A. E., R. F. Anderson and A. Pearson, (2004). Radiocarbon dating of diatom-bound organic compounds. Marine Chemistry 92, 91-105.
Ingalls, A. E., E. E. Ellis, G. M. Santos, K. E. McDuffee, L. Truxal, R. G. Keil and E. R. M. Druffel, (2010). HPLC Purification of Higher Plant-Dervied Lignin Phenols for Compound Specific Radiocarbon Analysis. Analytical Chemistry 82, 8931-8938.
Itoh, N., Y. Tani and M. Soma, (2003). Sedimentary photosynthetic pigments of algae and phototrophic bacteria in Lake Hamana, Japan: temporal changes of anoxia in its five basins. Limnology 4, 139-148.
Jeffrey, S. W., R. F. C. Mantoura and S. W. Wright (1996). Phytoplankton pigments in oceanography: Guidelines to modern methods, UNESCO Publishing.
Jull, A. J. T. and G. S. Burr, (2006). Accelerator mass spectrometry: Is the future bigger or smaller? Earth and Planetary Science Letters 243, 305-325.
Keely, B. J. (2006). Geochemistry of chlorophylls. Chlorophylls and Bacteriochlorophylls: Biochemistry, Biophysics, Functions and Applications, Advances in Photosynthesis and Respiration. B. Grimm, R. J. Porra, W. Rudiger and H. Scheer. Dordrecht, The Netherlands, Springer. 25**:** 535 - 561.

Kiernan, K., D. B. Gore, D. Fink, D. A. White, A. McConnell and I. A. Sigurdsson, (2009). Deglaciation and weathering of Larsemann Hills, East Antarctica. Antarctic Science 21, 373-382.
Killops, S. and V. Killops (2005). Introduction to Organic Geochemistry, Blackwell Publishing.
Kjeldsen, H., J. Churchman, P. Leach and C. B. Ramsey, (2008). On the prospects of AMS C-14 with real-time sample preparation and separation. Radiocarbon 50, 267-274.
Kusch, S., Y. Kashiyama, N. O. Ogawa, M. Altabet, M. Butzin, J. Friedrich, N. Ohkouchi and G. Mollenhauer, (2010). Implications for chloro- and pheopigment synthesis and preservation from combined compound-specific delta C-13, delta N-15, and Delta C-14 analysis. Biogeosciences 7, 4105-4118.
Laurie, I. C., (1985). Landscape gardeners at Eaton Park: II. Garden History 13, 126 - 155.
Macdonald, G. M., R. P. Beukens and W. E. Kieser, (1991). Radiocarbon dating of limnic sediments - A comparative-analysis and discussion. Ecology 72, 1150-1155.
Madeja, J. and D. Latowski, (2008). Too old AMS radiocarbon dates obtained from moss remains from Lake Kwiecko bottom sediments (N Poland). Geochronometria 32, 13-19.
Mann, W. B., (1983). An international reference material for radiocarbon dating. Radiocarbon 25, 519-527.
Mantoura, R. F. C. and C. A. Llewellyn, (1983). The rapid-determination of algal chlorophyll and carotenoid-pigments and their breakdown products in natural-waters by reverse-phase high-performance liquid-chromatography. Analytica Chimica Acta 151, 297-314.
Matile, P., S. Hortensteiner and H. Thomas, (1999). Chlorophyll degradation. Annual Review of Plant Physiology and Plant Molecular Biology 50, 67-95.
Matile, P., S. Hortensteiner, H. Thomas and B. Krautler, (1996). Chlorophyll breakdown in senescent leaves. Plant Physiology 112, 1403-1409.
Matsuzaki, H., C. Nakano, Y. Tsuchiya, K. Kato, Y. Maejima, Y. Miyairi, S. Wakasa and T. Aze, (2007). Multi-nuclide AMS performances at MALT. Nuclear Instruments & Methods in Physics Research Section B-Beam Interactions with Materials and Atoms 259, 36-40.
McNichol, A. P. and L. I. Aluwihare, (2007). The power of radiocarbon in biogeochemical studies of the marine carbon cycle: Insights from studies of dissolved and particulate organic carbon (DOC and POC). Chemical Reviews 107, 443-466.
Morellon, M., B. Valero-Garces, A. Moreno, P. Gonzalez-Samperiz, P. Mata, O. Romero, M. Maestro and A. Navas, (2008). Holocene palaeohydrology and climate variability in northeastern Spain: The sedimentary record of Lake Estanya (Pre-Pyrenean range). Quaternary International 181, 15-31.
Moreton, S. G., G. C. Rosqvist, S. J. Davies and M. J. Bentley, (2004). Radiocarbon reservoir ages from freshwater lakes, south Georgia, sub-Antarctic: Modern analogues from particulate organic matter and surface sediments. Radiocarbon 46, 621-626.
Naylor, C. C. (1997). Early oxidative transformation products of chlorophyll in contemporary environments. Chemistry, University of York. Ph. D. thesis.
Nelson, D. E., R. G. Korteling and W. R. Stott, (1977). C-14 - direct detection at natural concentrations. Science 198, 507-508.

O'Connell, T. C. and R. E. M. Hedges, (2001). Isolation and isotopic analysis of individual amino acids from archaeological bone collagen: A new method using RP-HPLC. Archaeometry 43, 421-438.
Ognibene, T. J., G. Bench, J. S. Vogel, G. F. Peaslee and S. Murov, (2003). A high-throughput method for the conversion of CO2 obtained from biochemical samples to graphite in septa-sealed vials for quantification of C-14 via accelerator mass spectrometry. Analytical Chemistry 75, 2192-2196.
Ohkouchi, N., T. I. Eglinton and J. M. Hayes, (2003). Radiocarbon dating of individual fatty acids as a tool for refining Antarctic margin sediment chronologies. Radiocarbon 45, 17-24.
Owens, T. G. and P. G. Falkowski, (1982). Enzymatic degradation of chlorophyll-a by marine-phytoplankton invitro. Phytochemistry 21, 979-984.
Paul, W. and H. Steinwedel (1960). Apparatus for separating charged particles of different specific charges. U. patent. 2939952.
Pearce, G. E. S., P. J. Harradine, H. M. Talbot and J. R. Maxwell, (1998). Sedimentary sterols and steryl chlorin esters: distribution differences and significance. Organic Geochemistry 28, 3-10.
Pearson, A., A. P. McNichol, R. J. Schneider, K. F. Von Reden and Y. Zheng, (1998). Microscale AMS C-14 measurement at NOSAMS. Radiocarbon 40, 61-75.
Pell, E. M., (1960). Ion drift in an N-P junction. Journal of Applied Physics 31, 291-302.
Povinec, P. P., M. Betti, A. J. T. Jull and P. Vojtyla, (2008). New isotope technologies in environmental physics. Acta Physica Slovaca 58, 1-154.
Ramsey, C. B. and M. J. Humm, (2000). On-line combustion of samples for AMS and ion source developments at ORAU. Nuclear Instruments & Methods in Physics Research Section B-Beam Interactions with Materials and Atoms 172, 242-246.
Reimer, P. J., M. G. L. Baillie, E. Bard, A. Bayliss, J. W. Beck, P. G. Blackwell, C. B. Ramsey, C. E. Buck, G. S. Burr, R. L. Edwards, M. Friedrich, P. M. Grootes, T. P. Guilderson, I. Hajdas, T. J. Heaton, A. G. Hogg, K. A. Hughen, K. F. Kaiser, B. Kromer, F. G. McCormac, S. W. Manning, R. W. Reimer, D. A. Richards, J. R. Southon, S. Talamo, C. S. M. Turney, J. van der Plicht and C. E. Weyhenmeye, (2009). Intcal09 and Marine09 radiocarbon age calibration curves, 0-50,000 years cal BP. Radiocarbon 51, 1111-1150.
Rezanka, T., (1989). Very-long-chain fatty-acids from the animal and plant kingdoms. Progress in Lipid Research 28, 147-187.
Richter, B. E., B. A. Jones, J. L. Ezzell, N. L. Porter, N. Avdalovic and C. Pohl, (1996). Accelerated solvent extraction: A technique for sample preparation. Analytical Chemistry 68, 1033-1039.
Ruff, M., S. Szidat, H. W. Gaggeler, M. Suter, H. A. Synal and L. Wacker, (2010). Gaseous radiocarbon measurements of small samples. Nuclear Instruments & Methods in Physics Research Section B-Beam Interactions with Materials and Atoms 268, 790-794.
Ruff, M., L. Wacker, H. W. Gaggeler, M. Suter, H. A. Synal and S. Szidat, (2007). A gas ion source for radiocarbon measurements at 200 kV. Radiocarbon 49, 307-314.
Santos, G. M., M. Mazon, J. R. Southon, S. Rifai and R. Moore, (2007). Evaluation of iron and cobalt powders as catalysts for C-14-AMS target preparation. Nuclear Instruments & Methods in Physics Research Section B-Beam Interactions with Materials and Atoms 259, 308-315.

Santos, G. M., R. B. Moore, J. R. Southon, S. Griffin, E. Hinger and D. Zhang, (2007). AMS C-14 sample preparation at the KCCAMS/UCI facility: Status report and performance of small samples. Radiocarbon 49, 255-269.
Scheer, H. (1991). Chlorophylls, RCR Press, Inc.
Schoch, S., H. Scheer, J. A. Schiff, W. Rudiger and H. W. Siegelman, (1981). Pyropheophytin a Accompanies Pheophytin a in Darkened Light Grown Cells of Euglena. Zeitschrift Fur Naturforschung C-a Journal of Biosciences 36, 827-833.
Shah, S. R., G. Mollenhauer, N. Ohkouchi, T. I. Eglinton and A. Pearson, (2008). Origins of archaeal tetraether lipids in sediments: Insights from radiocarbon analysis. Geochimica Et Cosmochimica Acta 72, 4577-4594.
Shah, S. R. and A. Pearson, (2007). Ultra-microscale (5-25 mu g C) analysis of individual lipids by C-14 AMS: Assessment and correction for sample processing blanks. Radiocarbon 49, 69-82.
Shapira, D., R. M. Devries, H. W. Fulbright, J. Toke and M. R. Clover, (1975). Rochester heavy-ion detector. Nuclear Instruments & Methods 129, 123-130.
Smith, K. M. (1975). Porphyrins and metalloporphyrins, Elsevier Scientific Publishing Company.
Smith, K. M., D. A. Goff, J. Fajer and K. M. Barkigia, (1982). Chirality and structures of bacteriochlorophyll-d. Journal of the American Chemical Society 104, 3747-3749.
Smith, K. M., L. A. Kehres and H. D. Tabba, (1980). Structures of the bacteriochlorophyll-c homologs - Solution to a longstanding problem. Journal of the American Chemical Society 102, 7149-7151.
Smittenberg, R. H., E. C. Hopmans, S. Schouten and J. S. S. Damste, (2002). Rapid isolation of biomarkers for compound specific radiocarbon dating using high-performance liquid chromatography and flow injection analysis-atmospheric pressure chemical ionisation mass spectrometry. Journal of Chromatography A 978, 129-140.
Soma, Y., N. Rob, N. Itoh, Y. Tani and M. Soma, (2005). Sterol composition of steryl chlorin esters (SCEs) formed through grazing of algae by freshwater crustaceans: relevance to the composition of sedimentary SCEs. Limnology 6, 45-51.
Squier, A. H., D. A. Hodgson and B. J. Keely, (2002). Sedimentary pigments as markers for environmental change in an Antarctic lake. Organic Geochemistry 33, 1655-1665.
Stafford, G. C., P. E. Kelley, J. E. P. Syka, W. E. Reynolds and J. F. J. Todd, (1984). Recent improvements in and analytical applications of advanced ion trap technology. International Journal of Mass Spectrometry and Ion Processes 60, 85-98.
Stuiver, M. and H. A. Polach, (1977). Reporting of C-14 data - Discussion. Radiocarbon 19, 355-363.
Suter, M., (2004). 25 years of AMS - a review of recent developments. Nuclear Instruments & Methods in Physics Research Section B-Beam Interactions with Materials and Atoms 223, 139-148.
Synal, H. A., M. Dobeli, S. Jacob, M. Stocker and M. Suter, (2004). Radiocarbon AMS towards its low-energy limits. Nuclear Instruments & Methods in Physics Research Section B-Beam Interactions with Materials and Atoms 223, 339-345.
Talbot, H. M., R. N. Head, R. P. Harris and J. R. Maxwell, (1999). Distribution and stability of steryl chlorin esters in copepod faecal pellets from diatom grazing. Organic Geochemistry 30, 1163-1174.

Tikkanen, P., V. Palonen, H. Jungner and J. Keinonen, (2004). AMS facility at the University of Helsinki. Nuclear Instruments & Methods in Physics Research Section B-Beam Interactions with Materials and Atoms 223, 35-39.
Uhl, T., W. Kretschmer, W. Luppold and A. Scharf, (2004). Direct coupling of an elemental analyzer and a hybrid ion source for AMS measurements. Radiocarbon 46, 65-75.
Vailaya, A. and C. Horvath, (1998). Retention in reversed-phase chromatography: partition or adsorption? Journal of Chromatography A 829, 1-27.
Valero-Garces, B. L., A. Navas, J. Machin, T. Stevenson and B. Davis, (2000). Responses of a saline lake ecosystem in a semiarid region to irrigation and climate variability - The history of Salada Chiprana, central Ebro basin, Spain. Ambio 29, 344-350.
Verkouteren, R. M. and G. A. Klouda, (1992). Factorial design techniques applied to optimization of AMS graphite target preparation. Radiocarbon 34, 335-343.
Verleyen, E., D. A. Hodgson, K. Sabbe and W. Vyverman, (2004). Late Quaternary deglaciation and climate history of the Larsemann Hills (East Antarctica). Journal of Quaternary Science 19, 361-375.
Vidondo, B., B. Martinez, C. Montes and M. C. Guerrero, (1993). Physicochemical characteristics of a permanent spanish hypersaline lake - La-Salada-de-Chiprana (NE Spain). Hydrobiologia 267, 113-125.
Vila, X., R. Guyoneaud, X. P. Cristina, J. B. Figueras and C. A. Abella, (2002). Green sulfur bacteria from hypersaline Chiprana Lake (Monegros, Spain): habitat description and phylogenetic relationship of isolated strains. Photosynthesis Research 71, 165-172.
Vogel, J. S., K. W. Turteltaub, R. Finkel and D. E. Nelson, (1995). Accelerator mass-spectrometry - isotope quantification at attomole sensitivity. Analytical Chemistry 67, A353-A359.
Volkman, J. K., S. M. Barrett and S. I. Blackburn, (1999). Eustigmatophyte microalgae are potential sources of C-29 sterols, C-22-C-28 n-alcohols and C-28-C-32 n-alkyl diols in freshwater environments. Organic Geochemistry 30, 307-318.
Volkman, J. K., S. M. Barrett, S. I. Blackburn, M. P. Mansour, E. L. Sikes and F. Gelin, (1998). Microalgal biomarkers: A review of recent research developments. Organic Geochemistry 29, 1163-1179.
Walker, J. S., A. H. Squier, D. A. Hodgson and B. J. Keely, (2002). Origin and significance of 13(2)-hydroxychlorophyll derivatives in sediments. Organic Geochemistry 33, 1667-1674.
Wilson, M. A. (2004). Analysis of complex distributions of bacteriochlorophylls: Development and application of HPLC and LC - MS methods. Chemistry, University of York. Ph. D.
Wilson, M. A., D. A. Hodgson and B. J. Keely, (2004). Structural variations in derivatives of the bacteriochlorophylls of Chlorobiaceae: Impact of stratigraphic resolution on depth profiles as revealed by methanolysis. Organic Geochemistry 35, 1299-1307.
Wilson, M. A., D. A. Hodgson and B. J. Keely, (2005). Atmospheric pressure chemical ionisation liquid chromatography/multistage mass spectrometry for assignment of sedimentary bacteriochlorophyll derivatives. Rapid Communications in Mass Spectrometry 19, 38-46.
Wilson, M. A., S. R. M. Saleh, D. A. Hodgson and B. J. Keely, (2003). Atmospheric pressure chemical ionisation liquid

chromatography/multistage mass spectrometry of isobaric bacteriophaeophorbide dmethyl esters. Rapid Communications in Mass Spectrometry 17, 2455-2458.
Woszczyk, M., A. Bechtel, R. Gratzer, M. J. Kotarba, M. Kokocinski, J. Fiebig and R. Cieslinski, (2011). Composition and origin of organic matter in surface sediments of Lake Sarbsko: A highly eutrophic and shallow coastal lake (northern Poland). Organic Geochemistry 42, 1025-1038.
Zale, R., (1994). C-14 age corrections in Antarctic lake-sediments inferred from geochemistry. Radiocarbon 36, 173-185.
Zapata, M., A. M. Ayala, J. M. Franco and J. L. Garrido, (1987). Separation of chlorophylls and their degradation products in marine-phytoplankton by reversed-phase high-preformance liquid-chromatography. Chromatographia 23, 26-30.
Zelles, L., (1997). Phospholipid fatty acid profiles in selected members of soil microbial communities. Chemosphere 35, 275-294.